2024

DISORGANIZATION OF ACTIN WITHIN THE SHAFTS OF STEREOCILIA IS A KEY DIFFERENCE BETWEEN TEMPORARY AND PERMANENT NOISE-INDUCED HEARING LOSS (NIHL)

Shadan Hadi
University of Kentucky, shadanhadi3@gmail.com
Author ORCID Identifier:
https://orcid.org/0000-0002-7482-0250
Digital Object Identifier: https://doi.org/10.13023/etd.2024.242

STUDENT AGREEMENT:

I represent that my thesis or dissertation and abstract are my original work. Proper attribution has been given to all outside sources. I understand that I am solely responsible for obtaining any needed copyright permissions. I have obtained needed written permission statement(s) from the owner(s) of each third-party copyrighted matter to be included in my work, allowing electronic distribution (if such use is not permitted by the fair use doctrine) which will be submitted to UKnowledge as Additional File.

I hereby grant to The University of Kentucky and its agents the irrevocable, non-exclusive, and royalty-free license to archive and make accessible my work in whole or in part in all forms of media, now or hereafter known. I agree that the document mentioned above may be made available immediately for worldwide access unless an embargo applies.

I retain all other ownership rights to the copyright of my work. I also retain the right to use in future works (such as articles or books) all or part of my work. I understand that I am free to register the copyright to my work.

REVIEW, APPROVAL AND ACCEPTANCE

The document mentioned above has been reviewed and accepted by the student's advisor, on behalf of the advisory committee, and by the Director of Graduate Studies (DGS), on behalf of the program; we verify that this is the final, approved version of the student's thesis including all changes required by the advisory committee. The undersigned agree to abide by the statements above.

Shadan Hadi, Student

Dr. Gregory I. Frolenkov, Major Professor

Dr. Lance Johnson, Director of Graduate Studies

DISORGANIZATION OF ACTIN WITHIN THE SHAFTS OF STEREOCILIA IS A KEY DIFFERENCE BETWEEN TEMPORARY AND PERMANENT NOISE-INDUCED HEARING LOSS (NIHL)

DISSERTATION

A dissertation submitted in partial fulfillment of the
requirements for the degree of Doctor of Philosophy in the
College of Medicine
at the University of Kentucky

By
Shadan Hadi
Lexington, Kentucky
Director: Dr. Gregory I. Frolenkov, Professor of Physiology
Lexington, Kentucky
2024

https://orcid.org/0000-0002-7482-0250

ABSTRACT OF DISSERTATION

DISORGANIZATION OF ACTIN WITHIN THE SHAFTS OF STEREOCILIA IS A KEY DIFFERENCE BETWEEN TEMPORARY AND PERMANENT NOISE-INDUCED HEARING LOSS (NIHL)

During sound stimulation, mechanosensory stereocilia of the auditory hair cell pivot around their bases, where their actin cores become denser and form rootlets protruding into the cuticular plate. It is believed that actin-based cuticular plate provides a stable mechanical support for stereocilia, while rootles are responsible for their pivotal flexibility and life-long resilience to mechanical stimuli. Not surprisingly, damage to the stereocilia bundles is known as a hallmark of permanent noise-induced hearing loss (NIHL). Yet, despite decades of NIHL studies, it is still unknown which ultrastructural changes in the stereocilia bundles are evoked directly by mechanical overstimulation.

Here, we explored the changes in the actin cores of stereocilia, their rootlets, and cuticular plates, immediately after noise exposures. We compared the effects of noise that reliably generate either temporary (TTS) or permanent (PTS) shifts of hearing thresholds in the adult C57BL/6 mice in the frequency region of 16-20 kHz. Samples from this region of the organ of Corti were dissected from unexposed control and noise-exposed animals. Then, the samples were high pressure frozen, freeze-substituted, and low-temperature embedded for serial sectioning with focused ion-beam (FIB) and backscatter scanning electron microscopy (FIB-SEM).

We found that noise exposure causes global disorganization of actin within the stereocilia shafts and the cuticular plate, likely initiated by a global increase in intracellular Ca^{2+}, and expansion of the rootlet, possibly due to local mechanical breakage in the connection between the rootlet and the surrounding cuticular plate. Disorganization of actin within the cuticular plate occurred in both TTS and PTS while expansion of the rootlet started to occur in TTS and became more prominent in PTS. The only pathology that was consistently different between TTS and PTS was the disorganization of actin filaments (F-actin) in the shaft of stereocilia, the region that is known to have minimal or no turnover in mammalian auditory hair cells. We conclude that loss of F-actin integrity within stereocilia shafts is a key determinant for PTS.

KEYWORDS: Noise-induced hearing loss, temporary threshold shift, permanent threshold shift, stereocilia bundles, ultrastructure, actin.

Shadan Hadi

(Name of Student)

04/15/2024

Date

DISORGANIZATION OF ACTIN WITHIN THE SHAFTS OF STEREOCILIA IS A KEY DIFFERENCE BETWEEN TEMPORARY AND PERMANENT NOISE-INDUCED HEARING LOSS (NIHL)

By
Shadan Hadi

Dr. Gregory I. Frolenkov
Director of Dissertation

Dr. Lance Johnson
Director of Graduate Studies

04/15/2024
Date

To my late grandmother

ACKNOWLEDGMENTS

This long-awaited moment has come as I finally sit down to write this section of my dissertation. Although I began my doctoral program in 2018, the road to my Ph.D. journey started 11 years ago. From starting in Dr. Frolenkov's lab at the end of my undergraduate studies, through my master's degree, and now concluding my Ph.D. career, I have truly grown up in his lab. These past years have been transformative and pushed me to be the person I am today. This journey has granted me tremendous academic growth, scientific achievements, courage, and priceless long-term friendships with wonderful colleagues. Today, I am grateful that I experienced this opportunity.

My wonderful advisor, Dr. Gregory Frolenkov, has made the biggest impact in helping me stay strong and focused throughout these years. He embodied the perfect figure with his passion for research, scientific rigor, resilience, patience, and outstanding mentorship. Dr. Frolenkov, I am beyond grateful for you being my lead supporter. Thank you for your limitless guidance. You built true scientific wisdom in me, and I appreciate all the enthusiastic discussions we have shared. I will cherish every moment I spent in your lab, my "home" that nurtured my growth since the early years of my scientific experience.

I have also been fortunate to have amazing and supportive committee members: Dr. Steven Estus, Dr. Hiroshi Saito, Dr. Christopher Waters, and Dr. Donna Wilcock. I want to thank all of you for your time and guidance. I would not have been able to complete this project without your feedback and valuable advice. I want to express my sincere gratitude to each of you in pushing me and challenging me through this process. Thank you for listening, motivating, and encouraging me. Dr. Robin Cooper, thank you for your encouragement and for serving as the outside examiner for this dissertation. Thank you for

your wisdom and guidance through this process. I would also like to thank Dr. Lance Johnson, the director of graduate studies, and Dr. Brett Spear, the director of the Integrated Biomedical Sciences program, for their outstanding leadership and eagerness to support and foster graduate student success.

I would also like to thank my fabulous former lab colleague: Dr. Catalina Velez-Ortega. Cata, I appreciate you opening the doors of your current lab and sharing your equipment to support my experiments. I would also give special thanks to Dr. Thad Wilson, my teaching mentor, who inspired me to consider pursuing medical teaching as a terminal career path. Dr. Wilson, I have been lucky to cross the path with you, joining the department during my Ph.D. I appreciate you giving me the learning opportunity and the experience to teach. Thank you for all your feedback and for being the perfect role model. You are the physiology professor I envision myself to be in my future teaching career.

I would like to thank my wonderful lab mates: Abigail Dragich, Isabel Aristizabal-Ramirez, Emma Bondy, and Aileen Khosravi. You all have been a wonderful team. I will always remember our laughs, snacks, and fun lab dinners.

I would like to thank our amazing administrative team in the Department of Physiology and the Office of Biomedical Education. Special thanks to Tanya Graf, Jennifer Kennedy, and Taylor Petersen. I appreciate all your hard work in making this journey smooth.

I would like to thank my friends, Dr. Rebecca Norcross, Jennifer Holleman, M.A., Dr. Diana Zajac, Dr. Nicholas Devanney, Carolina Galeano-Naranjo, M.S., and Robert Larson. Knowing you all is a precious gift that I earned during grad school. Rebecca, the strongest and most focused person I have ever known. Thank you for always listening and

motivating me, I would not have been able to do it without you. Jenny (Jen pal), the kindest and most inventive person I have ever met. I appreciate our weekly dinners and priceless laughs, which are truly therapeutic for me. Thank you for being the sunshine that keeps the smile on my face. Diana, the one with the vibrant energy, you have been a true inspiration for success as a scientist and for the influence of your positive attitude to overcome difficult times. You and Nick were amazing classmates. Carolina (Caro), and her wonderful husband Robert, thank you to both of you for listening to me express my frustrations and for always giving me the hope that things will get easier.

Finally, and most importantly, I want to express my sincere appreciation to my family: my mother, my father, my sister, my late grandmother, and my uncles Dheeya and Wadee for all their support and encouragement. My grandmother and my uncles provided a warm house while I grew up, but also pushed me to explore my interests and passions. My parents planted the seeds of academic ambitions and strong willingness to work hard in me. My father has taught me the persistence and the patience to pass through storms because “everything happens for a reason, and everything comes at the right time”. My mother, my best friend, whom I also consider my “classmate” because she has been there with me since day 1. She has been my first listener, supporter, and teacher. Throughout all these years, my family has been my backbone, which I leaned on and kept me strong until today. I admit that I would not have been able to reach where I am today without my family. Thank you, mom, and dad, for your unconditional love and selfless efforts to support me and keep me focused. No matter what I do, it will not be enough compared to what you have offered me. With completing my Ph.D. successfully, I hope I can fulfill my promise of making you proud of me today.

TABLE OF CONTENTS

ACKNOWLEDGMENTS iii

TABLE OF CONTENTS vi

LIST OF TABLES viii

LIST OF FIGURES ix

CHAPTER 1. SOUND DETECTION IN THE INNER EAR 1

1.1 The pathway of sound to the inner ear 1

1.2 The cochlea 2

1.3 The cochlear auditory hair cells: structure and mechanosensitive function 2

1.3.1 The organ of Corti: the inner and outer hair cells 2

1.3.1.1 Stereocilia bundles 4

1.3.1.2 Stereocilia rootlets 9

1.3.1.3 The cuticular plate 13

1.3.1.4 How do stereocilia bend during acoustic stimulation? 16

1.3.1.5 Hair cell mechanotransduction and Ca^{2+} homeostasis 17

1.4 Auditory hair cell innervation 20

1.5 The stria vascularis 21

CHAPTER 2. ACOUSTIC OVERSTIMULATION AND NOISE-INDUCED HEARING LOSS (NIHL) 23

2.1 NIHL prevalence and susceptibility 23

2.2 Types of NIHL 25

2.3 Known mechanisms of NIHL 25

2.3.1 Auditory hair cell death 25

2.3.2 Stereocilia bundle damage 26

2.3.3 Excitotoxicity and neural damage 28

2.3.4 Noise-induced metabolic changes 29

2.4 Limited efficacy of currently available treatments 30

2.5 Uknown mechanisms potentially involved in NIHL 32

CHAPTER 3. EXPERIMENTAL METHODS AND TECHNIQUES 33

3.1 Mouse model and cohorts 33

3.2 Auditory brainstem responses (ABRs) and noise exposures 33

3.3 Fluorescence confocal microscopy 35

3.3.1 Organ of Corti sample preparation 35
3.3.2 Fluorescent imaging 36
3.3.3 Data analysis 36
3.4 Focused ion beam scanning electron microscopy (FIB-SEM) 37
3.4.1 Significance and rationale of using the FIB-SEM technology 37
3.4.2 Organ of Corti sample preparations 40
3.4.3 FIB-SEM imaging 42
3.4.4 FIB-SEM image processing for data analysis 42
3.4.5 Quantification of stereocilia with irregular actin 42
3.4.6 Fast Fourier Transform (FFT) analysis 43
3.4.7 Quantification of dense actin structures within the shafts of stereocilia 43
3.4.8 Quantification of rootlet widths 44
3.4.9 Quantification of the cuticular plate non-uniformity 45
CHAPTER 4. RESULTS 46
4.1 Generating TTS or PTS in the middle frequency region of the cochlea 46
4.2 Noise-induced disorganization of F-actin in the shafts of IHC stereocilia 50
4.3 Appearance of dense actin structures within the shafts of stereocilia in IHCs . 54
4.4 Noise exposure causes expansion of the rootlets in IHCs 58
4.5 Noise exposure produces actin disorganization in IHC cuticular plates 62
4.6 Noise changes the positioning of stereocilia in the cuticular plates of IHCs 66
4.7 Actin disorganization in the shafts of stereocilia is also a key distinction between TTS and PTS in OHCs 69
CHAPTER 5. DISCUSSION 75
5.1 Noise exposure causes disorganization of actin within the shafts of stereocilia… 75
5.2 Noise causes loss (disorganization) of actin within the cuticular plate 77
5.3 Appearance of dense actin structures within the shafts of stereocilia in IHCs . 79
5.4 Expansion of the rootlets during noise exposure 81
CHAPTER 6. CONCLUSION 84
REFERENCES 85
VITA…….. 94

LIST OF TABLES

Table 4.1 Detailed summary for the quantification of IHC stereocilia with “rootlet-like” dense actin structures within their shafts. 58

LIST OF FIGURES

Figure 1.1 Structures of the mammalian ear. 1
Figure 1.2 Scanning electron microscopy images of stereocilia bundles of the sensory hair cells in the mammalian cochlea. 3
Figure 1.3 A hair cell has a bundle of stereocilia projections that are made of F-actin. 5
Figure 1.4 Old model on F-actin treadmilling along the shaft of stereocilia. 7
Figure 1.5 New model with F-actin stability within the shaft of stereocilia..... 8
Figure 1.6 Stereocilia rootlets have sophisticated molecular machinery. 13
Figure 1.7 Hair cell apex contains the cuticular plate and the surrounding narrow area of vesicular traffic. 15
Figure 1.8 Two different models demonstrating changes in F-actin upon stereocilia deflection by sound. 17
Figure 1.9 Stereocilia rows are connected via tip links which are associated with MET channels at their lower part. 18
Figure 1.10 Hair cells express different PMCA pumps to extrude Ca^{2+}. 19
Figure 1.11 The stria vascularis maintains endo-cochlear potential in the inner ear. 22
Figure 2.1 Loud noise produces damage to actin structures within stereocilia bundles... 27
Figure 3.1 FIB-SEM imaging of hair cells. 40
Figure 4.1 Establishing parameters of the noise exposure to differentiate temporary (TTS) and permanent (PTS) hearing losses in the mid-frequency (16-20 kHz) region of the cochlea. 49
Figure 4.2 Disruption of F-actin within the shafts of IHC stereocilia is produced by noise causing PTS but not TTS. 53
Figure 4.3 Wrinkling of the stereocilia's plasma membranes in PTS is not an artifact of embedding resin. 54
Figure 4.4 Shafts of stereocilia in IHCs exhibit dense rootlet-like actin structures. 57
Figure 4.5 Noise exposure causes expansion of rootlets in IHCs. 62
Figure 4.6 Noise induces loss of F-actin within the IHC cuticular plates. 66
Figure 4.7 Noise exposure alters the positioning of stereocilia insertions within the cuticular plates in IHCs. 68
Figure 4.8 Typical F-actin compartments in control OHCs. 72
Figure 4.9 F-actin compartments in the OHCs exposed to noise producing TTS. 73
Figure 4.10 Disruption of F-actin within the shafts of stereocilia is a key pathology in OHCs induced by noise producing PTS. 74

CHAPTER 1. SOUND DETECTION IN THE INNER EAR

1.1 The pathway of sound to the inner ear

Sound pressure waves travel through the external ear, the auricle (also named as pina), the ear canal, reaching the tympanic membrane in the middle ear (figure 1.1 A) (for more details of these processes, see (Lehnhardt and Lehnhardt 2003)). These pressure waves vibrate the tympanic membrane, which subsequently causes a displacement motion of the physically associated bones (the ossicles): malleus, incus, and stapes (figure 1.1 A). The movement of the latter transfers the wave pressure into the inner ear via its footplate pushing onto the oval window of the cochlea (figure 1.1 A). Sound stimuli can be presented with different intensities (loudness) in decibel sound pressure level (dB SPL) at given frequencies (kHz).

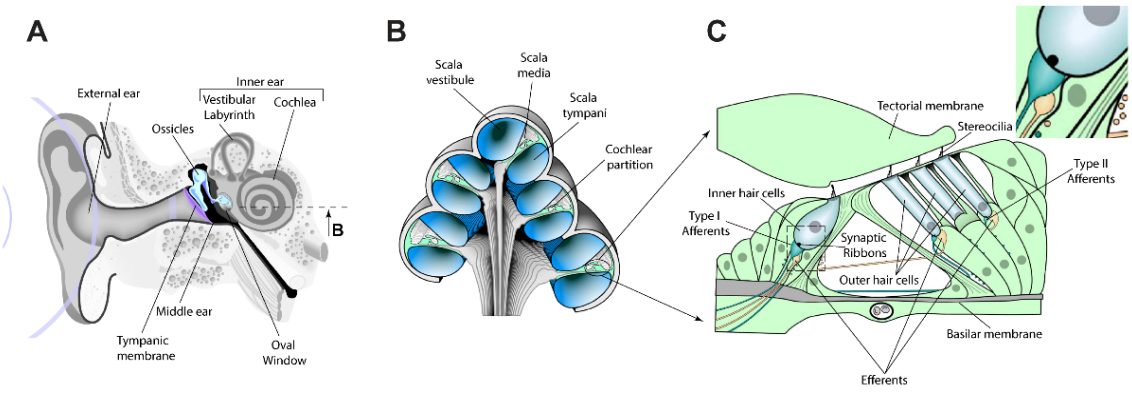

Figure 1.1 Structures of the mammalian ear.
(A) Incoming sound waves reach the cochlea in the inner ear. **(B)** Sagittal cross section through the cochlear bone showing three fluid-filled scalae. The organ of Corti is located between scala media and scala tympani. **(C)** The organ of Corti with its mechanosensory cells, the inner and outer hair cells. Tectorial membrane is located above hair cells and physically touches the outer hair cells. Afferent (green) and efferent (yellow) nerve fibers innervate the sensory hair cells. Type I afferents group to form the auditory nerve going towards the brain. A dashed rectangle with magnified insert marks the synaptic end of an inner hair cell, where neurotransmitter release occurs. This synapse contains a unique structure - synaptic ribbon. The figure is modified from (Frolenkov et al. 2004).

1.2 The cochlea

The cochlea is located inside the temporal bone. It is a key inner ear structure that is responsible for auditory sensation. The cochlea is a fluid-filled bone casing with three domains (figure 1.1 B): the scala vestibule and the scala tympani, which both are filled with perilymph, and the scala media in middle is filled with endolymph (Marcus 1998). Unlike the perilymph which resembles extracellular and cerebrospinal fluids, the endolymph is special due to its high potassium [K^+], exactly like that inside the cell, which is necessary for cochlear function (Harrison 1988; Marcus 1998). The endolymph surrounds the mechanosensory organelles of hair cells at their apex (figure 1.1 B), and therefore, maintaining its environment is essential for hearing.

1.3 The cochlear auditory hair cells: structure and mechanosensitive function

1.3.1 The organ of Corti: the inner and outer hair cells

The mammalian organ of Corti consists of thousands (15,000-30,000) of auditory cells (Frolenkov et al. 2004): inner (IHCs) and outer (OHCs) hair cells, which either detect or amplify the sound-induced vibrations, respectively. Hair cells are arranged in four rows: one row of IHCs and three rows of OHCs (figure 1.1 C). The apical surface of each cell has specialized microvilli projections known as stereocilia, which are the key mechanonsensitive structures of the hair cell (figure 1.1 C and figure 1.2). In contrast to the IHC's stereocilia, which are stimulated by the sound-induced vibration of fluid within the scala media, OHC's stereocilia make physical contact with the tectorial membrane, a collagenous-fibrous mixture covering the organ of Corti (Harrison 1988). The shear motion between tectorial membrane and the OHC surface is essential for the mechanical stimulation and the overall function of OHCs (figure 1.1 C).

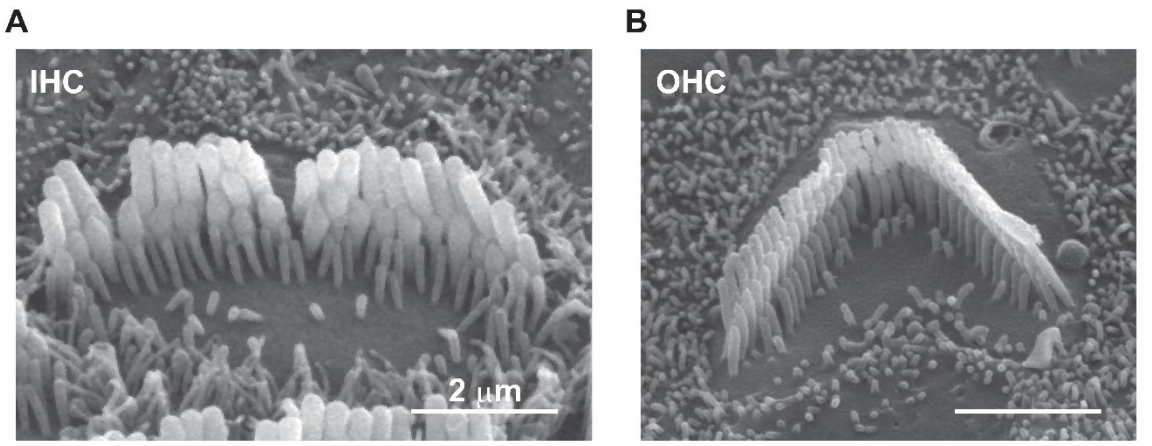

Figure 1.2 Scanning electron microscopy images of stereocilia bundles of the sensory hair cells in the mammalian cochlea.
(A) An inner hair cell. **(B)** An outer hair cell. Cells (A) and (B) come from mice with early postnatal ages, postnatal day (P) 10 and 8, respectively. Each hair cell has stereocilia projections arranged in rows, making a stereocilia bundle. Extra microvilli-like projections resorb throughout postnatal development, and a mature hair cell bundle has only three stereocilia rows. Inner and outer hair cells can be distinguished by the differences in the shape of their bundles. Images in the figure are from (Hadi and Frolenkov, unpublished).

Hair cells are arranged tonotopically along the length of the cochlea, and each cell detects a specific frequency – the cells at the apex of the cochlea detect low frequencies, while the cells at the base of the cochlea detect high frequencies. Since mechanical stiffness of the basilar membrane is gradually increasing from apex to the base of the cochlea while the mass of the organ of Corti is decreasing from apex to the base, each region of the organ of Corti along the length of the cochlea has its own resonant frequency that increases from apex to the base (Békésy 1960). Thus, the cochlea operates as a frequency analyzer (Békésy 1960). See basilar membrane in (figure 1.1 C).

In mammals, the size of the organ of Corti and frequency range of hearing could be different. For example, the human's organ of Corti size is 3.5 cm (Harrison 1988) and detects 20-20,000 Hz (reviewed in (Reynolds et al. 2010)) while that of mouse is 7 mm (Manley and Gummer 2017) and detects 1-100 kHz (reviewed in (Reynolds et al. 2010)). Differences in the organ of Corti size among mammals is believed to contribute to

determining their abilities to hear lower frequency sounds (Manley and Gummer 2017). However, it is known that across all mammals, the shape cochlea seems to be highly preserved (Harrison 1988). It is also worth mentioning that mammalian auditory hair cells do not regenerate. Therefore, maintaining hair cells and protecting them from damage is crucial for hearing.

1.3.1.1 Stereocilia bundles

Stereocilia bundles are hair-like actin structures that project from the apical surface of the hair cells (figure 1.2 and figure 1.3 A). A mature hair cell has more than 50 stereocilia forming a hair "bundle", whereas during early postnatal development, the number of stereocilia within the bundle is significantly higher (Hadi et al. 2020). Within a bundle, stereocilia are positioned in three rows with a staircase-like shape due to differences in lengths between the rows: first row stereocilia are the tallest, and third row stereocilia are the shortest (figure 1.3 A). The tips of stereocilia within a row are connected to the side of their neighboring stereocilia from the taller rows via small (~5 nm in diameter) filaments known as tip-links (Pickles et al. 1984) (figure 1.3 A). Mature tip links are composed of cadherin-23 and protocadehrin-15 (Kazmierczak et al. 2007) and are mechanically linked to mechano-electrical transduction (MET) channels at their lower (protocadherin-15) ends (Beurg et al. 2009) (figure 1.9 A). Only second and third row stereocilia have MET channels at their tips (Beurg et al. 2009), and therefore are known as transducing stereocilia (figure 1.3 A and figure 1.9 A). During acoustic stimulation, sound-induced vibrations deflect the stereocilia, which pull on their tip-links to open the MET channels allowing for influx of positive ions and depolarization of the cell (Fettiplace 2017) (figure 1.9 B).

In addition to their lengths, stereocilia rows also have different widths, where first and second row stereocilia are equally thickest, and third row stereocilia are the thinnest

(as quantified in my previous study (Hadi et al. 2020)). Interestingly, despite that the heights of stereocilia bundles change tonotopically from base to apex (taller bundles detect low frequency sounds, and the shorter ones detect high frequency sounds), all stereocilia within one row of a hair bundle have equal dimensions, and these dimensions are also equal to the stereocilia of the same row on the adjacent cell, indicating that hair cells are highly precise in forming their stereocilia bundles during development (Vélez-Ortega and Frolenkov 2019). Accordingly, since hair cells do not regenerate in mammals, it is not surprising that any disruption to the shape of their stereocilia bundles is detrimental for life-long hearing.

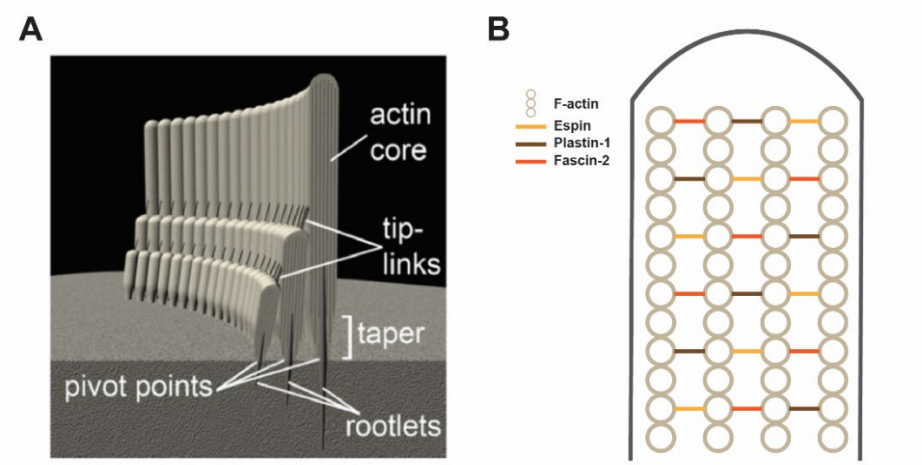

Figure 1.3 A hair cell has a bundle of stereocilia projections that are made of F-actin.
(A) Rod-like stereocilia with parallel actin filaments inside, arranged in staircase-like rows connected with tips links. Each stereocilium has a rootlet that anchors it at its base where it pivots. This panel is adopted from (Kitajiri et al. 2010). **(B)** F-actin core of one stereocilium with side-to-side actin filaments connected with crosslinkers. The most common crosslinking proteins are espin, pastin-1, and fascin-2.

Within a bundle, each stereocilium is supported by up to thousands of parallel actin filaments (F-actin) that are crosslinked (Tilney et al. 1980) with espin (Zheng et al. 2000), plastin-1 (Taylor et al. 2015), and fascin-2 (Shin et al. 2010), (figure 1.3 B). These crosslinker proteins maintain spacing distances between the filaments of ~ 12 nm (Kitajiri

et al. 2010). The F-actin core becomes denser at the tapered base of a stereocilium forming a rootlet, a structure that anchors the stereocilium into the surface of the cell (or the cuticular plate) (Tilney et al. 1980), as shown in figure 1.3 A. Because of the crosslinking within F-actin core, the shafts of stereocilia are thought to be highly rigid and mimic straight rods that are mechanically flexible only at their bases (Tilney et al. 1980). Moreover, because pivoting movements constantly occur at the base of stereocilia during sound stimulation (Tilney et al. 1980), it is highly likely that the F-actin at these sites is more susceptible to damage (breakage) during acoustic overstimulation, e.g. by damaging noise (Belyantseva et al. 2009).

Every actin filament is a double helix of two filaments, and all of the filaments supporting stereocilia have the exact polarity with barbed ends at the tips of stereocilia (Tilney et al. 1980). This is the site where actin monomers are added at the stereocilia tips (Schneider et al. 2002). In mammalian hair cells, the F-actin core is made of beta (β) actin (from *actb* gene) and gamma (γ) actin (from *actg1*gene), the two known non-muscle actin isoforms that are distinguished from each other by only four amino acids at their N-termini (Perrin and Ervasti 2010). In mouse hair cells, it was shown that *β* and *γ*-actin have similar distribution along the shafts of stereocilia, and hair cells need at least one of them to be present for proper development of their stereocilia bundles (Perrin et al. 2010). Similarly, conditional knock-out mutations of β or γ-actin independently have been shown to cause degeneration of adult stereocilia bundles and progressive hearing loss, suggesting that both are essential for hair bundle maintenance (Perrin et al. 2010).

Within the past two decades, several labratories have explored F-actin turnover within the shafts of stereocilia, and how they could keep their shapes and heights without

changing throughout the life span. Two decades ago, Kachar's group suggested that F-actin within the shafts of stereocilia is fully dynamic and treadmills (figure 1.4). This means monomers are added at the barbed ends of F-actin at the tip of a stereocilium, and the whole filament slides down to allow removal of actin monomers from the pointed ends at the base (figure 1.4). Therefore, the stereocilium's height remains the same (Schneider et al. 2002; Rzadzinska et al. 2004). This idea was proposed based upon *in-vitro* gene-gun transfection experiments in the neonatal mammalian organ of Corti, which involved tracing GFP-β-actin starting from the stereociliary tips, and implied a complete exchange of the F-actin core in two days (Schneider et al. 2002; Rzadzinska et al. 2004).

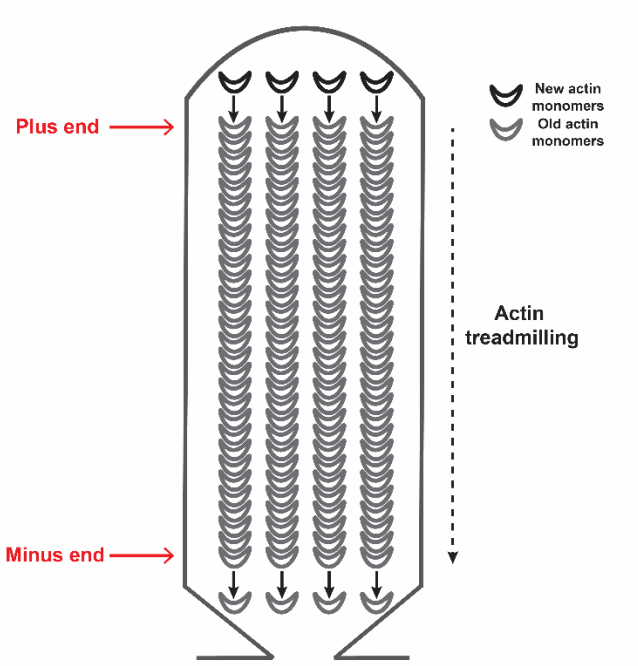

Figure 1.4 Old model on F-actin treadmilling along the shaft of stereocilia.
A schematic representation drawn based on the idea by (Schneider et al. 2002; Rzadzinska et al. 2004) suggesting actin monomers which are added at the tip of a stereocilium move the filament downward to allow removal of actin monomers at the base of a stereocilium.

This treadmilling model was later refuted by several studies which demonstrated that the F-actin core is only dynamic at the tips of stereocilia (within a region of ~500 nm)

and is highly stable within their shafts (Zhang et al. 2012; Drummond et al. 2015; Narayanan et al. 2015) (figure 1.5). Based on the new model, it is therefore speculated that persistent heights of stereocilia are maintained by controlled activity of actin severing proteins only at the tips of stereocilia (Narayanan et al. 2015). One example is gelsolin, which is an actin severing and capping protein that is specifically found at the tips of stereocilia and is essential for maintaining their lengths (Mburu et al. 2010).

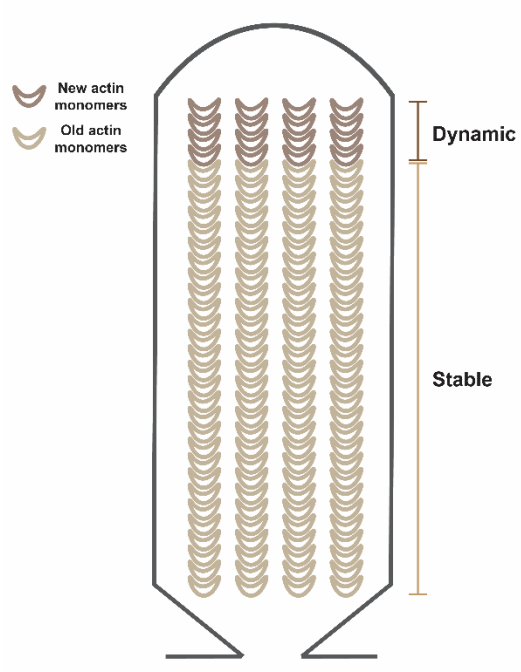

Figure 1.5 New model with F-actin stability within the shaft of stereocilia.
A schematic showing actin turnover only at the tips of stereocilia while the shaft remains intact.

In conclusion, it is currently established that the F-actin core is extremely stable with minimal or no turnover within the shafts of stereocilia (Zhang et al. 2012; Drummond et al. 2015; Narayanan et al. 2015). Correspondingly, it is also presumed that F-actin crosslinkers may not only contribute to the rigidity of the shafts but also to the normal stability of their actin cytoskeleton (McGrath et al. 2017). However, despite that fascin-2 has been shown to have fast turnover (Roy and Perrin 2018), turnover of the other actin

crosslinkers espin and plastin-1 is still not known. Likewise, it is yet unknow whether there are any potential differences in the turnover dynamics between β and γ-actin within the shaft of stereocilia. However, based on *in-vitro* observations, it was proposed that γ-actin has slower polymerization rate in the presence of Ca^{2+} compared to β-actin (Bergeron et al. 2010).

It is also not known whether F-actin within the shafts of stereocilia remains stable after acoustic damage. Noise-exposure experiments in guinea pigs have demonstrated that γ-actin might be involved in repair since it was observed to be recruited to fill-in mechanical breaks in F-actin anywhere within the shafts of injured stereocilia after noise overstimulation (Belyantseva et al. 2009). Following studies in mice suggested that both β and γ-actin might be involved in this repair, and Xin actin binding containing 2 (XIRP2) seems to be essential for this as it brings actin monomers to the location of damage (Wagner et al. 2023). However, these findings were observed only in the case of acoustic exposure causing temporary NIHL (Wagner et al. 2023). It is yet unknown which damages to stereocilia F-actin differentiate between temporary and permanent NIHLs.

1.3.1.2 Stereocilia rootlets

Rootlets are specialized structures that insert stereocilia into the surface of the cell, the cuticular plate. This is the site where stereocilia pivot upon deflection by sound (Karavitaki and Corey 2010). Based on classical transmission electron microscopy (TEM) studies of hair cells in the alligator lizards (Tilney et al. 1980) and birds (Tilney et al. 1983), it is believed that rootlets are just denser extensions of the actin filaments within stereocilia shafts (Tilney et al. 1980) (figure 1.3 A). Recent reports in mammalian hair cells have revealed that both β and γ-actin are found within the rootlets (Furness et al. 2008), but it has also been suggested that rootlets could be made of mostly of β-actin (Furness et al.

2005). The maximum thickness of the rootlets is ~100 nm at the stereocilia pivots, and their lengths "mirror" the staircase-like organization of stereocilia rows (Furness et al. 2008) (figure 1.3 A). Interestingly, hair cells build and position the rootlets in the cuticular plate with extreme precision — with a few nanometers' accuracy of the distances between the rootlets. This distance (between the rows) determines the amount of tip link stretch during bundle deflection upon sound stimulation.

Each rootlet is composed of an upper part, which protrudes to a maximum length that is half of the stereocilium shaft, and a lower part that is deeply embedded into the cuticular plate (Furness et al. 2008; Pacentine et al. 2020) (figure 1.6). The cuticular plate represents a meshwork of F-actin (DeRosier and Tilney 1989; Furness et al. 2008). Interestingly, although they have same F-actin, the molecular properties of the upper and lower pats of the rootlets are not only different from the F-actin core within stereocilia shafts but also are different from each other (Pacentine et al. 2020).

Unlike the F-actin core within the shaft of stereocilia that is highly crosslinked (Tilney et al. 1980), there seem to be no "classical" actin crosslinkers within the rootlets of mammalian hair cells. TRIO and F-actin binding protein (TRIOBP) is the only known actin bundler in the rootlets that is crucial for hearing (Kitajiri et al. 2010). It is hypothesized that, due to limited space between rootlet actin filaments which are about 8 nm apart, TRIOBP cannot physically localize between actin filaments within the rootlets. It was proposed that TRIOBP wraps around actin filaments within the rootlets (Kitajiri et al. 2010) (Figure 1.6). Correspondingly, filaments free of crosslinkers are speculated to easily slide relative to each other giving the rootlets and stereocilia pivots flexible dynamics during sound stimulation (Kitajiri et al. 2010) (figure 1.8 B). While TRIOBP (isoform 4)

is essential for rootlet formation and is present in the upper part of the rootlets and within the shafts of stereocilia, TRIOBP (isoform 5) is required for proper morphology of the rootlets and is present only in their lower part within the cuticular plate (Katsuno et al. 2019) (figure 1.6).

To provide long lasting support for stereocilia bundles, the lower part of the rootlet is equipped with a special molecular complex to further enhance its stability within the actin meshwork of the cuticular plate (Pacentine et al. 2020) (figure 1.6). Originally, several TEM studies have characterized the structure of the lower part of the rootlet, which seems to be surrounded by a puzzling "empty" space that is lighter in density than the rest of the actin meshwork of the cuticular plate, presumably due to lacking or having less actin (Tilney et al. 1980; DeRosier and Tilney 1989; Furness et al. 2008). Within this "empty" space that has been described as "tube"-like (Liberman 1987), there seem to be ~3 nm actin-free filaments coming out of the rootlets (Tilney et al. 1983), referred to as "whiskers" (DeRosier and Tilney 1989) or radial fibrils (Pacentine et al. 2020). See these thin filaments in figure 1.6.

Recently, several proteins forming the molecular machinery of the "tube" that frames the lower rootlet have been identified (figure 1.6). Spectrin αII and βII isoforms have been reported to self-aggregate and make up rings around rootlet insertions and the lower part of the rootlet within the cuticular plate (Liu et al. 2019) (figure 1.6). Knocking out spectrin results into both abnormal stereocilia bundles and hair cell polarity in addition to deafness (Liu et al. 2019). In their published work, Liu and colleagues suggest that spectrin has some degree of elasticity which could make rootlets somewhat flexible during bundle displacement (Liu et al. 2019). Given that rootlets lack crosslinkers and their actin

filaments are speculated to slide relative to each other during sound stimulation (Kitajiri et al. 2010), spectrin may provide an elastic link between the filaments, thereby making this sliding elastic. Interestingly, after acoustic overstimulation, spectrin seems to be affected and definition of its rings are lost in the noise damaged stereocilia bundles (Liu et al. 2019).

Similarly, ankyrin repeat domain protein (ANKRD24) is another key protein, which has been recently proposed to physically interact with TRIOBP-5 as part of the "tube" around the lower part of the rootlet within the cuticular plate and the stereocilia insertion points (figure 1.6). *Ankrd* $^{KO/KO}$ deletion affects localization of TRIOBP-5, and, correspondingly, mutation of TRIOBP-5 completely disrupts normal ANKRD24 localization (Krey et al. 2022). Interestingly, EM imaging of hair cells from *Ankrd* $^{KO/KO}$ mice (which have hearing impairments) demonstrate that their stereocilia bundles exhibit hollow rootlets (Krey et al. 2022). Therefore, it is currently suggested that ANKRD24 restrains F-actin of the lower rootlet preventing their expansion within the cuticular plate (Krey et al. 2022). So far, ANRKRD24 is the only currently known molecule that is speculated to surround the rootlet immediately after TRIOBP-5 (figure 1.6). Perhaps, ANRKR24 is one of the first components to connect the lower rootlet to the actin meshwork and maintain it. Not surprisingly, Krey and colleagues have shown that hearing thresholds in mice lacking ANKRD24 are more susceptible to noise exposure (Krey et al. 2022).

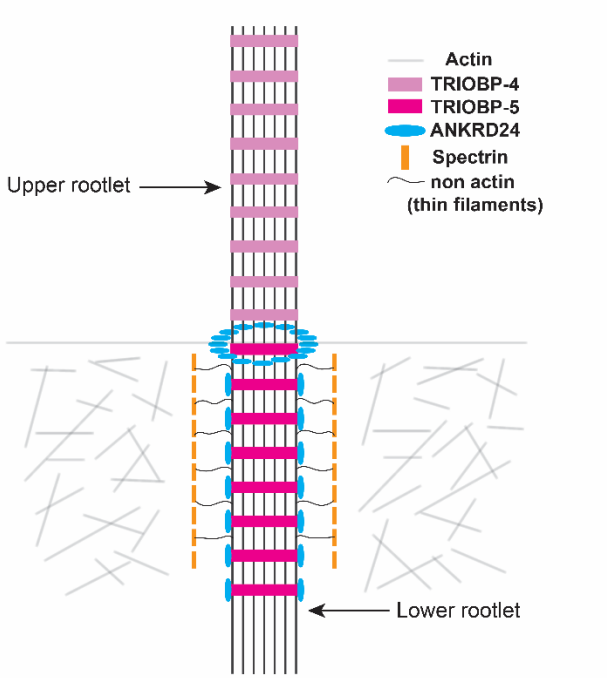

Figure 1.6 Stereocilia rootlets have sophisticated molecular machinery.
A single stereocilium rootlet with TRIOBP (isoforms 4 and 5) shown. Other proteins which make up the anchoring machinery of the lower rootlet within the cuticular plate are also shown. Note F-actin of the rootlet is connected with the cuticular plate's actin meshwork via thin actin-free filaments. ANKRD24 was recently discovered to interact with TRIOBP (isoform 5), and both are hypothesized to "wrap around" the lower part of the rootlet within the cuticular plate (Krey et al. 2022).

It is important to note that nothing is known about the turnover of any of the above-mentioned proteins. We also still do not currently understand how they could potentially re-form if damaged or broken, for example, by acoustic trauma. Furthermore, actin turnover within the rootlet itself is also not completely understood. One may hypothesize that rootlets might be similar to stereocilia in F-actin dynamics since they are believed to be extensions of the stereocilia's F-actin cores. However, this hypothesis has not been experimentally tested.

1.3.1.3 The cuticular plate

The cuticular plate is a bowl-like structure, which underlies the surface of the hair cell and provides foundation for stereocilia (Pacentine et al. 2020) (figure 1.7). Although

it makes up the upper portion of the hair cell body (with the approximate depth of 3 μm), the cuticular plate lacks cellular organelles and is rather made of a gel-like mixture of F-actin that is randomly distributed with nonunified polarity (DeRosier and Tilney 1989). Recent studies in mammalian hair cells suggest that the cuticular plate is composed of β-actin and (perhaps more abundant) γ-actin (Furness et al. 2005; Perrin et al. 2010).

Furthermore, immunofluorescence and immunogold labeling experiments reveal that the cuticular plate also contains spectrin (Slepecky and Ulfendahl 1992; Furness et al. 2008; Liu et al. 2019), alpha-actinin (actin crosslinker) (Slepecky and Chamberlain 1985; Slepecky and Ulfendahl 1992), the rootlet associated tropomyosin, fimbrin, and other key proteins which are believed to contribute to proper structure of the actin meshwork and support stereocilia bundles (Slepecky and Chamberlain 1985). Fimbrin is the same as plastin-1, which is present in shaft of stereocilia in mammalian hair cells (Taylor et al. 2015). Interestingly, fimbrin seems to be highly expressed in the cuticular plate of OHCs compared to IHCs, and therefore possibly contributing to even more sturdy cuticular plates (Slepecky and Chamberlain 1985) in OHCs that are more susceptible to damage. XIRP2 (long isoform) has also been shown to be present in the cuticular plate (Scheffer et al. 2015).

Interestingly, at the edge of the cuticular plate, there is a narrow region lacking F-actin, which defines the shape of the actin meshwork and isolate it from the hair cell's junctional region (consisting tight junction and adherent junctions) (Kachar et al. 1997) (figure 1.7). EM studies in bullfrogs by Kachar and colleagues suggest that these regions contain microtubules serving as tracks for vesicular trafficking within the hair cell (Kachar et al. 1997) . At these locations, vesicles are usually endocytosed or exocytosed from the

cell body, providing pathway for membrane protein trafficking to the stereocilia bundles (figure 1.7). Not surprisingly, this vesicular machinery meets on the cytoplasmic site the basal body, the microtubule structure of which the kinocilium develops from (Kachar et al. 1997; Pollock and McDermott 2015) (figure1.7).

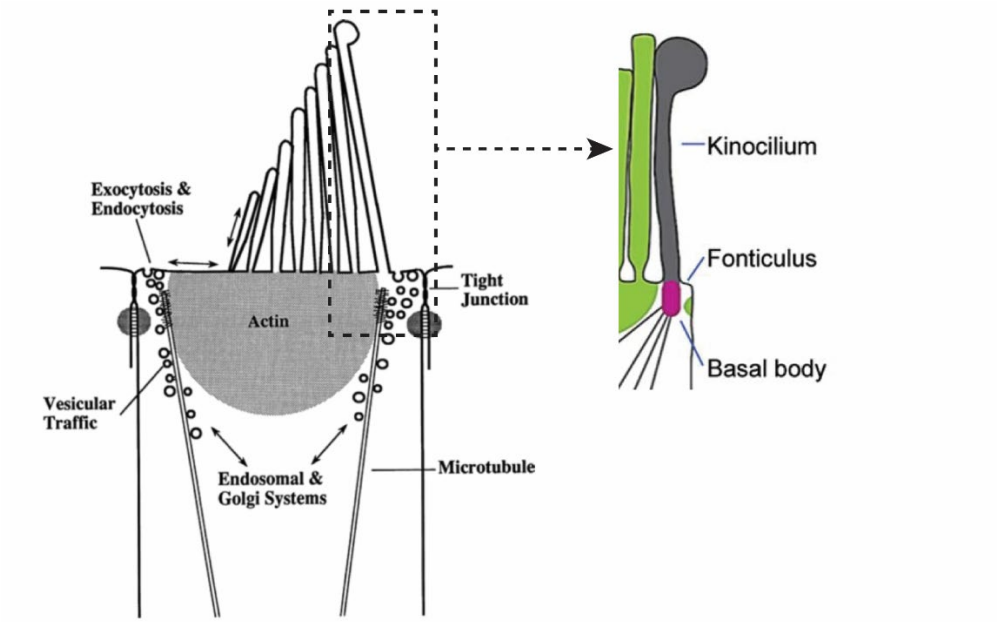

Figure 1.7 Hair cell apex contains the cuticular plate and the surrounding narrow area of vesicular traffic.
The spaces around F-actin meshwork of the cuticular plate are shown. Vesicles use microtubules to move in and out of the cell body. Main panel (left) is modified from (Kachar et al. 1997). Dashed rectangle marks the kinocilium, shown in the panel insert (right) that is modified from (Pollock and McDermott 2015). Kinocilium is found behind 1st row stereocilia only (Tilney et al. 1992). The kinocilium is also a hair like projection that looks like stereocilia but instead of F-actin, it is supported by microtubules (Pollock and McDermott 2015). During development, the kinocilium forms before the stereocilia bundles and establishes the hair cell polarity (Tilney et al. 1992), which is essential for normal hearing. When the exact orientation and the staircase structure of the stereocilia bundles are established, the kinocilium disappears (Tilney et al. 1992). In mammals, immature stereocilia bundles have kinocilium at postnatal day (P) 0, which then later retracts around ~P12 (Elkon et al. 2015) before all bundles become mature at P16-18 (Kaltenbach et al. 1994). To note, this is approximately the same time when mice start to hear at ~P12 (Akil et al. 2016).

Currently, we still do not clearly understand actin turnover and remodeling within the cuticular plate's meshwork. However, some experiments suggest that F-actin in the

cuticular plate is highly dynamic similar to the stereocilia tips (Zhang et al. 2012), and this is very different from the lack of actin turnover in the shaft of stereocilia (Zhang et al. 2012; Drummond et al. 2015; Narayanan et al. 2015).

1.3.1.4 How do stereocilia bend during acoustic stimulation?

Based on TEM visualization of F-actin within the shafts of stereocilia and the arrangement of cross-linkers between these filaments in bird hair cells, it was previously proposed that, upon acoustic stimulation, non-stretchable actin filaments slide against each other within the shafts of stereocilia (Tilney et al. 1983) (figure 1.8 A). Since the identity of the crosslinker molecules was not known at that time, it was assumed that the molecules crosslinking F-actin would be flexible enough to tilt along with the filaments to accommodate the change in orientation of the stereocilium upon stimulation (Tilney et al. 1983) (figure 1.8 A). However, following studies reveal the identity of some proteins in the mammalian hair bundle, and how they are differently distributed between the shaft and the base of stereocilia. It is now known that espin (Zheng et al. 2000), plastin-1(Taylor et al. 2015), and fascin-2 (Shin et al. 2010) crosslink F-actin within shafts of stereocilia making them rigid. These proteins are absent from the rootlet, which only have TRIOBP that is assumed to wrap around the rootlets (Kitajiri et al. 2010). Therefore, Tilney's model was modified by the recent model proposed by Kitajri et al., which suggests that actin filaments within the rigid stereociliary shafts do not slide relative each other, and this sliding occurs only at the base of the stereocilia right at the rootlets because actin filaments there lack "classical" cross-linkers (Kitajiri et al. 2010; Pacentine et al. 2020) (figure 1.8 B).

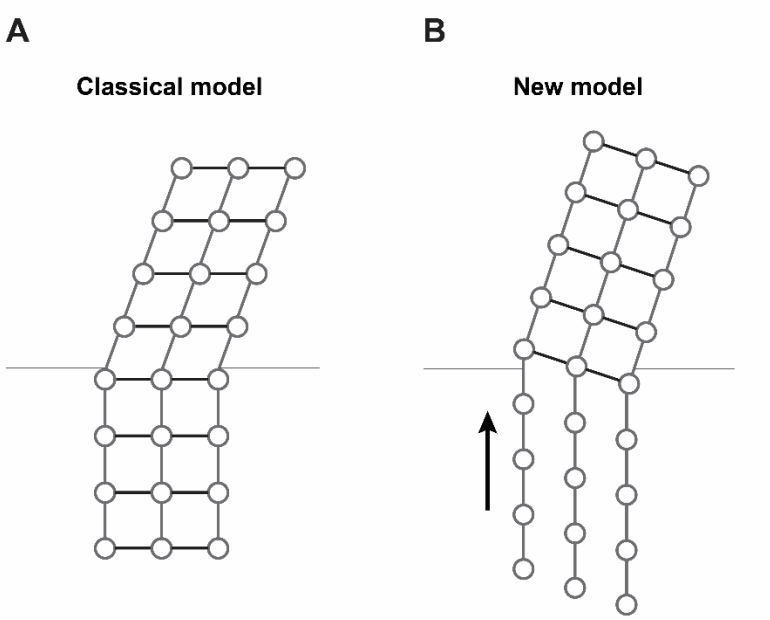

Figure 1.8 Two different models demonstrating changes in F-actin upon stereocilia deflection by sound.
(A) Illustration of actin filaments sliding within the shafts of stereocilia based on Tilney's model. **(B)** Sliding of actin filaments only at the rootlets based on Kitajiri's model.

Based on either of these models, if actin filaments within the stereocilia shafts were somehow to forcefully bend, it is very likely that the crosslinker proteins between the filaments would break. Indeed, breakage of crosslinker proteins have been previously reported after noise overstimulation (Tilney et al. 1982).

1.3.1.5 Hair cell mechanotransduction and Ca^{2+} homeostasis

In mammalian hair cells, the tips of transducing stereocilia (second and third row) harbor MET channels (Beurg et al. 2009). The pore of these non-selective cation channels consists of transmembrane channel-like protein 1 and 2 (TMC1/TMC2) (Kawashima et al. 2011; Kurima et al. 2015; Pan et al. 2018). The channels are mechanically connected to the tip links between stereocilia rows (Pickles et al. 1984) (figure 1.9 A). Tip links are composed of cadherin-23 and protocadehrin-15 (Kazmierczak et al. 2007). During sound stimulation, deflection of stereocilia in the positive direction stretches the tip links and

opens MET channels allowing for positive ions K^+, Ca^{2+}, and Na^+ to enter the cell (reviewed in (Fettiplace 2017)) (figure 1.9 B). Conversely, deflection of bundle in the negative direction closes MET channels. However, at resting position of the bundle, a certain number of MET channels remain open allowing for constant resting current. This resting current has been found to be required for the stability of F-actin core of stereocilia (Vélez-Ortega et al. 2017).

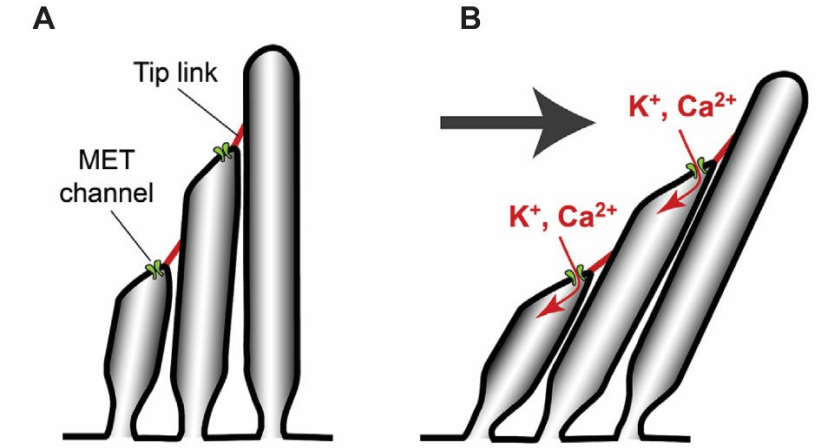

Figure 1.9 Stereocilia rows are connected via tip links which are associated with MET channels at their lower part.
(A) Stereocilia bundle at rest has most of their MET channels closed. **(B)** Sound-induced mechanical stimulation opens MET channels and results in influx of positive ions inside the cell. In IHCs, transduction-induced depolarization of the IHCs is essential for detection of sound and signal transmission to the brain. In OHCs, depolarization of the OHCs activates prestin, a protein on the plasma membrane of hair cell body, which is crucial for OHC's electromotility and sound amplification within the cochlea (reviewed in (Fettiplace 2017)). Figure panels are adopted from (Vélez-Ortega and Frolenkov 2019).

MET channels are highly permeable to Ca^{2+} compared to other ions, and there are known large differences in Ca^{2+} concentrations between the endolymph (20-40 µM) versus that of the hair cell body (approximately 0.1µM) (Fettiplace and Nam 2019). Therefore, while Ca^{2+} is speculated to contribute to the MET dependent stability of F-actin in stereocilia (Vélez-Ortega et al. 2017), large concentration of Ca^{2+} could be overwhelming to the hair cell and detrimental to its viability (Fettiplace and Nam 2019). Indeed, OHCs at

the base which detect high frequencies, are believed to be more prone to Ca^{2+} overload because they have larger MET currents, compared to IHCs and OHCs at the apex of the cochlea (Fettiplace and Nam 2019). To maintain proper levels of intracellular [Ca^{2+}], hair cells have unusually high density of Ca^{2+} ATPases known as PMCA1 (Dumont et al. 2001) and PMCA2 (Yamoah et al. 1998; Dumont et al. 2001) on the plasma membrane of their cell body and stereocilia, respectively (figure 1.10). More specifically, the PMCA2a isoform pumps are crucial for removing extra Ca^{2+} as soon as it enters the stereocilia bundles, and thereby are vital for hearing (Dumont et al. 2001).

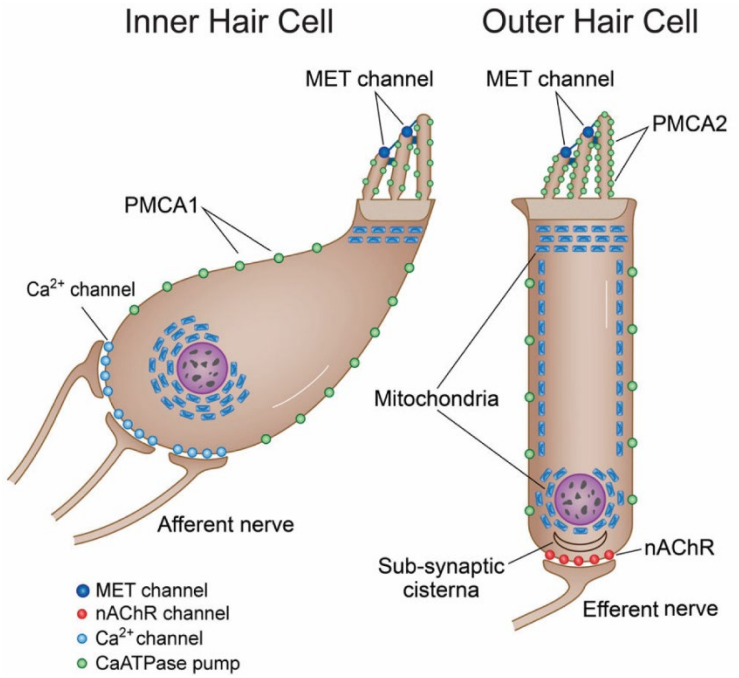

Figure 1.10 Hair cells express different PMCA pumps to extrude Ca^{2+}.
PMCA2 is found in the shafts of stereocilia, and a stereocilia bundle could have up to ~2000 pumps/μM2 (Yamoah et al. 1998; Dumont et al. 2001). As shown, OHCs stereocilia shafts have a larger number of PMCA2 and a larger number of mitochondria below the cuticular plate to further protect them. Besides MET channels, Ca^{2+} may enter the cell via voltage gated Ca^{2+} channels at the basolateral plasma membrane and through nicotinic acetylcholine receptors at the base of the cell. The figure is adopted from (Fettiplace and Nam 2019).

Hair cells utilize their mitochondria to uptake any remaining Ca^{2+} before it reaches further down into the hair cell body (Fettiplace and Nam 2019). Therefore, a number of

them are strategically located below the cuticular plate (figure 1.10). Ca^{2+} uniporter (MCU) is known to be pivotal for the mitochondrial Ca^{2+} uptake (Baughman et al. 2011) at large $[Ca^{2+}]_i$ of ~ 10 μM (Fettiplace and Nam 2019).

Besides PMCAs and mitochondria, hair cells also could regulate their $[Ca^{2+}]_i$ through buffering proteins and the uptake into endoplasmic reticulum (Fettiplace and Nam 2019). Published work by Hackney and colleagues reported calbindin, parvalbumin α and β (also known as oncomodulin), and calretinin as examples of Ca^{2+} buffering proteins found in mammalian hair cells. Not surprisingly, the concentration of these buffering proteins in OHCs seems to be 10 times larger than that of IHCs. Furthermore, the data also show that concentration of these proteins may vary throughout postnatal development. For example, parvalbumin β seems to be predominant in OHCs at later postnatal ages (around the time of hearing) in contrast to calbindin which is predominant in the neonatal IHCs (Hackney et al. 2005). This unusual Ca^{2+} buffering would suggest that Ca^{2+} homeostasis is crucial for hair cell function. Interestingly, shafts of stereocilia seem to be the compartment with the least concentrations of Ca^{2+} buffering proteins compared to the cuticular plate and cell body (Hackney et al. 2005). This further emphasizes the necessity for PMCA2 pumps in that region.

1.4 Auditory hair cell innervation

Both afferent and efferent nerve fibers innervate the auditory hair cells in the mammalian organ of Corti (figure 1.1). There are two types of afferent nerve fibers, ~95% of them are type I which innervate the IHCs (at the ratio of ~10-20 to one IHC), and 5% are type II which innervate OHCs (at the ratio of one to ~10 OHCs) (Fuchs and Glowatzki 2015; Fettiplace 2017). IHCs are primarily involved in the sound signal transmission to the

brain. The type I nerve fibers are thick and myelinated (Fuchs and Glowatzki 2015), thereby ensuring faster conduction velocity. In contrast, type II fibers are thin and unmyelinated (Fuchs and Glowatzki 2015). The cell bodies of the afferent nerve fibers are located in the spiral ganglion.

The postsynaptic terminals of afferent fibers have AMPA receptors which bind glutamate that is released from that hair cell upon depolarization during sound stimulation (Fuchs and Glowatzki 2015). Interestingly, hair cells have synaptic ribbons (figure 1.1). These special structures hold clusters of readily releasable vesicles with glutamate, and these vesicles released at the postsynaptic cleft through Ca^{2+} dependent exocytosis, as Ca^{2+} enters the hair cell from the voltage gated Ca^{2+} channels at the base of the hair cell body (Fuchs and Glowatzki 2015) (figure 1.10). Synaptic ribbons are uniquely suited for faster rate of transmission and are present only in the auditory system.

In contrast to afferents, efferent fibers transmit neural feedback to hair cells. Efferent fibers either directly innervate the OHCs or form synaptic connections with Type I afferents innervating IHCs (Figure 1.1). Efferent nerve fibers release acetylcholine which bind on nicotinic acetylcholine receptors on OHCs, thereby are believed to be involved in dampening cochlear amplification during overstimulation and/or adjusting it to achieve better signal detection in noise (reviewed in (Fettiplace 2017)). See these acetylcholine receptors in figure 1.10.

1.5 The stria vascularis

One side of the scala media, right next to the organ of Corti, is confined by the stria vascularis, which is attached to the lateral wall of the cochlea (figure 1.11). The stria vascularis consists of the basal, intermediate, and marginal cells which contribute to its

function (Kiernan et al. 2002) (figure 1.11). Known functions of the stria vascularis which are essential for the hearing: 1) sustain oxygen and metabolic supply to the organ of Corti, 2) production of potassium rich endolymph, and 3) establishing endo-cochlear potential (+100 mV) (Kiernan et al. 2002; Kazmierczak et al. 2015).

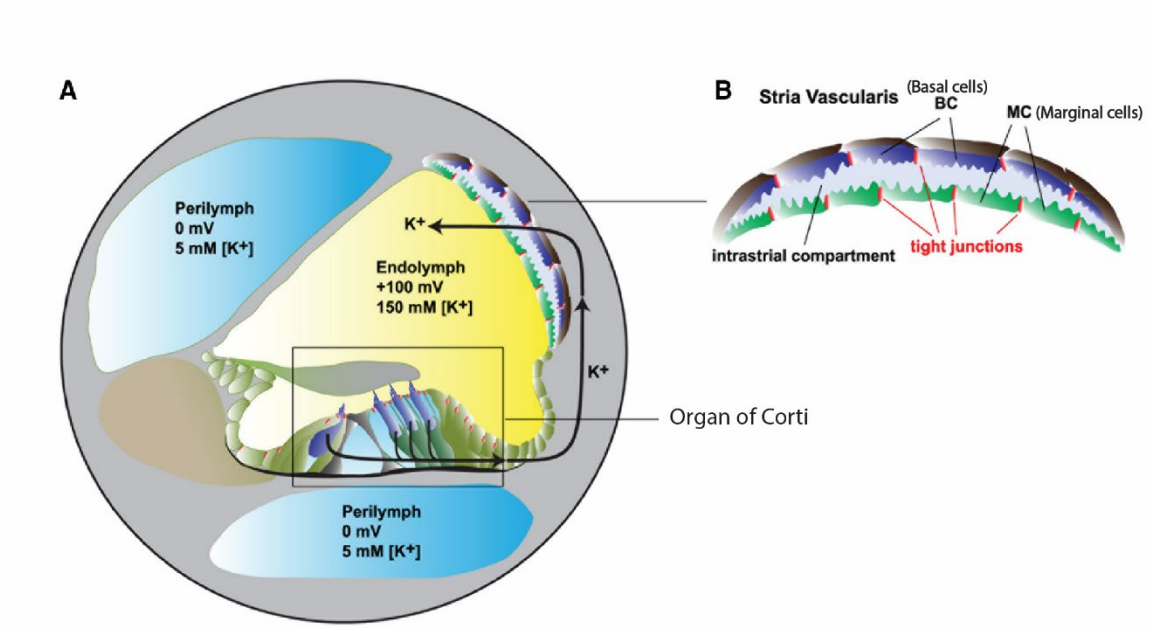

Figure 1.11 The stria vascularis maintains endo-cochlear potential in the inner ear. **(A)** Organ of Corti is surrounded by endolymph with rich potassium and high endo-cochlear potential. **(B)** The stria vascularis consists of basal, intermediate, and marginal cells. This figure is modified from (Kazmierczak et al. 2015).

CHAPTER 2. ACOUSTIC OVERSTIMULATION AND NOISE-INDUCED HEARING LOSS (NIHL)

2.1 NIHL prevalence and susceptibility

Acoustic trauma is the leading cause of hearing impairments after aging (Natarajan et al. 2023). According to the Center for Disease Control and Prevention (CDC), "hearing loss is the third most common chronic physical condition in the United States and is twice as prevalent as diabetes or cancer." (Reviewed in (CDC 2018)). It is defined as pathological changes in hearing threshold 0-20 dB above the normal human hearing thresholds (WHO 2023). Current international statistics by the World Health Organization suggests that 5% of the people around the globe have hearing dysfunction, and this percentage is speculated to double (>700 million individuals) within the next 25 years (WHO 2023). Given the increased usage of musical and electronic tools, teenagers make up a large number of those impacted with greater than a billion being at risk (WHO 2023).

Hearing loss due to acoustic overstimulation can depend upon the amplitude and length of exposure (Konings et al. 2009; Natarajan et al. 2023). For example, a high intensity noise produced by a siren (120 dB SPL, sound pressure levels re 2×10^{-5} Pa) for one minute generates NIHL whereas a milder intensity noise by a leaf blower (90 dB SPL) may take up to two hours to cause hearing loss (CDC 2020). Additionally, exact parameters of acoustic overstimulation may not produce the same type of hearing loss in those who are exposed. These differences are believed to be determined by environmental and biological mediators (Konings et al. 2009). Indeed, people with military or industrial professions are known to be particularly susceptible due to the nature of their exposure (or so-called occupational noise) (Natarajan et al. 2023). Correspondingly, the National Institute for Occupational Safety and Health (NIOSH) have imposed restrictions on

acoustic exposure higher than 85 dB for 8 hours during a workday (Natarajan et al. 2023). Moreover, the modern generation's exposure to loud entertainment surroundings or utilization of headphones (or so-called recreational noise) has major consequences on hearing (Konings et al. 2009; Natarajan et al. 2023).

Besides the environment, several genes have been identified in animal and human subjects to underline susceptibility to NIHL (Konings et al. 2009; Natarajan et al. 2023). In 2002, Kozel and colleagues performed a mouse study where they discovered that heterozygous ablation of PMCA2, (previously discussed in Chapter 1), increases vulnerability to hearing loss after loud exposure (Kozel et al. 2002). Other labratories have also demonstrated mutations in genes that are known to be essential for reversing the deleterious effects of reactive oxygen species (ROS) could compromise protection from acoustic overstimulation (Konings et al. 2009). For instance, Ohlimiller's group showed that mutations in superoxide dismutase (*Sod1*) (Ohlemiller et al. 1999) or glutathione peroxidase (*Gpx1*) (Ohlemiller et al. 2000) in mice makes them more prone to hearing loss after acoustic exposure.

Furthermore, published reviews by (Konings et al. 2009) and (Natarajan et al. 2023) have additionally provided a list of other genes including heat shock protein (*HSP70*), heat shock factor 1 (*Hsf1), CJB1-4,6* (encoding connexins), *SLC12A2,* and *KCNE1, KCNJ10, KCNQ1,* and *KCNQ4* genes encoding K^+ channels that are essential for maintaining K^+ concentration in the endolymph. Even though we are learning more information about the possible causes, NIHL continues to escalate and will be more concerning as it increases further in the next years.

2.2 Types of NIHL

Acoustic trauma can produce temporary increase of hearing thresholds (TTS) that is recoverable within two weeks after exposure, or permanent (PTS) when the hearing thresholds do not recover even two weeks after noise exposure (Liberman 2016). For decades, significant body of research was accumulated regarding pathological mechanisms of noise-induced hearing loss.

2.3 Known mechanisms of NIHL

2.3.1 Auditory hair cell death

Hair cell death in the inner ear is a predominant pathology associated with NIHL, ototoxicity (i.e. induced by aminoglycosides), and age-related hearing loss. In all these pathologies, increased ROS and resultant apoptosis are believed to be key driving phenomena (Furness 2015). Since mammalian hair cells do not regenerate, it has been assumed that loss of the mechanosensitive hair cells (IHCs and OHCs) in the organ of Corti is the primary reason for permanent NIHL after noise exposure (reviewed in (Harrison 1988; Fridberger et al. 1998)). Loss of hair cells have been postulated to be caused by increases in $[Ca^{2+}]_i$ due to prolonged mechanical stimulation during exposure (reviewed in (Fridberger et al. 1998)). Indeed, studies have shown increases in $[Ca^{2+}]_i$ in OHCs immediately after overstimulation *in-vitro* (Fridberger et al. 1998). Despite that such changes might be temporary and associated with TTS (Fridberger et al. 1998), irreversible increase in $[Ca^{2+}]_i$ is believed to cause apoptosis, particularly in OHCs since they are more prone to Ca^{2+} overload (Fridberger et al. 1998; Fettiplace and Nam 2019). Therefore, loss of OHCs, especially at the high frequency regions, is a known condition in PTS (reviewed in (Harrison 1988)).

2.3.2 Stereocilia bundle damage

In contrast to the conventional wisdom which associates hair cell death with PTS, classical studies by Liberman and colleagues have demonstrated that hair cells could remain viable in PTS but rather have damaged stereocilia bundles in noise-exposed mammalian cochleae (Liberman and Beil 1979; Liberman 1987). Because stereocilia have rigid shafts due to actin crosslinkers and only bend at their bases during stimulation (Tilney et al. 1980), their pivot points can be most vulnerable to breakage by overstimulation. Indeed, electron microscopy (EM) studies in alligator lizards exposed to intense noise (105 dB SPL, 24h) identified prominent actin depolymerization at the base of the stereocilia that was associated with increase in hearing thresholds (Tilney et al. 1982) (figure 2.1 A). Moreover, experiments in cats exposed to intense noise (115 dB SPL, 2h) producing PTS, reveal similar F-actin depolymerization at the base of stereocilia, fused or floppy stereocilia and disruption (breakage) of their rootlets (Liberman 1987) (figure 2.1 B). All the PTS associated ultrastructural pathologies to the stereocilia and rootlets were not recoverable, as observed several months after exposure (Liberman 1987) and were not seen in TTS (Liberman and Dodds 1987).

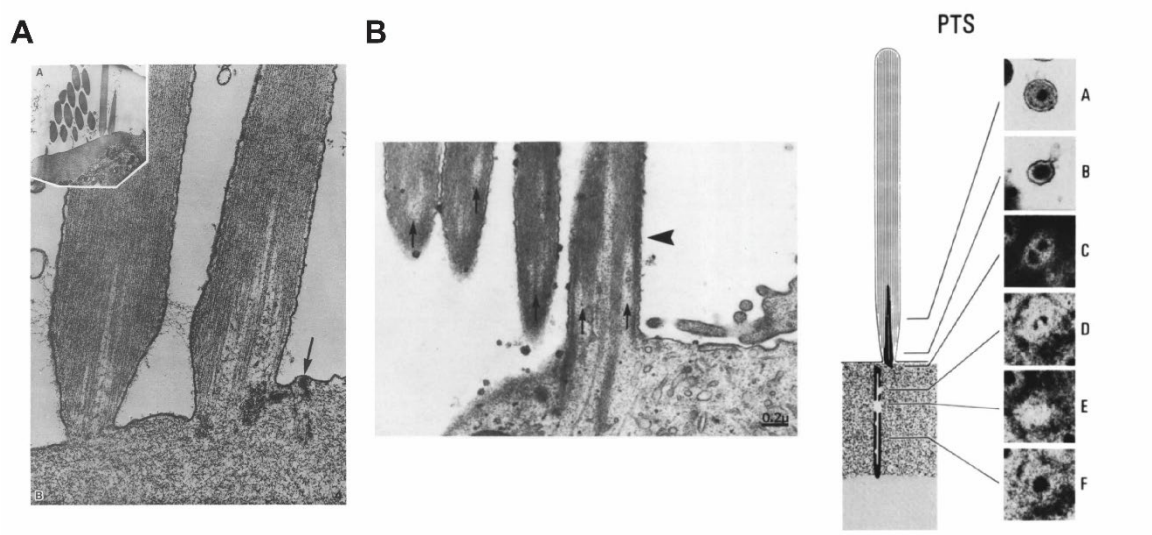

Figure 2.1 Loud noise produces damage to actin structures within stereocilia bundles.
(A) TEM images of noise-induced depolymerization of F-actin at the base of stereocilia in a non-mammalian hair cell. This panel is reproduced from (Tilney et al. 1982). **(B)** TEM images of stereocilia bundles in cats with permanent NIHL showing depolymerized F-actin at their bases and further up within their shafts (left). F-actin within the lower rootlet seems also depolymerized within the cuticular plate (right). These bundles were examined 63 days after noise exposure (Liberman 1987). Therefore, it is not known exactly when the loss of actin within stereocilia or their rootlet occurred and what initiated this loss. However, one may predict that breakage of rootlet at pivot point (right) is likely a mechanical damage happening during noise exposure. Panel B is reproduced from (Liberman 1987).

Unlike in PTS, noise-induced damage in TTS has been seen mostly in the hair cell bodies or their synaptic innervation as temporary swelling of hair cells and their afferent fibers (Liberman and Dodds 1987). Therefore, it was speculated that the pathological changes in TTS do not involve stereocilia bundles themselves or their actin (Liberman and Dodds 1987). One interesting phenomenon that is worth noting is that TTS hair cells presented reduction in the length of the upper of part of the rootlets after noise exposure, which was hypothesized to produce recoverable changes in the mechanical properties (stiffness) of stereocilia (Liberman and Dodds 1987). The latter speculation is consistent with the results from Saunders and Flock, who showed that stereocilia become less stiff

after fluid-jet overstimulation in-vitro, and this effect was recoverable (Saunders and Flock 1986). Indeed, repetition of Saunder's experiments in our lab have also validated the findings of that study (Grossheim et al., unpublished).

2.3.3 Excitotoxicity and neural damage

Besides hair cells, several labratories have also investigated the effects of acoustic exposure contributing to TTS or PTS on hair cell innervation, particularly Type I afferent neurons, which innervate IHCs and transmit signals to the brain (previously discussed in Chapter 1). Early studies in guinea pigs suggests that noise exposure producing temporary shift in hearing thresholds causes swelling of the postsynaptic dendrites of the afferent neural fibers within 20 minutes after exposure, which seems recoverable within 7 days post exposure (Puel et al. 1998). Temporary swelling of the dendrites was hypothesized to be a result of glutamate excitotoxicity due to increased glutamate release during noise overstimulation (Puel et al. 1998). Indeed, Puel and colleagues have illustrated that elevation in hearing thresholds and associated swelling of the dendrites after noise can be mitigated with kynurenate, a glutamate antagonist (Puel et al. 1998). Other studies in mice suggest that despite complete recovery of the auditory threshold shifts after noise leading to TTS, resulting neural damage could involve permanent decrease in the number of IHC's pre-synaptic ribbons and postsynaptic afferent nerve fibers, and their detachment from the IHCs within 3 days after exposure, particularly, at the higher frequency regions of the organ of Corti (Kujawa and Liberman 2009). Permanent loss of afferent nerve fibers, presumably their "retraction", could ultimately contribute to spiral ganglion cell death, which could occur years after exposure (Kujawa and Liberman 2009).

2.3.4 Noise-induced metabolic changes

Researchers have also examined cellular and metabolic changes after acoustic trauma in the lateral wall and stria vascularis, the structures that are essential for sustaining oxygen supply to the organ of Corti and for the generation of the endo-cochlear potential (EP) (Kiernan et al. 2002), (Previously discussed in Chapter 1). Indeed, decreased EP was observed in mice within 3 hours after intense noise (110dB SPL, 2h), and was associated with vascular or cellular defects and degeneration in the stria and lateral wall (Ohlemiller and Gagnon 2007). Although the noise-induced abnormalities in the stria were temporary in some mouse strains or permanent in others, the resulted decrease in EP seems to be recoverable (Ohlemiller and Gagnon 2007). This suggests that damage to the stria may not be a primary contributor to PTS. Similar studies in rats also report temporary vascular constriction, irregular fluctuations or brief suspension of the blood flow, and red blood cells aggregation in the lateral wall immediately after noise (Quirk and Seidman 1995). Despite that, the vascular abnormalities were recoverable within 15 minutes after noise. However, potential short-term ischemia after noise exposure is believed to impart metabolic pathological outcomes in the inner ear (Quirk and Seidman 1995). Indeed, ROS contributing to TTS or PTS have been observed within 1-2h after intense exposure (Ohlemiller et al. 1999). Similarly, increased nitric oxide (NO) that is associated with TTS (Chen et al. 2005) and superoxide anion radical (O^{2-}) (Yamane et al. 1995) in the stria within minutes after exposure, seem to recover within hours to 1 week, respectively. Free radicals are speculated to result from normal return of blood flow in hypoxic tissues after exposure but can be possibly treated with scavenger therapies (Quirk and Seidman 1995; Yamane et al. 1995; Chen et al. 2005).

2.4 Limited efficacy of currently available treatments

As of today, there is no effective clinical treatment for NIHL (Natarajan et al. 2023). A wide range of drugs with potential targets against ROS, apoptosis, inflammation, and other noise-induced damaging changes have been used in both laboratory and clinic, and yet have failed to provide solid answers on whether they are effective against NIHL (Kurabi et al. 2017; Natarajan et al. 2023).

To prevent hair cell damage leading to permanent NIHL, several investigators have tried to use antioxidant drugs to possibly minimize the effects of ROS after acoustic exposure. N-acetylcysteine (NAC) and D-methionine are examples of majorly known amino-acid based antioxidants (free radical chelators) that have been tested over the past two decades (Cheng et al. 2008; Kurabi et al. 2017; Natarajan et al. 2023). A study by Kopke et al. in chinchillas exposed to several rifle-like impulse stimuli (155 dB SPL) producing PTS revealed that NAC significantly decreased auditory hair cell death (both IHCs and OHCs) as well as changes in hearing threshold by a maximum of 30 dB (Kopke et al. 2005). In the following years, another study by the same group used different doses of NAC, whether given orally or through intraperitoneal injection, in animals with noise-induced PTS. This study has confirmed the success of NAC in reducing hearing threshold by < 30 dB (approximately at maximum dose) (Bielefeld et al. 2007). Unfortunately, human trials with NAC seem to be not as enncouraging even with temporary NIHL (Kurabi et al. 2017; Natarajan et al. 2023). Similarly, experiments in guinea pigs exposed to moderate noise leading to temporary NIHL demonstrated the benefits of D-methionine in speeding up recovery and decreasing theshold shifts by about 10-13 dB (Cheng et al. 2008). However, these results seem to be contradicted by clinical data involving more severe noise conditions - for more details on this clinical study, see review by (Natarajan et al. 2023).

A number of projects have also been focusing on preventing hair cell death by using anti-apoptotic agents, which could interfere with key molecules associated with apoptotic pathways or mitochondrial failure after noise exposure (reviewed by (Le Prell et al. 2007; Kurabi et al. 2017)). Examples of these agents are Cyclosporin A, FK506, CEP-1347, caspase inhibitors, and others. In most cases, these drugs seem to be beneficial in animals. For example, one study has shown that cyclosporin A and FK506 decrease the noise-induced changes in hearing threshold by 13-21 dB (Minami et al. 2004). Yet, we still do not know whether anti-apoptotic agents would be practical in humans given the safety concerns and the uncertainty regarding the route of administration and timing (Le Prell et al. 2007).

Steroid drugs have been used against inflammatory responses resulting from increased cytokines and aggravated immune cells like macrophages after noise exposure (Xu et al. 2023). In fact, steroids seem to be the only clinically approved medication currently prescribed to mitigate the effects of NIHL (Xu et al. 2023). Experiments in guinea pigs exposed to intense noise (118 dB SPL, 5 hours) have demonstrated that trans-tympanic treatment with dexamethasone through the round window decreases hair cell death and associated changes in hearing thresholds by less than or equal to 30 dB (Shih et al. 2019). Clinical experiments which used steroids alone or in combination with other drugs reinforce that steroids could be useful, however the majority were performed in individuals with TTS (for more details see (Natarajan et al. 2023)).

Overall, although many of the currently available treatments may show some degree of protection, most of them typically decrease threshold shifts by no more than 20-30 dB ((Minami et al. 2004; Kopke et al. 2005; Bielefeld et al. 2007; Cheng et al. 2008;

Shih et al. 2019); see also data from studies revisited by (Le Prell et al. 2007)). This suggests that perhaps there is another unknown component underlying residual NIHL that is left untreated.

2.5 Uknown mechanisms potentially involved in NIHL

Noise damage to the inner ear during TTS and PTS is a complex process, and the pathophysiological mechanisms distinguishing these phenomena are poorly understood even after decades of research. According to Liberman, damage to the stereocilia bundles is the hallmark to permanent NIHL (Liberman and Beil 1979; Liberman 1987). Yet, clinical efforts to prevent PTS have often focused on protecting hair cells from dying rather than repairing their damaged stereocilia. Furthermore, in the studies by Liberman, the primary mechanism/time course driving the ultrastructural damage to the stereocilia is not clear because these hair cells were examined *several* months after exposure.

In this study, we explored the ultrastructural pathologies happening during noise exposure, and which of them are associated with TTS or PTS. Using focused ion beam scanning electron microscopy (FIB-SEM), we revealed that actin structures in the stereocilia bundles exhibit two types of damage after exposure: local mechanical damage in individual stereocilia and global actin disorganization within a hair cell. The most fundamental conclusion of our study is that actin disorganization in the stereocilia shafts during noise exposure determines the difference between TTS and PTS.

CHAPTER 3. EXPERIMENTAL METHODS AND TECHNIQUES

3.1 Mouse model and cohorts

We used C57BL/6J mice (strain #000664, Jackson Laboratory) for experiments performed in this study. First, several cohorts of young adult male and female mouse littermates (postnatal days 25-26, P25-P26) were used for auditory brainstem responses (ABRs) experiments. These animals survived until all longitudinal time points (days 0-14 after noise exposure) of the ABR study were completed. Based on this study, we determined noise exposure protocols that reliably produce either TTS or PTS. Then, the other cohorts of male and female littermates (P25-P27) were exposed to broadband noise of different intensity and duration and euthanized immediately (within minutes) after noise exposure. These noise-exposed animals were compared with the control non-exposed groups to examine the short-term effects of acoustic trauma on their hair cell stereocilia bundles. Hence, their cochleae were processed for analysis with high resolution confocal microscopy or focused ion beam scanning electron microscopy (FIB-SEM).

All animal procedures were approved by the University of Kentucky Institutional Animal Care and Use Committee (IACUC) (protocols #903M2005 and #2019-3414).

3.2 Auditory brainstem responses (ABRs) and noise exposures

We recorded ABRs to determine the noise amplitudes (intensities) and duration, which would reliably generate temporary (TTS) or permanent (PTS) shifts in hearing thresholds in a well-defined region of the cochlea. Male and female littermates were either exposed to a high intensity noise of 110 dB SPL for 1 hour or a milder intensity noise of 100 dB SPL for 30 minutes. Other non-exposed animals served as controls. Prior to the ABR experiment, we anesthetized the animals intraperitonially with tribromoethanol

(avertin) (0.02g/ml) with the dosage of (22µl/g). Then, a mouse was placed about one inch away facing a speaker with three subdermal electrodes, two inserted behind each left and right ears and one under the scalp. We initially measured the ABR thresholds of the animal prior to noise exposure. The evoked potentials in response to different intensity stimuli were recorded at the frequencies: 8 kHz, 16 kHz, 20 kHz, and 32 kHz with Tucker Davis Technologies ABR system and BioSig RP software, ver. 4.4.11. At high stimuli intensities, the ABR responses were revealed by averaging neural activity to 500 presentations of the same acoustic stimulus. To record reliable ABR waveform at the intensities close to the threshold, more averaging was needed (up to 2000). The neural activity was high pass filtered at 300 Hz and low pass filtered at 5 kHz. Simultaneously, electrocardiogram was monitored through the same electrodes on an external digital oscilloscope (Rigol DS1052E).

After performing baseline ABR recordings, the animal was exposed to the noise of high or mild intensities, and the hearing was re-evaluated on the same day (designated as day 0), immediately after the end of noise exposure. Both unexposed and noise-exposed animals were returned to the housing facility, and their hearing was re-evaluated again at days 5 and 14 for TTS cohort or at day 14 only for PTS cohort. We determined that, in the 16-20 kHz region of the cochlea, exposure to white noise of 100 dB SPL for 30 minutes reliably produced only TTS, while noise of 110 dB SPL for 1 hour generated prominent PTS. Hearing thresholds are presented as mean±SE (dB SPL) for each of the control, TTS, and PTS groups relative to time (days) for each frequency tested and plotted with OriginPro 2023.

The other non-survival animal groups were exposed to the previously determined noise intensities resulting in TTS or PTS and euthanized immediately after noise exposure. Cochleae from these animals and their control non-exposed counterparts were extracted and perfused with fixative through the oval window (within ~15 minutes post noise). These cochleae were stored at 4˚C for *in parallel* preparations for fluorescence or electron microscopy.

3.3 Fluorescence confocal microscopy

3.3.1 Organ of Corti sample preparation

Control unexposed and noise exposed cochleae were dissected in Lebovitz 15 medium (Gibco), perfused gently through the oval window with 4% paraformaldehyde (EMS, cat# 15710) and stored in 2 mL of this fixative overnight at 4˚C. Next day, the fixative was diluted in 1:4 with 1X PBS (Gibco), and the samples were stored at 4˚C for later microdissection. Then, we dissected the organ of Corti in 1X PBS using the place-frequency map (Müller et al. 2005) to obtain the region corresponding to 10-20 kHz, which include the frequencies of interest (figure 4.1 C-D). Tectorial membrane was physically removed by fine forceps, and samples were stored in 1 ml 1X PBS at 4˚C. In the following days, the organ of Corti samples were washed with fresh 1X PBS and stained with 1:100 Alexa Fluor 488™ bright green phalloidin (Invitrogen, cat# A12379) for 2 hours in the dark at room temperature to stain actin structures. Organs of Corti samples were carefully washed 5 times with 1X PBS and mounted on micro slides (VWR, cat# 48311-600) with sapphire coverslips (Olympus, # 20200901) using ProLong™ Glass Antifade mounting medium (Invitrogen, ref. P36980). Mounted samples were stored in the dark at room temperature for imaging in the following 2-3 days, after the medium was completely cured.

3.3.2 Fluorescent imaging

We used the Olympus 100X oil objective (cat# APON100XHOTIRF) with 1.7 numerical aperture (NA) to resolve the small nano-sized stereocilia rootlet insertions. One drop of series M oil medium with refractive index 1.7800 (Cargille Labratories, cat# 18151) was placed on the coverslip. Using Leica SP8 confocal microscope, we first located the hair cells approximately in the middle of the region corresponding to 10-20 kHz. IHCs were imaged with pinhole size of 0.20-0.30 Airy units with z-planes separated by 0.05 μm and covering the region starting from the brightly fluorescent stereocilia tips to the end of the cuticular plate where actin was no longer present. Low magnification images were obtained first to confirm the hair cell location along the length of the cochlea. All stacks were collected at high magnification covering the region of interest with a maximum of 2 neighboring IHCs (~25 × 25 × 5 μm, X Y Z correspondingly).

3.3.3 Data analysis

We used the "Object Stabilizer" tool in Huygens Professional software (ver. 22.10) to align the z-planes of fluorescent stacks. Then, the stacks were rotated utilizing the "Interactive Stack Rotation" tool under the Transform plugin in FIJI/Image J (ver.1.53t), so that the cuticular plate was parallel to (facing) the screen view. A single plane below the stereocilia pivot points was selected where almost all stereocilia disappeared while the cuticular plate actin and rootlet insertions were fully visible. Then the stack was rotated in X,Y,Z axis such that two opposing (front and back or right and left) edges of the cuticular plate would be equally visible. Rotation of the cell was essential to ensure proper measurement of the rootlet insertions at the proper angle. We systematically quantified the distances of rootlet insertions from center to center between neighboring stereocilia within

(intra) each of row 1 and row 2 or between (inter) row 1 and row 2. Two or three stereocilia from each lateral side of the hair cell bundle were disregarded. Histogram of stereocilia counts representing a particular distance, mean±SE distance (μm), and statistical analysis was performed with OriginPro 2023. In an independent series of experiments, we tested whether the location along the cochlea would affect measurements of the distances between rootlets. We examined the correlation between these rootlet distances and heights of stereocilia, known to be dependent on cochlear position, and we found no correlation.

3.4 Focused ion beam scanning electron microscopy (FIB-SEM)

3.4.1 Significance and rationale of using the FIB-SEM technology

Here, we explore the effects of acoustic trauma on the actin-based structures of auditory hair cells: the stereocilia, the rootlets, and the cuticular plate. In hair cells, even 1st row stereocilia, the tallest and the most pronounced protrusions on the cell's surface, have a maximum thickness of ~350 nm (as previously quantified in my study (Hadi et al. 2020)). Imaging of the thinner stereocilia from shorter rows (100-150 nm in diameter) is limited by the wavelength of light and could be done only with super-resolution for light microscopy. Of course, none of the currently available optical techniques could resolve organization of actin filaments within a stereocilium (spaced ~ 8 nm apart from each other). Therefore, electron microscopy is essential for this study. In addition, actin filaments in the shaft of stereocilia, rootlets, and the cuticular plate have unique ultrastructural morphology, which is extremely hard to study with classical TEM and requires some sort of 3-D electron microscopy.

Current technologies known for high resolution imaging and 3-D reconstruction are focused ion beam and scanning electron microscopy (FIB-SEM), transmission electron

microscopy (TEM) tomography, serial block face scanning electron microscopy (SBF-SEM), and array tomography (Narayan and Subramaniam 2015). In the following paragraphs, we present each technique and compare its major cons and pros with FIB-SEM, the primary technique we chose to use in our study.

In the TEM tomography, a single section of the sample is placed on TEM grid and imaged at different angles. These images can be used to reconstruct 3-D representation of a particular structure of interest with sub-nanometer resolution (Narayan and Subramaniam 2015). However, the overall thickness of the section used for tomography must be still relatively small, 200-300 nm (Haruta 2018; Peddie et al. 2022). Thicker sections not only lead to issues of the beam not penetrating through the sample, but also inability to image the full size of structures (Haruta 2018). Considering the approximate thickness of a single stereocilium (~300 nm), a 200 nm tomography section will only cover half of the stereocilium or one stereocilium from thinner shorter rows within a bundle. In addition, according to Baumeister and colleagues, for adequate tomography results, it is necessary to acquire several images with the least rotation decrements possible over the maximum rotation range (180˚) (Baumeister et al. 1999). However, they argue that this may not only damage the sample due to the strength of the beam, but also would require re-adjustment of alignment parameters every time the sample is rotated. Failure to do so results into inconsistency and insufficient imaging details (Baumeister et al. 1999).

In SBF-SEM, a diamond knife, that is built-in within the microscope, is used to slice ~50 nm sections through the sample block while the SEM beam images the block face upon serial slicing (Haruta 2018). These sections are slightly thicker than those we use in FIB-SEM (~20 nm). Strong knife artifacts are possible with SBF-SEM compared to FIB-

SEM, which uses a gallium ion beam for milling instead (Narayan and Subramaniam 2015). Furthermore, in contrast to FIB-SEM where the sample could be positioned very close to the pole piece, SBF-SEM sample cannot be as close due to possible physical interference with the diamond knife. Imaging samples at a far distance decreases signal to noise ratio, making high resolution imaging impossible.

The array tomography is a version of classical serial section TEM. Here, several serial sections with the thickness of ~70 nm are placed on wafer, and each is imaged with SEM (Haruta 2018). Similar to the known problems with classical TEM serial sectioning, this technique needs careful handling and attention to details to prevent losing serial sections, and thereby it is time and labor consuming.

In FIB-SEM (figure 3.1), a resin block containing the sample (i.e. organ of Corti) is mounted on a FIB-SEM specimen holder. A focused ion beam (FIB) that is parallel to the block face automatically mills through the sample at the z-step of 20 nm, while the backscattered electron beam (SEM) images the sample after each milling step. With this tool, not only that the samples can be positioned within ~2 mm distance from the pole piece, but the beam can be adjusted to a small region within the sample, providing a reasonable compromise between resolution and information obtained. In our case, we were able to achieve 2 nm/pixel resolution with a reasonable volume through the whole hair cell (approximate full z-size is 8μm) or at least half a cell. This allowed us to re-construct z-projections through several stereocilia and rootlets within a bundle and examine them in 3-D.

Other benefits of using FIB-SEM discussed by (Narayan and Subramaniam 2015) include: i) reliability, since hundreds of consecutive sections are collected through

automatic slicing with precise and equal z-thickness, ii) flexibility in changing imaging and milling beam parameters to reduce beam damage, iii) several detectors appropriate for imaging of a particular sample to prevent imaging artifacts.

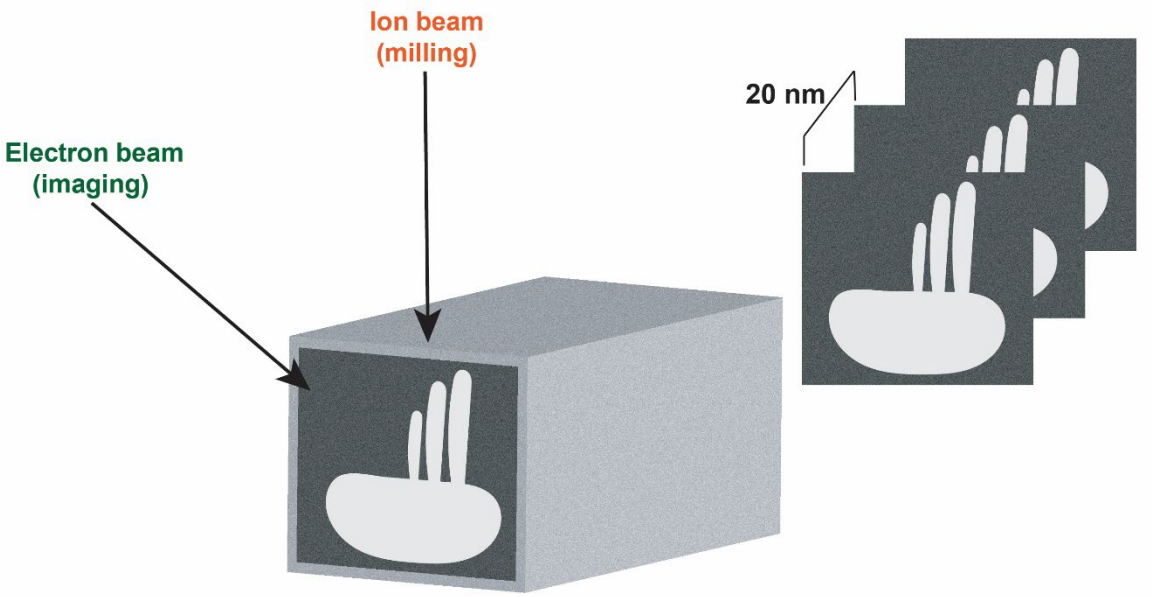

Figure 3.1 FIB-SEM imaging of hair cells.
Organ of Corti sample is embedded within a resin block. A hair cell is sectioned with ion beam at the z-step of 20 nm and imaged with electron beam. A stack of serial sections is generated. All sections are aligned with software-based registration plugins for hair cell 3-D reconstruction.

3.4.2 Organ of Corti sample preparations

Control unexposed and exposed cochleae were extracted in Lebovitz 15 medium (Gibco) and carefully perfused through the oval window with 2.5% glutaraldehyde, 3% paraformaldehyde in 0.1 sodium cacodylate buffer, pH 7.4 (EMS, cat# 19560) supplemented with 1% tannic acid stain (EMS, cat# 21710). Cochleae were stored in 1 ml of the tannic acid fixative overnight at 4˚C. Then, cochleae were postfixed with the same fixative without tannic acid to prevent precipitation and were stored in 1 ml of clear fixative at 4˚C. In the next days, organ of Corti samples were dissected in distilled water according to the place-frequency map (Müller et al. 2005) (figure 4.1 C-D). We did not use any

calcium chelators such as EDTA to soften the bone of the adult cochleae because we have previously observed deleterious effects of these chemicals on ultrastructural features resolvable by EM. Following dissections, organs of Corti were stored in distilled water at 4˚C. On later days, the samples were cryoprotected with graded glycerol series (EMS, cat#16550) at the concentrations of 5%, 10%, 15%, 20%, 25% (at least 45-60 minute on shaker per incubation), and a final 30% overnight incubation at room temperature.

Next day, we froze the samples with plunge freezing or high pressure freezing with the Leica EM ICE. High pressure freezing ensures preservation of membranes within a larger depth of the sample due to less ice crystallization. Then, organ of Corti samples were placed in the Leica AFS2 freezing substitution machine and incubated in 1% uranyl acetate (EMS, cat# 22400) and methanol solution at -90˚C for 34 hours, replaced with clean methanol for the next 11 hours at -45˚C, and then washed and dehydrated with 100% methanol (EMS, cat# 1850) for 24 hours. After that, we incubated the samples at graded concentrations of the monostep HM-20 lowicryl resin (EMS, cat# 14345) or the monostep K4M (polar) lowicryl (cat# 14335): 50, 75%, 100%, and then UV polymerized the lowicryl resin into hard blocks. Additional 100% lowicryl washes (12-24 hours) ensured better infiltration of the resin into the sample. Any residual methanol does affect curing of the resin. Blocks were then thinned with Leica EM TRIM2 and mounted with epoxy on the specimen pin holders (Ted Pella, cat# 16104). Each block was then sectioned using the Leica UC7 ultramicrotome from the block-face side and from the top so that the distance was within less than 50 µm away from the top surface. Samples were coated with 25 nm platinum using a sputter coater (EMS150T ES). Organs of Corti imaged with FIB-SEM

(Helios Nanolab Systems 660, FEI, OR) to obtain 20 nm serial sections of the hair cell stereocilia bundles of control and noise-exposed hair cells.

3.4.3 FIB-SEM imaging

Samples were automatically sectioned with the ion beam and imaged with the backscattered electron detector using "Slice and View" mode of the FEI Helios 660 Nanolab system. Raw FIB-SEM stacks typically contained several hundreds of images with 4096×3536 pixels each and a voxel size of ~2x2x20 nm.

3.4.4 FIB-SEM image processing for data analysis

Serial sections within each FIB-SEM stack were aligned translationally with "Linear Stack Alignment with SIFT" tool of the Registration plugin in FIJI. The initial Gaussian blur value was adjusted to 4.00 pixels. Registered stacks were then scaled with the correct nm/pixel size and voxel depth of 20 nm/pixel and filtered with median filter (radius: 1 or 2 pixels). Brightness and contrast were adjusted to match the contrast among the different stacks or images within a stack. To generate maximum intensity projections, we generated sub-stacks of several slices through structures of interest, and the sub-stack was then inverted and converted to a projection by the "Z-project" tool in FIJI. In some of the figures' images, these maximum intensity projections were re-inverted for transmission EM (TEM-like) representation. All figures were constructed using Adobe Illustrator (23.0.3) after converting all images from 16-bit to 8-bit.

3.4.5 Quantification of stereocilia with irregular actin

In each FIB-SEM stack from control non-exposed and noise exposed (TTS and PTS) animals, we first counted the total number of imaged IHC stereocilia within a hair

cell bundle. Then, we counted the number of stereocilia that have normal (organized) or irregular (disorganized) F-actin in the same bundle, and the percentage of the latter was calculate per IHC per animal (figure 4.2 D). Normal stereocilia were counted based on the following criteria: large enough sectioned area with hints of striations or compact actin with the appearance of non-patchy (uniform) density, and smooth plasma membrane. Irregular stereocilia criteria: large enough sectioned area with fuzzy looking or patchy actin with rough plasma membrane. For these quantifications, we only focused on taller 1st and 2nd row stereocilia because they have thicker shafts providing a relatively large surface area to accurately characterize their actin filaments. We disregarded 3rd row stereocilia because they are thin making it difficult to evaluate F-actin.

3.4.6 Fast Fourier Transform (FFT) analysis

To assess quantitatively F-actin organization in the shaft of the stereocilia, we performed 2-D Fast Fourier Transform (FFT) analysis of manually drawn region of interest covering the stereocilia shaft in available images containing longitudinal sections of IHC stereocilia of the first and second rows. Standard FFT function of ImageJ2 (FIJI) was used. The resulting FFT images were examined for the presence of the peaks indicating periodicity of the stereocilia actin core.

3.4.7 Quantification of dense actin structures within the shafts of stereocilia

Within each FIB-SEM stack of control non-exposed and noise exposed (TTS and PTS) animals, we counted the total number of stereocilia within a cell per IHC bundle. Then, we applied additional median filtering (radius: 3-5 pixels) for the stack to blur F-actin within stereocilia shafts. This makes the abnormally dense “rootlet-like” actin structures within the shafts of stereocilia more visible by decreasing the surrounding noisy

signals. Then we searched through a particular stereocilium frame by frame to find the section that shows the dense actin structures at their maximum thickness. Once finding that frame, using FIJI, a transverse line was drawn from edge to edge, and the length of the line was determined as the diameter of these aberrant structures. We did observe that the dense actin structures have large variability in their thickness, and some were extremely thin making it difficult to differentiate them from possible artifacts. Therefore, we set 25 nm threshold as the minimum width of the structure that would be considered in our counts. If a stereocilium exhibited multiple of these structures, as long as one of them passed the 25 nm threshold, that stereocilium was included in the counts. The percentage of stereocilia exhibiting rootlet-like dense actin structures per cell in all control, TTS, and PTS animals was calculated (see table 4.1 for details). The mean± SE percentage per treatment group was also plotted in bar graph with statistical analysis using OriginPro 2023 (figure 4.4 D). Here we also analyzed only taller 1st and 2nd row stereocilia because their shafts are thick enough for this sort of analysis.

3.4.8 Quantification of rootlet widths

Using maximum intensity projections in FIJI, a longitudinal line was drawn on top of the lower rootlet in such a way that it is parallel to the axis and the tilt of that rootlet. Then, a second line was drawn perpendicularly to the longitudinal line, right at the point where the lower rootlet meets the surface of the cell, the cuticular plate. This point was determined as 0 nm. Then, we quantified the diameter of the rootlet from edge to edge by descending 200 nm step size from the surface of the cell along its length. We obtained measurements up to 1 micron. Because rootlet dimensions are proportional to that of their stereocilia, 1st and 2nd row stereocilia rootlets were quantified because shorter 3rd row

stereocilia rootlets are very thin and difficult to quantify. Mean±SE rootlet diameters (nm) were calculated per row at a particular distance from the surface of the cell, and plotted using OriginPro for control, TTS, and PTS groups. See figure 4.5 B and C.

3.4.9 Quantification of the cuticular plate non-uniformity

Using FIJI, single FIB-SEM planes (slices) of the cuticular plate were selected from the approximated center of the cell and at lateral distances of 400 nm, 800 nm, and 1200 nm away from that center plane. Then, in each plane, a trace line was drawn to outline the actin meshwork of the cuticular plate. The standard deviation (StDev), the maximum (I_{MAX}), and the minimum (I_{MIN}) intensity of the meshwork area(s) in that plane were recorded. Then, the averages of the I_{MAX} and I_{MIN} of the analyzed slices within a stack were calculated. Non-uniformity of the actin meshwork within the cuticular plate in each plane was calculated by the formula $StDev/(I_{MAX}-I_{MIN})$. Data were plotted and statistical analysis was performed with OriginPro 2023 as shown in figure 4.6 F.

CHAPTER 4. RESULTS

4.1 Generating TTS or PTS in the middle frequency region of the cochlea

First, we wanted to identify noise intensities/durations that produce either TTS or PTS in a well-defined region of the cochlea. We performed ABR assessments in mice that were exposed to a broadband noise at high intensity (110 dB SPL, 1h) or moderate intensity (100 dB SPL, 30 min) at the frequencies: 8 kHz, 16 kHz, 20 kHz, and 32 kHz.

At 8 kHz (figure 4.1 A), immediately after moderate noise exposure, mice exhibited only 5 dB SPL shift in their average hearing thresholds compared to their pre-exposure levels. Such a minimal increase seems to remain stable over the next two weeks but, overall, was not significantly different from the control animals' hearing thresholds, even at 5- and 14-days post exposure. In contrast, the high intensity noise produced a significantly larger (~50 dB SPL) threshold shift immediately after exposure. Yet, the animals' hearing recovered by two weeks after exposure. The low frequency (apical) regions in the cochlea are known to be the least susceptible to noise, and therefore, in our study, even the high intensity noise did not produce PTS (figure 4.1 B).

At 16 kHz and 20 kHz (figure 4.1 A), we observed that (100 dB SPL, 30 min) and (110 dB SPL, 1h) reliably generated TTS and PTS, respectively. At 16 kHz, moderate intensity noise (100 dB SPL, 30 min) produced a significant (53 dB SPL) increase in thresholds immediately after exposure. This increase recovered by 5 days post exposure and was not significantly different from control thresholds at both 5 and 14 days after exposure (figure 4.1 A and B). In contrast, intense noise (110 dB SPL, 1h) produced increase in hearing thresholds to more than 112 dB SPL immediately after exposure, which then started to decrease but remained significantly higher than control levels by ~42 dB

SPL at 2 weeks post exposure, suggesting non-recoverable hearing loss or PTS (figure 4.1 B). Similarly, for the 20 kHz, moderate noise caused significant threshold shift (51.5 dB SPL) compared to that of pre-exposure levels, which also recovered within the next 5 days and was not significantly different from the control group at 5- and 14-days post exposure (figure 4.1 A and B). In contrast, intense noise produced significant change in auditory thresholds to more than 112 dB SPL immediately after exposure. This hearing loss decreased over the next 2 weeks, but hearing thresholds remained significantly elevated by (~45 dB SPL) from control levels, suggesting PTS (figure 4.1 A and B).

At 32 kHz, both moderate and intense noise generated non-recoverable hearing loss, i.e. PTS (figure 4.1 A). This is not surprising because high frequency regions within the organ of Corti are known to be most susceptible to noise damage. Both types of noise exposures caused significant changes in hearing thresholds, more than 100 dB SPL, immediately after exposure. These changes remained significantly higher than their control groups' levels at 2 weeks post exposure, suggesting PTS (figure 4.1 B). Although threshold shift in the "moderate noise" group showed some recovery 5 days post exposure, these mice progressively lost their hearing later on to the levels observed immediately after exposure (figure 4.1 A). Both mouse groups with the different noise types were compared independently to their own control groups, and there was no statistical significance between these control groups.

We conclude that we have identified the types of noise (intensity and duration), which would consistently generate either TTS or PTS in the mid-cochlear region corresponding to the frequencies of 16-20 kHz (figure 4.1 B). In this region, two weeks post exposure, hearing thresholds of the "TTS group" are not significantly different from

control groups while hearing thresholds of the “PTS group” are significantly higher (figure 4.1 B). Therefore, this is the region we focus on for the ultrastructural analysis of this study. We did not consider 32 kHz since both noise intensities generated PTS, as clearly seen in figure 4.1 B. Additionally, this region is highly susceptible for mechanical damage during dissection making it unreliable to study or differentiate from potential effects of noise.

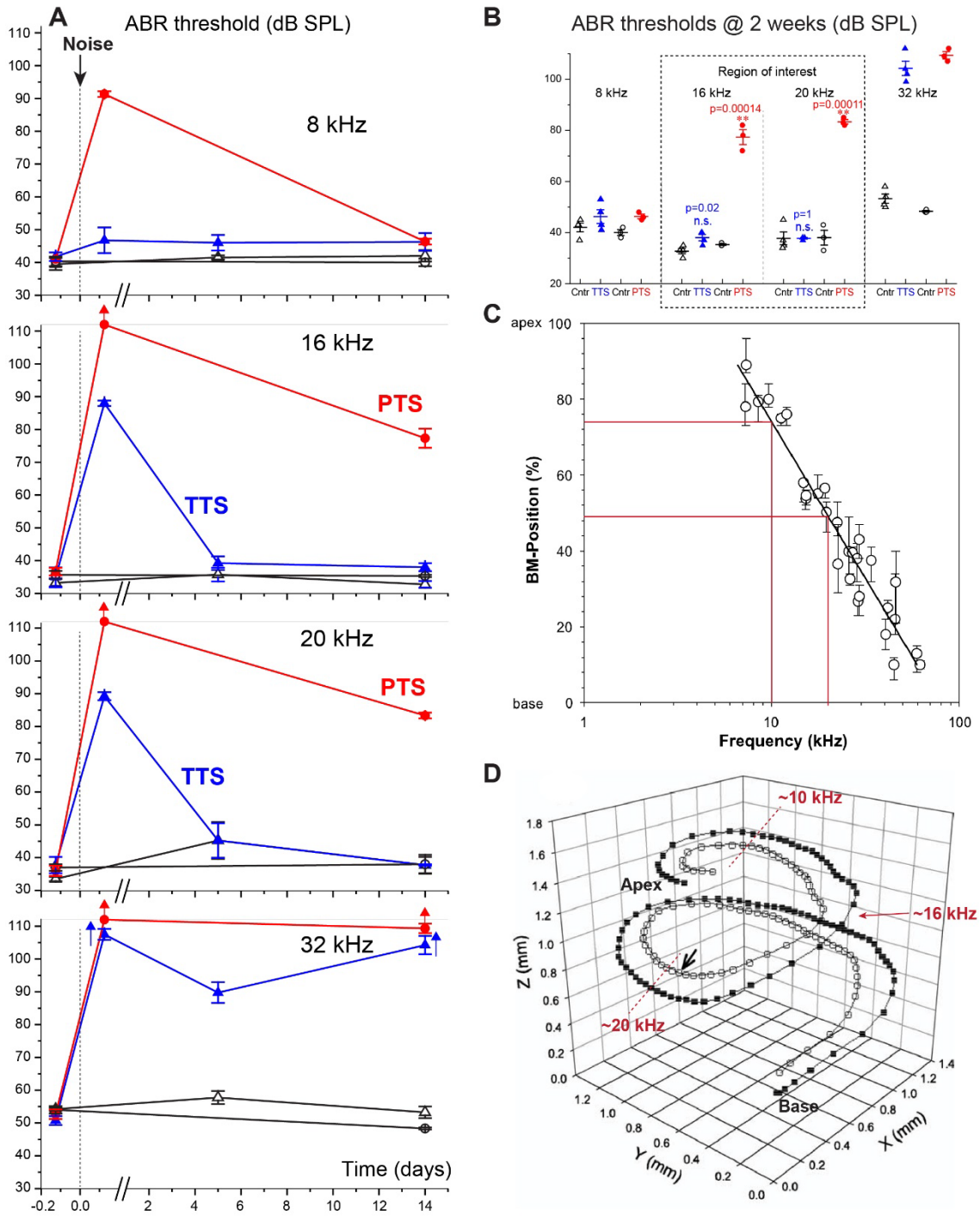

Figure 4.1 Establishing parameters of the noise exposure to differentiate temporary (TTS) and permanent (PTS) hearing losses in the mid-frequency (16-20 kHz) region of the cochlea.

(A) Hearing thresholds in dB SPL (y-axis) assessed by the auditory brainstem responses (ABRs) at 8, 16, 20, and 32 kHz before, immediately after, and 5 or 14 days (x-axis) after noise exposure. Dashed vertical lines indicate timing of the noise exposure. There are four mouse groups in each graph: high intensity noise of 110 dB SPL for 1 hour (PTS, filled circles, red, n=3), moderate intensity noise of 100 dB SPL for 30 minutes (TTS, filled

triangles, blue, n=4), and separate controls for PTS (open circles, black, n=3) and TTS (open triangles, black, n=4). Males and females were combined in each group since we did not observe sex differences. Solid horizontal line indicates the upper limit of the stimulating hardware at 112 dB SPL. Hearing thresholds above this limit are indicated with upward arrows. **(B)** ABR thresholds 2 weeks after noise exposure at all frequencies tested. Note that, in the range of 16-20 kHz, TTS groups recovered completely while PTS group still had elevated thresholds. Individual data points are shown plus SE of the mean. Asterisks indicate statistical significance: *, $p<0.01$; **, $p<0.001$; ***, $p<0.0001$, Student's t-test. **(C-D)** Mouse cochlea 2D (C) and 3D (D) place-frequency maps reproduced from (Müller et al. 2005). Dark red solid lines mark the region between 10 and 20 kHz that we aimed to dissect for sample preparation electron microscopy. Then, the most apical part of this region was sectioned out during block preparation, and actual FIB-SEM imaging started from the middle of dissected piece (~16 kHz) toward the base of the cochlea.

4.2 Noise-induced disorganization of F-actin in the shafts of IHC stereocilia

It was previously demonstrated that stereocilia bundle disorganization after acoustic overstimulation is a hallmark pathology associated with PTS (Liberman and Beil 1979; Liberman 1987). Several months or years after noise exposure in mammals, shafts of damaged auditory hair cell stereocilia exhibited loss of F-actin from their base (Liberman 1987). Studies in alligator lizards also reported loss of F-actin besides breakage of actin cross-linkers and formation of wavy filaments within the stereocilia shafts (Tilney et al. 1982). However, it is still unclear which of these effects represent the direct effect of acoustical overstimulation. To answer this question, here we explored the changes in stereocilia F-actin immediately after noise exposure.

We have performed 20 nm FIB-SEM serial sections of stereocilia in the IHCs located in the 16-20 kHz region of the cochlea in control mice and mice experiencing either TTS or PTS (referred later on as "TTS" or "PTS" mice). In these sections, we compared stereocilia from samples that were prepared *in parallel* during the same freezing round and embedded in the same type of resin. In the panels illustrated in figure 4.2 A-C, we show two different representations of the actin core within a stereocilium, single longitudinal

(main images) and transverse (top inserts) sections. Within the stereocilia shafts of both control and TTS IHCs (figure 4.2 A and B), we observed compact actin with hints of striations indicating the presence of intact actin filaments. The F-actin cores seem to have a smooth and even appearance and completely fill a sectioned area of the stereocilia in frame. In contrast, in the PTS stereocilia shafts (figure 4.2 C), the actin cores are not organized and seem to have a rough or "fuzzy" appearance suggesting that integrity of actin filaments is likely to be affected. In PTS, actin cytoskeleton in the shafts of the stereocilia looks less dense (figure 4.2 C), with lighter patches indicating loss of F-actin (figure 4.2 C, top insert), that is not seen in control and TTS (figure 4.2 A and B).

To confirm whether the observed noise-induced changes of F-actin are happening in PTS only, we used Fast Fourier transform (FFT) in FIB-SEM sections from control, TTS, and PTS mice (figure 4.2 A-C, bottom insets). This mathematical procedure allows us to evaluate the organization pattern of actin filaments within the shafts of stereocilia. According to the FFT theory, if periodicity is present, i.e. actin filaments are organized in a uniform repeated pattern, it is expected to observe the brightest point that is perpendicular to the axis of the filaments (arrow heads in figure 4.2 A-B, bottom insets). The intensity and amplitude of this brightest point correspond to the frequency (or number of occurrences) of the organized pattern of F-actin. If periodicity is absent, i.e. there is no organized re-occurring pattern of the F-actin, then a signal of brightest point does not exist (its amplitude is 0). Based on this analysis, our FFT data reveals periodicity of F-actin in the shafts of IHC stereocilia in control and TTS mice but not in PTS mice (arrow heads in figure 4.2 A-C, bottom insets). This further suggests, actin organization is only present within the shafts of stereocilia in control and TTS, but not in PTS.

Additionally, our data also show that membranes of the stereocilia surrounding the actin cores in control and TTS appear smooth and intact with no visible breaks, as shown in figure 4.2 A and B. However, single sections of PTS stereocilia shafts demonstrate that they exhibit less defined and wrinkled plasma membrane indicating that the anchors between the membrane and the actin core could be disrupted after noise exposure (figure 4.2 C). To ensure that the PTS associated changes in the membrane are not artifacts of embedding, we processed the other cohorts of mice using the same freeze-substitution protocol but with the K4M polar resin, which is known for enhanced labeling of membrane contained organelles. We observed similar wrinkling in the stereocilia plasma membranes after noise exposure but only in PTS but not in control or TTS samples (Figure 4.3 A and B).

Finally, we calculated the percentage of stereocilia with irregular (disorganized) F-actin core per IHC in control, TTS, and PTS animals in all FIB-SEM stacks that show longitudinal sections through stereocilia (figure 4.2 D). Our data show that in control and TTS IHCs, there is no single stereocilium with the irregular actin cytoskeleton in its shaft. In contrast, in PTS IHCs, 90-100% of stereocilia within a cell have disorganized F-actin cores (figure 4.2 D). Yet, there was one PTS IHC where all stereocilia appeared normal, with no single stereocilium with irregular F-actin within that cell (figure 4.2 D).We conclude that: i) noise produces irregularity of actin in the shafts of IHC stereocilia but we see this phenomenon only in PTS; ii) irregularity of F-actin in the shafts seems to result from some global changes in the actin within a hair cell because whenever we see it, we see it in all stereocilia within that cell. It is possible that disorganization of actin cytoskeleton within the shafts of stereocilia is due to disassembly or loss of F-actin, which

we hypothesize to be initiated by Ca^{2+} induced severing after noise exposure (figure 4.2 E).

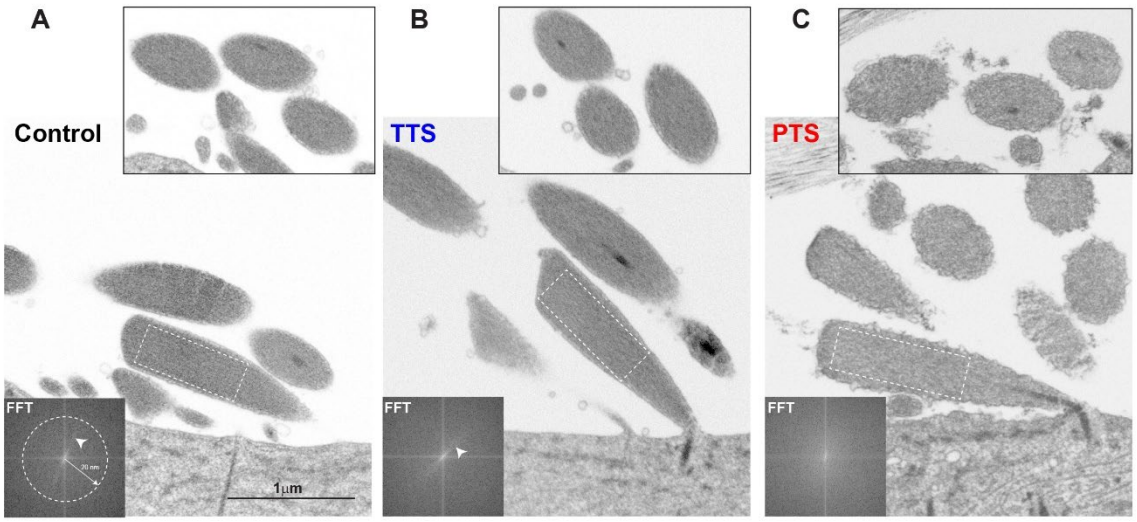

D

		# stereocilia with irregular actin	# stereocilia with normal actin	% stereocilia with irregular actin
Control (N=3, mice)	IHC1	0	33	0
	IHC2	0	25	0
	IHC3	0	11	0
	IHC4	--	--	--
TTS (N=3, mice)	IHC1	0	14	0
	IHC2	0	17	0
	IHC3	0	7	0
PTS (N=3, mice)	IHC1	32	0	100
	IHC2	39	0	100
	IHC3	0	31	0
	IHC4	28	3	90.32
	IHC5	--	--	--

n.s.
***

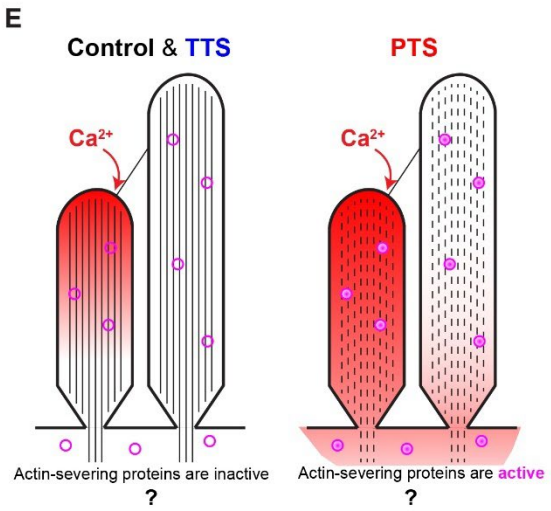

Figure 4.2 Disruption of F-actin within the shafts of IHC stereocilia is produced by noise causing PTS but not TTS.

(A-C) Single 20 nm longitudinal FIB-SEM section through stereocilia in IHCs from control (A), TTS (B) and PTS (C) mouse organ of Corti samples that were processed *in parallel*, in the same high pressure freezing freeze-substitution round and embedded *in parallel* in HM20 lowicryl resin. Top inserts show more transverse sections through neighboring stereocilia within the same cells. Fast Fourier transform revealed actin filament periodicity within the shafts (areas outlined by dashed rectangles) in control and TTS but not in PTS hair cells (bottom insets, arrowheads). Note in all FFT image insets, there is an x-y coordinate. This determines the directionality that is perpendicular to the periodic pattern. In contrast to the FFT shown in (C), FFT in (A-B) shows a bright signal that extends far from the origin with the direction that is perpendicular to actin filaments within the shafts of stereocilia in these longitudinal sections. The amplitude (how far that

signal extends) corresponds to the frequency of the periodic pattern of F-actin. White dashed circle in (A) shows a trace of that distance. **(D)** Percentage of stereocilia with irregular actin among all 1st and 2nd row stereocilia in available serial sections. Cells came from three different animals per treatment group. For simplicity, different cells within a treatment group are numbered. Two samples were embedded in a different resin (K4M), which produced worse imaging contrast and, therefore, cannot be used to determine the presence of organized actin filaments (labeled with "—"). Statistical significance: ***, $p<0.001$, Student's t-test. Note that PTS noise produces "yes or no" effect on F-actin filaments in nearly all individual stereocilia of a particular cell but not every hair cell is affected. Green vs. red text indicates healthy vs. nonhealthy state of stereocilia, respectively, which were scored by two independent observers. **(E)** A potential mechanism of noise-induced F-actin disorganization in the stereocilia shaft. In control or TTS IHCs, Ca^{2+} entering through mechanotransduction channels is extruded from stereocilia by abundant plasma membrane ATPases (left). During PTS overstimulation, we hypothesize that Ca^{2+} may reach cell body and activate actin-severing proteins that would disrupt F-actin (right).

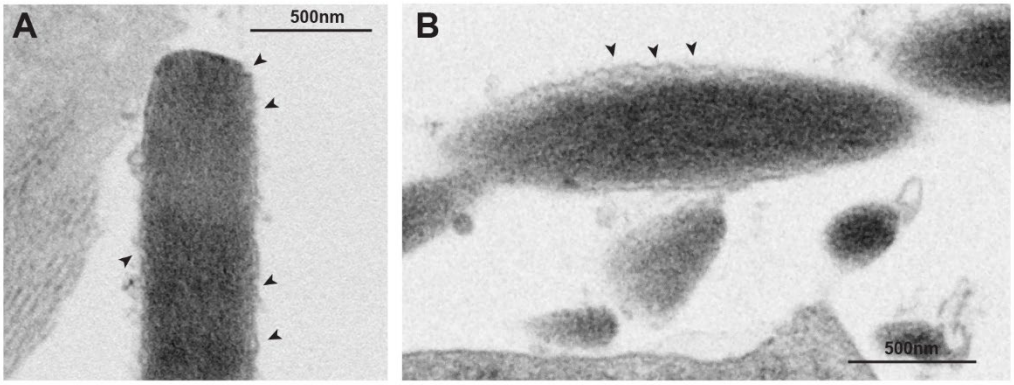

Figure 4.3 Wrinkling of the stereocilia's plasma membranes in PTS is not an artifact of embedding resin.
(A-B) Single 20 nm sections of IHC stereocilia in PTS sample that was plunge-frozen and freeze-substituted and embedded in the K4M resin. Black arrow heads point to sites of membrane wrinkling that is not present in control samples.

4.3 Appearance of dense actin structures within the shafts of stereocilia in IHCs

Besides normal rootlets located at the pivot point of each stereocilium, serial sections in control and noise FIB-SEM stacks revealed additional areas with abnormally dense F-actin within the shaft of a stereocilium. In our study, we define these areas as "rootlet-like" dense actin structures. To trace the "rootlet-like" dense structures, we

constructed maximum intensity projections of stereocilia shafts in control, TTS, and PTS IHC bundles (figure 4.4 A-C). In all these samples, we found some but not all stereocilia exhibiting abnormally dense structures (specifically from row 1, figure 4.4 A-C, arrow heads). A stereocilium could have as many as 2-3 of these structures. Sometimes, these structures are thin and less prominent while in other case they resemble the thickness and density of the rootlets. These structures are different from rootlets which are found at the pivot point and continue to protrude into the shaft of a stereocilium and into the cuticular plate (Furness et al. 2008; Pacentine et al. 2020), as clearly seen in figure 4.4 B. In contrast, the abnormally dense actin structures seem to be disconnected from the rootlet and can be either found near a pivot point or along mid or upper shaft of a particular stereocilium (figure 4.4 A-C, arrows heads). Also, the upper part of the rootlet within stereocilia shafts exhibiting the dense actin structures appears to be normal and intact with no hints of thinning. This strongly suggests that these "rootlet-like" dense structures are not shattered pieces from the real rootlets.

We were interested to explore whether the abnormal "rootlet-like" actin structures would increase after mechanical damage due to noise overstimulation. We calculated the percentage of stereocilia with these dense structures within a cell in control, TTS, and PTS samples and found that all seem to have similar percentages (figure 4.4 D and table 4.1). Additionally, in all control non-exposed and noise-exposed IHCs, we found that less than 50% of stereocilia within a cell have the dense actin structures inside their shafts.

We conclude that: i) the "rootlet-like" dense actin structures in the shafts of IHCs stereocilia are not produced by noise exposure because they are also present in control IHCs, and ii) this phenomenon seems to be a result of local change in the F-actin within

the shaft of a particular stereocilium because we do not see it in every stereocilium within a cell. We speculate that these structures might be developmental and could be generated during normal formation of the stereocilia F-actin core. Alternatively, they could form due to abnormal bundling of neighboring actin filaments by TRIOBP-4 present in the shafts of stereocilia (Kitajiri et al. 2010) (figure 4.4, E). TRIOPB-4 is previously discussed in Chapter 1.

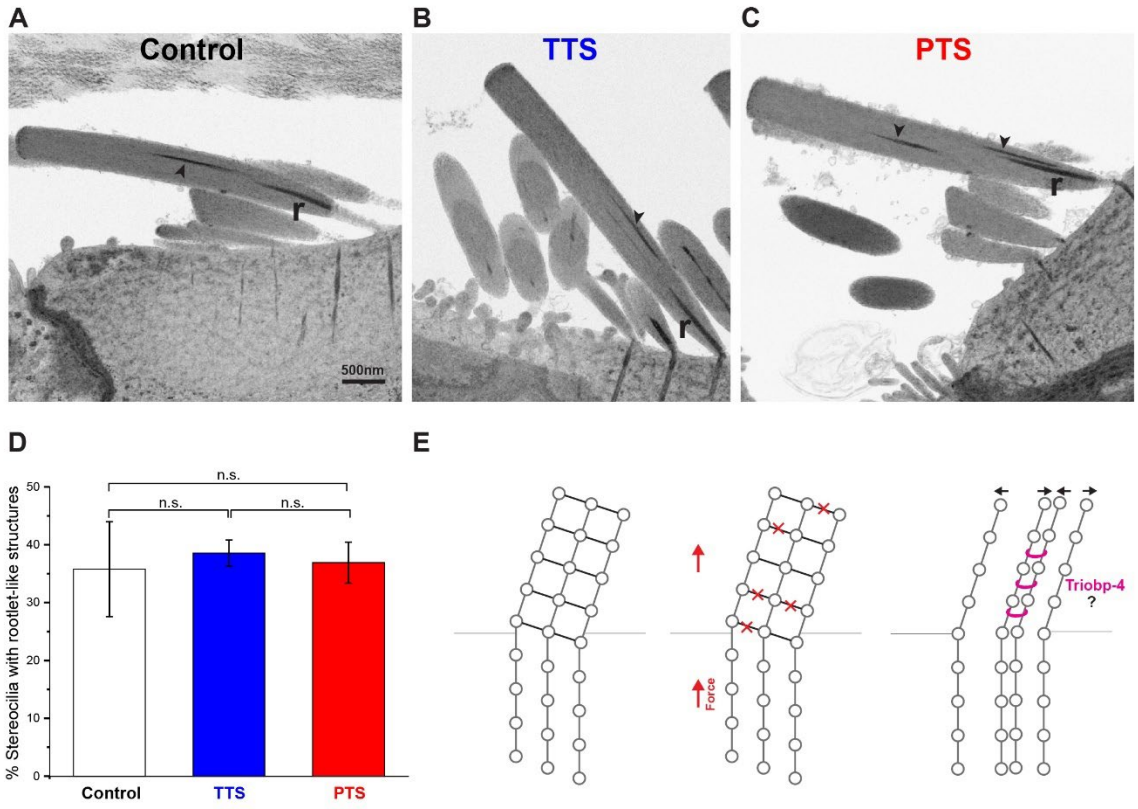

Figure 4.4 Shafts of stereocilia in IHCs exhibit dense rootlet-like actin structures. **(A-C)** Maximum intensity projections (inverted to "TEM-like" images) of FIB-SEM serial sections through stereocilia bundles in control (A), TTS (B), and PTS (C) IHCs from the organ of Corti samples processed *in parallel* during the same round of freezing/freeze-substitution/embedding. Actin-dense stereocilia rootlets (marked with "r") have an upper part extended into the stereocilia shaft and a lower part inserted into the cuticular plate. Arrowheads point to similar actin-dense structures but either appearing in close proximity to rootlet or further at mid-shaft. **(D)** Average percentages of the 1st (tallest) and 2nd row stereocilia with "rootlet-like" dense actin structures in control (white), TTS (blue), and PTS (red) groups (N=3 mice per group). Means±SE are shown, see Table 4.1 for detailed counts per cell. One-way ANOVA shows no significance ($p=0.95$) among all control and noise exposed groups. Brackets show results of the mean comparisons by Bonferroni test with no significance (n.s.) ($p>0.05$) between the treatment groups **(E)** A potential mechanism for formation of the dense F-actin patches within the shaft of a stereocilium. During non-damaging sound stimulation, sliding of actin filaments is restricted to the rootlets (left). During lifetime, excessive mechanical stimulation may break F-actin crosslinkers in stereocilia shafts (middle), allowing TRIOPB-4 to "wrap" them into "rootlet-like" dense structures. Apparently, formation of these, on first sight, aberrant structures does not affect hair cell function since they were observed in the control, normal hearing mice.

Table 4.1 Detailed summary for the quantification of IHC stereocilia with “rootlet-like” dense actin structures within their shafts.

Cells came from three different animals per group that were processed in three different rounds of freezing. For simplicity, different cells within a treatment group are numbered.

		Total number of stereocilia	# stereocilia with rootlet-like structures	% stereocilia with rootlet-like structures
Control (N=3, mice)	IHC1	**33**	**4**	**12.1**
	IHC2	**25**	**12**	**48**
	IHC3	**16**	**6**	**37.5**
	IHC4	**11**	**5**	**45.5**
TTS (N=3, mice)	IHC1	**16**	**6**	**37.5**
	IHC2	**17**	**6**	**35.3**
	IHC3	**7**	**3**	**42.9**
PTS (N=3, mice)	IHC1	**32**	**9**	**28.1**
	IHC2	**39**	**12**	**30.8**
	IHC3	**31**	**13**	**41.9**
	IHC4	**19**	**9**	**47.4**
	IHC5	**11**	**4**	**36.4**

4.4 Noise exposure causes expansion of the rootlets in IHCs

Besides stereocilia, we also examined the noise-induced ultrastructural changes in the rootlet, the other actin-based structure that anchors stereocilia and is required for mechanosensation. Rootlets have precise shapes (i.e. lengths and diameters) (Furness et al. 2008), which are essential for mechanical stiffness of the bundle (Kitajiri et al. 2010; Katsuno et al. 2019). However, rootlets can also be susceptible to damage by noise overstimulation.

We compared the morphology of the rootlets in the control, TTS, and PTS mice, and found that after noise exposure, rootlets become expanded (figure 4.5 A). Maximum intensity projections of several rootlets in a control IHC bundle show that 1st row stereocilia rootlets are somewhat thick and may have gap (hollowness) within their core, a feature that has been previously reported in other studies (Pacentine et al. 2020). Some of these rootlets do not appear to maintain the same thickness along their lower axis, and they widen towards their ends within the cuticular plate (figure 4.5 A, control). Rootlets of 2nd row stereocilia are most consistent in length along their lower axis, and they become thinner or more pointed towards their end within the cuticular plate (figure 4.5 A, control). In contrast, after noise exposure in both TTS and PTS, 2nd row rootlets seem to become thicker due to being expanded, hollow, or split towards the end (figure 4.5 A, TTS and PTS). Therefore, we hypothesized that noise may expand the lower part of the rootlet within the cuticular plate.

We obtained systematic measurements of the diameter of the 1st and 2nd row stereocilia rootlet up to ~1 micron down within the cuticular plate in control, TTS, and PTS groups (figure 4.5 B and C). We found that within ~600 nm down below the surface of the cell (within the cuticular plate), 1st row rootlets have thick diameters that are similar in the control and noise exposed stereocilia bundles (figure 4.5 C). Then, at 600 - 1000 nm distance from the surface of the cell, rootlets become progressively wider, with clear large variability towards the end, in all groups (figure 4.5 C). We conclude that there are no differences in the thickness of row 1 rootlets between control and noise exposed samples.

In contrast, our measurements demonstrate that 2nd row rootlets are less thick than 1st row rootlets. This is consistent with the previous knowledge that smaller row 2

stereocilia have normally thinner rootlets compared to larger row 1 stereocilia (Furness et al. 2008). According to our data, normal (control) row 2 rootlets become more pointed towards the ends down into the cuticular plate (dependence on the distance is statistically significant, p=0.018, two-way ANOVA) (figure 4.5 B). In the TTS condition, there is a tendency for expansion of the rootlets after noise exposure. However, in PTS, the rootlet expansion becomes prominent, and some rootlets become dramatically expanded after noise exposure. The ones that were severely expanded or splayed, which we designate as class II, were significantly thicker than control starting from -400 nm within the cuticular plate. The rootlets that were not as severely expanded, designated as class I, still showed significant statistical difference at -800 nm compared to control (figure 4.5 B). Both class I and class II rootlets are shown in figure 4.5 B, bottom panel.

We conclude that noise exposure causes expansion of the IHC lower rootlet, which somewhat seems to correlate with the intensity of noise exposure. Expansion of the rootlet started to occur in TTS and became more significantly prominent in PTS. Noise exposure causing PTS produces two types of rootlets depending on how severely they expand (or splay). This suggests rootlet expansion during noise exposure could be caused by mechanical breakage of the molecular complex that is essential for anchoring each rootlet and making them more constricted within the cuticular plate (figure 4.5 D). Proteins forming this molecular complex are previously discussed in Chapter 1.

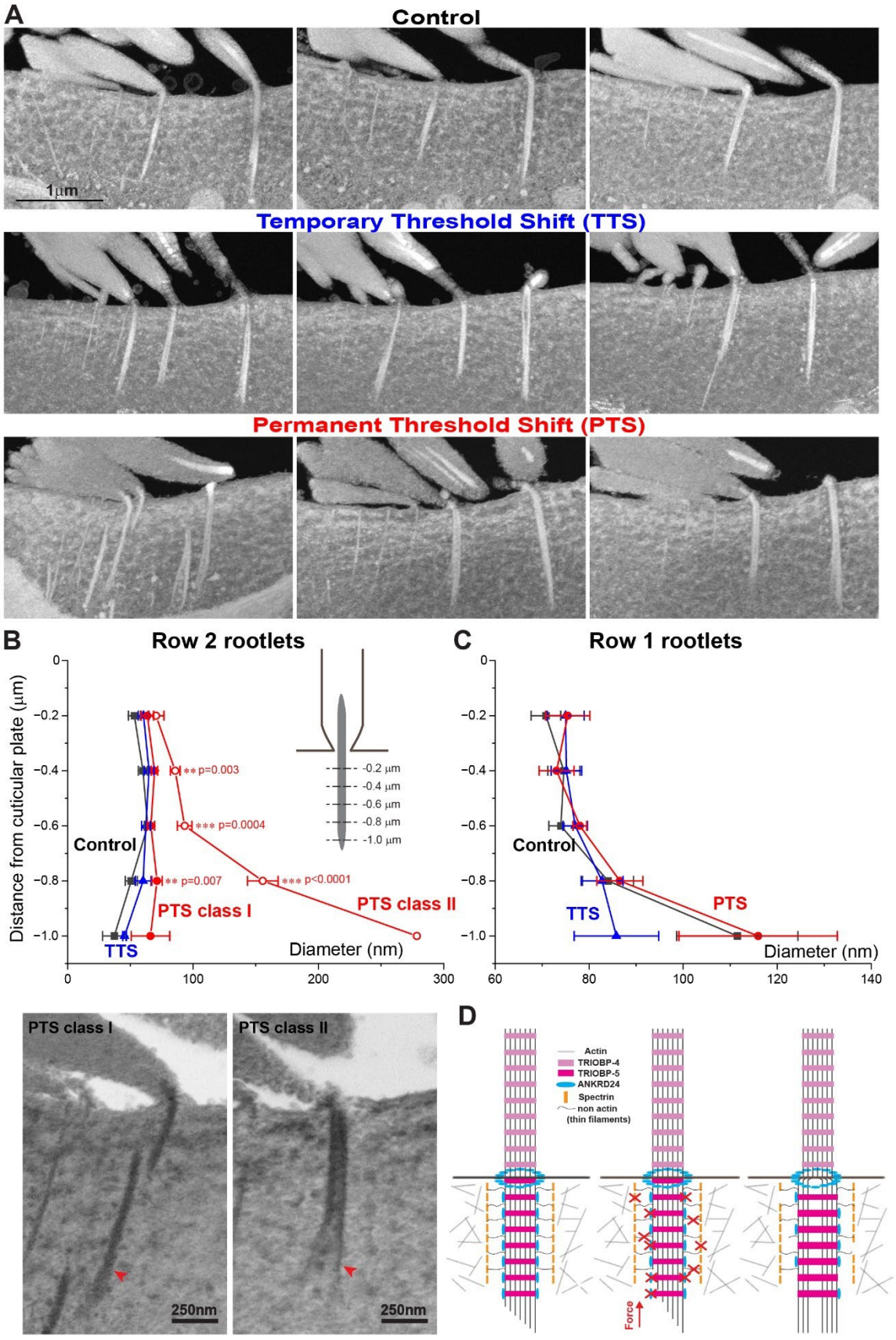
A
Control
1μm
Temporary Threshold Shift (TTS)
Permanent Threshold Shift (PTS)
B
Row 2 rootlets
Distance from cuticular plate (μm)
0
-0.2
-0.4
-0.6
-0.8
-1.0
** p=0.003
*** p=0.0004
** p=0.007
*** p<0.0001
Control
PTS class I
PTS class II
TTS
Diameter (nm)
0
100
200
300
-0.2 μm
-0.4 μm
-0.6 μm
-0.8 μm
-1.0 μm
C
Row 1 rootlets
Control
TTS
PTS
Diameter (nm)
60
80
100
120
140
PTS class I
PTS class II
250nm
250nm
D
Actin
TRIOBP-4
TRIOBP-5
ANKRD24
Spectrin
non actin
(thin filaments)
Force

Figure 4.5 Noise exposure causes expansion of rootlets in IHCs.
(A) Maximum intensity projections of the serial sections through several rootlets of 1st and 2nd row stereocilia control (top), TTS (middle), and PTS (bottom) IHCs processed *in parallel*. Number of slices per intensity projection ranged between 10-185 to cover rootlets from the different rows. **(B-C)** Measurements of the row 2 and row 1 rootlet diameters (mean±SE) at different distances from the surface of the cell (0 nm) down into the cuticular plate in controls (grey solid lines, filled squares), TTS (blue solid lines, filled triangles), and PTS (red solid line, filled circles or open circles) IHCs. Number of rootlets (N) per row per treatment group ranged between 7-11 rootlets, which came from two different independent experimental series. In panel (B) (top graph) there is a clear trend indicating widening of the rootlets within the cuticular plate, with the tendency to increase with the severity of noise exposure. Note that PTS rootlets separate into two classes depending on severity of widening. A two-way ANOVA among the treatment groups of control, TTS, and PTS class I rootlets indicates significant differences ($p=0.00073$). A two-way ANOVA among control, TTS, and PTS class II rootlets also shows significant differences ($p<0.00001$). Results of the mean comparisons by Student's t-test, with asterisks which indicate statistical significance, are shown on the plot, **, $P<0.01$; ***$p<0.001$. The bottom of panel (B) are maximum intensity projections (inverted to "TEM-like" images) representing class I and class II rootlets in PTS. Both rootlets are shown also in panel (A) PTS, but here, their z-projections contain smaller number of slices (3-16) to cover the structure of these individual rootlets only and show their apparent widening. Red solid arrows point to the site of thickening or splitting of the hollow rootlets towards their ends. **(D)** A potential model of how noise exposure produces mechanical damage and widening of the rootlets. The cartoon shows several essential proteins anchoring the rootlets to the actin meshwork (grey lines) of the cuticular plate (left). Force generated by mechanical overstimulation (red arrow) should increase relative sliding of the actin filaments within a rootlet (middle). This sliding may break connections with anchoring molecules producing "hollow" rootlets, such as that previously reported in mice lacking ANKRD24 (Krey et al. 2022) (right).

4.5 Noise exposure produces actin disorganization in IHC cuticular plates

We were interested to explore whether acoustic trauma impacts the cuticular plate, which is also another actin-based compartment in the hair cell, where stereocilia and their rootlets are embedded. Unlike stereocilia and rootlets that are supported by parallel and unidirectional actin filaments, the cuticular plate is a gel-like mixture of random F-actin and non-actin cytoskeletal proteins (DeRosier and Tilney 1989), refer to (Chapter 1). To investigate whether noise exposure disrupts this structure, we examined single 20 nm sections at different locations (z-frames) of the IHC cuticular plate with and without noise

exposure (figure 4.6). In some cases, we were only able to capture sections in the middle of the hair cell, as shown in figure 4.6 A and C, images 2-4 or B, images 1-6. In other cases, we were fortunate to capture ends of the cuticular plates from both lateral sides of the hair cell, as demonstrated in figure 4.6 D and E.

We observed that the actin meshwork within the cuticular plate has defined bowl-like borders with distinct and highly visible "speckles", which represent the random arrangement of the F-actin (figure 4.6). This actin meshwork almost covers the entire cuticular plate with the widest area in the middle of the cell, and progressively, gets smaller towards the lateral ends of the cell. An exception to that is a small area that normally lacks F-actin is where the speckles are absent. At this site, the kinocilium forms and vesicular trafficking of the hair cell usually happens (Kachar et al. 1997; Pollock and McDermott 2015), refer to (Chapter 1). Interestingly, our data show that unlike in control hair cells (figure 4.6 A), in both TTS and PTS (figure 4.6 B and C), this kinocilium region that is free of actin appears to become larger during exposure. This strongly suggests that noise causes loss of F-actin from the cuticular plate.

Furthermore, single FIB-SEM sections in the lateral ends of the cell show that the control cuticular plate maintains its bowl-like structure even when it gets smaller towards the end (figure 4.6 D, control). However, in PTS, we noticed formation of actin "islands" that are dispersed and seem to be interrupted with vesicular tracks-like patterns lacking actin (figure 4.6 E, PTS). This indicates that noise induces rearrangement of actin cytoskeleton within the cuticular plate. Although we did not observe actin islands in TTS (figure 4.6 B), the cuticular plates in both TTS and PTS groups seem to be shrinking from both side edges (figure 4.6 B and C, fourth images).

When we examined the non-uniformity of the actin structures within the remaining meshwork of the cuticular plate, we also found changes there after noise exposure (figure 4.6 F). This analysis was performed by first outlining the areas which represent the electron dense actin meshwork per single section along multiple z-frames of the cuticular plate in each FIB-SEM stack. Then, the non-uniformity of the cuticular plate was calculated per section as following: StDev/(I_{MAX}-I_{MIN}), where StDev is the standard deviation of the intensity of the actin meshwork area in a particular section while I_{MAX} and I_{MIN} are the average maximum and minimum intestines of the cuticular plate meshwork areas of all sections within a stack, respectively. Based on this analysis, we have found that in both TTS and PTS groups, there is a significant decrease in the non-uniformity within the cuticular plate compared to control group. Decreased non-uniformity indicates rearrangement and degradation of actin structures after exposure, and thereby making the cuticular plate's meshwork more uniform (i.e. homogenous), with even more gel-like composition.

We conclude that acoustic trauma causes loss or rearrangement of actin within the cuticular plate. This loss of F-actin could be due to Ca^{2+} induced depolymerization during acoustic exposure.

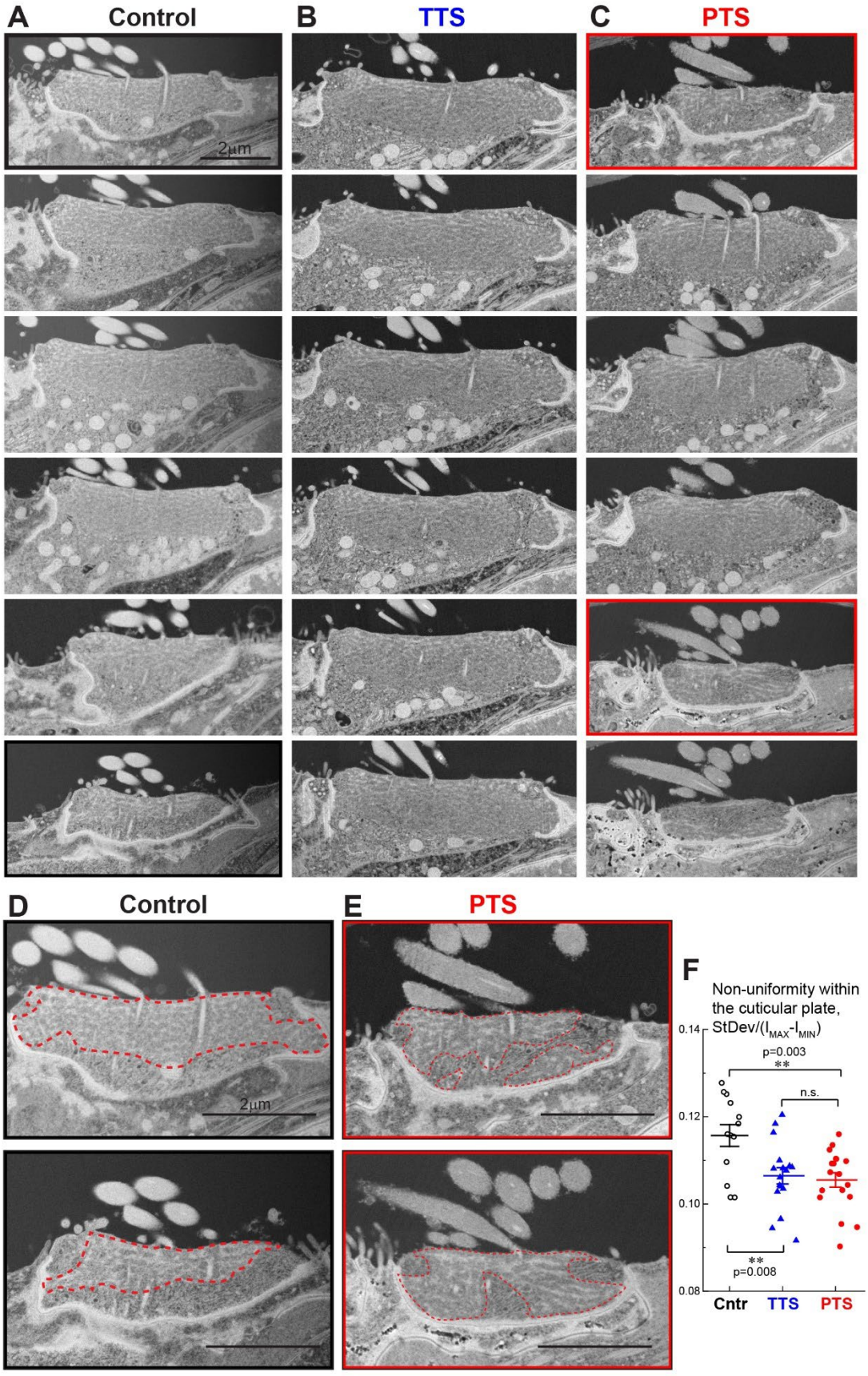
A
Control
B
TTS
C
PTS
2μm
D
Control
E
PTS
2μm
F
Non-uniformity within the cuticular plate, StDev/(I_MAX-I_MIN)
0.14
0.12
0.10
0.08
p=0.003
**
n.s.
**
p=0.008
Cntr
TTS
PTS

Figure 4.6 Noise induces loss of F-actin within the IHC cuticular plates.
Single FIB-SEM sections of the cuticular plates at different z-planes in control **(A)**, TTS **(B)**, and PTS **(C)** IHCs. **(D-E)** Magnified images which correspond to single planes from panel (A) of the control IHC (black borders), with normal cuticular plate, and PTS IHC (red borders) with the cuticular plate consisting of prominent islands of F-actin. Red dashed lines outlined F-actin meshwork of the cuticular plates in both panels (D) and (E). These areas of interest were determined by tracing the bowl-shaped electron dense actin meshwork containing "speckles" and lacking mitochondria and vesicles. **(F)** Quantification of the non-uniformity of actin structures within the meshwork of the cuticular plate in control (black open circles), TTS (blue filled triangles), and PTS (red filled circles). Each data point represents quantification of individual FIB-SEM sections at the approximated center of the cell and consecutive z-planes taken at 400 nm steps before and after the center of the cell. Cells came from two different independent experimental series. One-way ANOVA shows that there is a significant change ($p=0.0017$) in the non-uniformity within the cuticular plate among the control and noise-exposed groups. Brackets represent results of the mean comparisons by Bonferroni test indicating statistical significance between both control and TTS or control and PTS, and no significance (n.s.) between TTS and PTS ($p>0.05$); **, $p<0.01$.

4.6 Noise changes the positioning of stereocilia in the cuticular plates of IHCs

As discussed in Chapter 1, the stereocilia rows within a hair bundle are inserted into the cuticular plate's actin meshwork via rootlets with utmost accuracy. Here, we observed noise-induced rearrangement of the cuticular plate's actin meshwork in IHCs. Therefore, we hypothesized that acoustic trauma would in turn alter the insertions of stereocilia.

We compared changes in the rootlet insertions between the control non exposed and noise exposed IHC bundles. We used Alexa Fluor 488^{TM} phalloidin to stain actin in control, TTS, and PTS organs of Corti. Unfortunately, we were not able to detect fluorescent labeling of the rootlets, possibly due to their compact structure preventing the phalloidin from accessing F-actin. However, using high resolution confocal microscopy with 1.7 NA 100X objective, special high refraction index immersion oil, and sapphire coverslips, we resolved row 1 and 2 rootlet insertions. These nano-sized insertions appeared as prominent holes within the cuticular plate. We measured the distances between the "holes" within (intra) row 1 and row 2 in the control, TTS, and PTS IHCs (figure 4.7

B). We observed that the average distance between the “holes” within row 1 does not change in TTS, but significantly decreases in PTS compared to that of control. However, the average distance between the “holes” within row 2 are similar in control, TTS, and PTS IHCs, suggesting that they are not affected by noise. We also measured the distances between rootlet “holes” of row 1 and row 2 stereocilia (figure 4.7 C). We found that this distance significantly decreases in TTS, but does not change in PTS.

In summary, we conclude that noise exposure results into changes in the positioning of stereocilia within the cuticular plate. This is consistent with the changes in the actin meshwork of the cuticular plate after noise. It is likely that the noise-induced shrinkage or rearrangement of actin within the cuticular plate brings the stereocilia closer together.

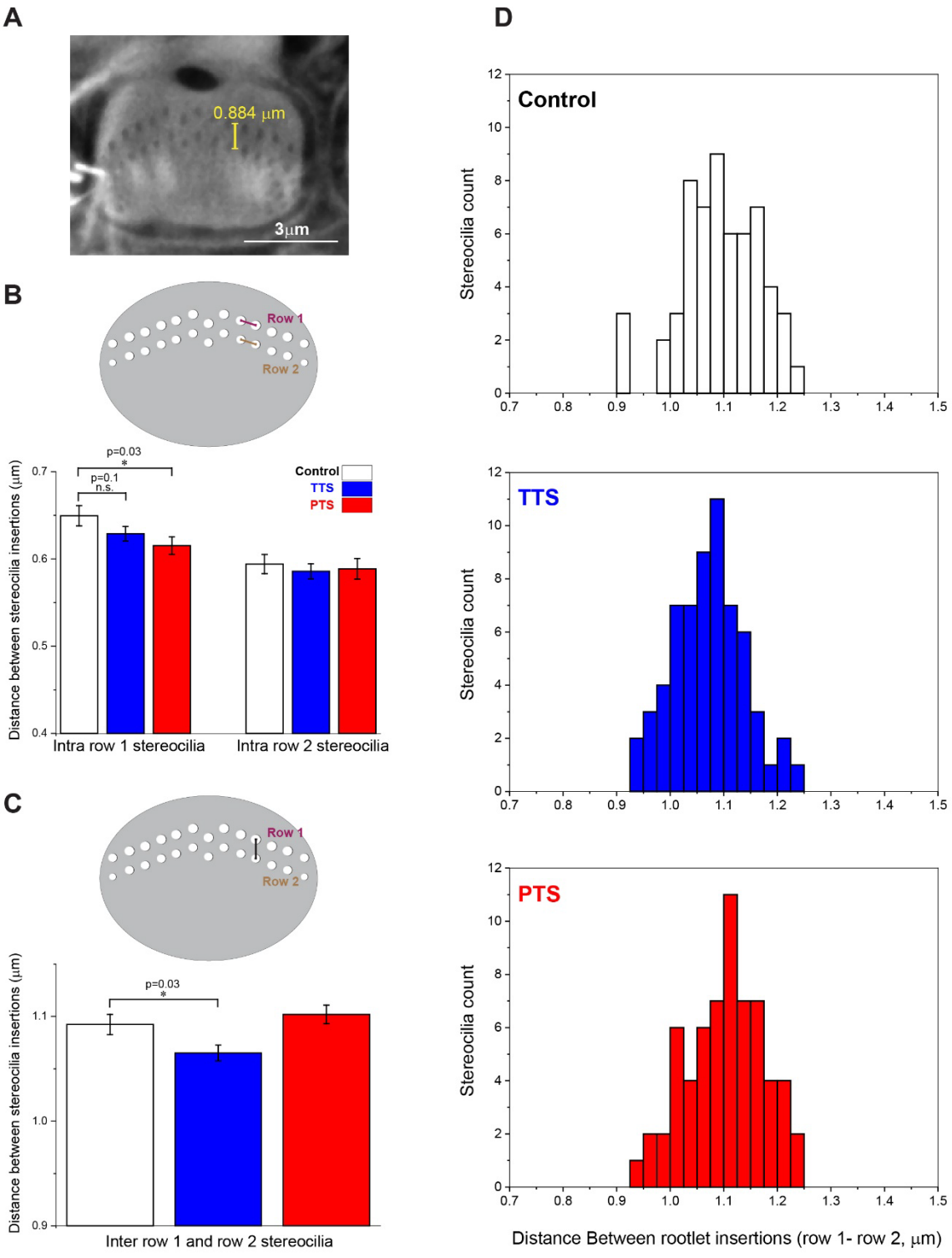

Figure 4.7 Noise exposure alters the positioning of stereocilia insertions within the cuticular plates in IHCs.

(A) Representative example of high-resolution confocal imaging of the stereocilia insertion points in the adult wild type IHC. **(B-C)** Distance (mean±SE) between stereocilia insertion points in the cuticular plate within stereocilia rows (B) and between 1st and 2nd row

stereocilia (C) in control (white), TTS (blue), and PTS (red) IHCs. Cartoon illustrations explain how measurements were performed. Distances between neighboring stereocilia insertion points were quantified by drawing a line in FIJI from center to center and measuring the length of that line. Averaged values are plotted along with their standard errors. There is a trend toward decreasing the distance between neighboring 1st row stereocilia with the increase of severity of noise trauma, but the differences reached significance only for PTS but not TTS (*, $p<0.05$, Student's t-test). Distance between stereocilia insertions in row 1 and row 2 decreased significantly in TTS but not in PTS (*, $p<0.05$, Student's t-test). **(D)** Histograms of inter-stereocilia distance counts for the data show in (C). Number of cells: 6 (control), 8 (TTS), 6 (PTS).

4.7 Actin disorganization in the shafts of stereocilia is also a key distinction between TTS and PTS in OHCs

Our data show that actin disorganization within stereocilia shafts in IHCs is the major distinction between TTS and PTS. We hypothesize that this phenomenon could be driven by a global mechanism within the cell, such as changes of intracellular Ca^{2+} concentration after noise exposure. To determine whether this is true also for OHCs, we examined the short-term effects of noise exposure on the actin structures in the OHCs. OHCs are known to be more sensitive to Ca^{2+} overload (Fettiplace and Nam 2019). Therefore, we compared FIB-SEM serial sections of the stereocilia, the rootlets, and the cuticular plate actin compartments in OHCs in the control, TTS, and PTS conditions (figures 4.8-10, respectively).

Single section of the cuticular plate in a control OHC shows that the actin meshwork is more defined and denser than that in IHCs (figure 4.8 A). This is consistent with the physiological function of OHCs in sound amplification - their stereocilia bundles need to have sturdier mechanical support. The kinocilium and associated vesicular trafficking site seems to be narrow and is distinctly visible by its prominent lighter density due to the absence of actin in control OHCs (figure 4.8 A, white arrow). In contrast, in TTS (figure 4.9 A, black arrow) and PTS (figure 4.10 A, black arrow), the kinocilium site that is devoid of actin looks larger and seem to be filled with a greater number of vesicles and

other non-actin material. These observations suggest that noise exposure produces cytoskeletal changes within the cuticular plate and loss of its F-actin. It is important to note that in one control OHC (figure 4.8 C), we noticed loss of actin from the cuticular plate similar to that of TTS and PTS, although this cell was not exposed to noise. However, the stereocilia bundle in that particular cell did not have an upright position and looked severely bent at their pivots. It indicates the possibility of mechanical damage during dissection since adult OHCs are more susceptible to mechanical damage.

Unlike in IHCs, we were not able to visualize actin filaments within the shafts of stereocilia in OHCs. This is due to limited resolution of FIB-SEM and more dense packing of F-actin in OHCs. Therefore, unfortunately, we were not able to characterize changes in the regularity of actin within the shafts of stereocilia in OHCs after noise exposure. However, maximum intensity projections of the stereocilia reveal that in both control and TTS, all stereocilia within a cell maintain their rod shape appearance (figure 4.8 B and figure 4.9 B, respectively). Interestingly, only in PTS, we observed that some stereocilia are bent at their mid-shaft (figure 4.10 C, red arrow heads). We have not observed such bending in TTS. This data is intriguing because it strongly suggests that noise exposure causes disorganization (disassembly) of F-actin within the shafts of stereocilia in PTS but not in TTS. It is worth mentioning that such bending could be easily detected even by scanning electron microscopy. Based on more than a decade-long experience of our lab, stereocilia with properly crosslinked parallel F-actin filaments never bend in wildtype OHCs that were not exposed to noise.

Finally, maximum intensity projections of the OHCs' rootlets within the cuticular plate reveal that OHCs' stereocilia have long rootlets that are proportional to lengths of

their stereocilia, as previously reported (Furness et al. 2008) and discussed in Chapter 1. Therefore, the rootlets of the tallest 1st row stereocilia extend deepest within the cuticular plate actin meshwork (figure 4.8 B). Surprisingly, we found several rootlets within a cell that were over-elongated and extended beyond the actin meshwork of the cuticular plate in all control (figure 4.8 D-E, arrow heads), TTS (figure 4.9 C-E, arrow heads), and PTS (figure 4.10 D-H, arrow heads). The ends of these over-elongated rootlets seem to have various morphologies as either normal (figure 4.10 D), split (figure 4.8 D, figure 4.9 D, and figure 4.10 E), or bent (figure 4.9 E and figure 4.10 G). Interestingly, all these over-elongated rootlets were in the 1st row stereocilia, close to the kinocilium site lacking actin. We have not observed any in the 2nd row stereocilia. We cannot conclude that the rootlets with atypical morphologies are produced by noise because we also see them in the control cells.

Overall, from this OHCs data, we summarize that noise exposure also induces rearrangement or changes in the actin cytoskeleton within the cuticular plate and the shafts of stereocilia. However, like in the IHCs, presumable loss (depolymerization) of F-actin from the stereocilia shafts during acoustic exposure in OHCs is the key determinant for PTS.

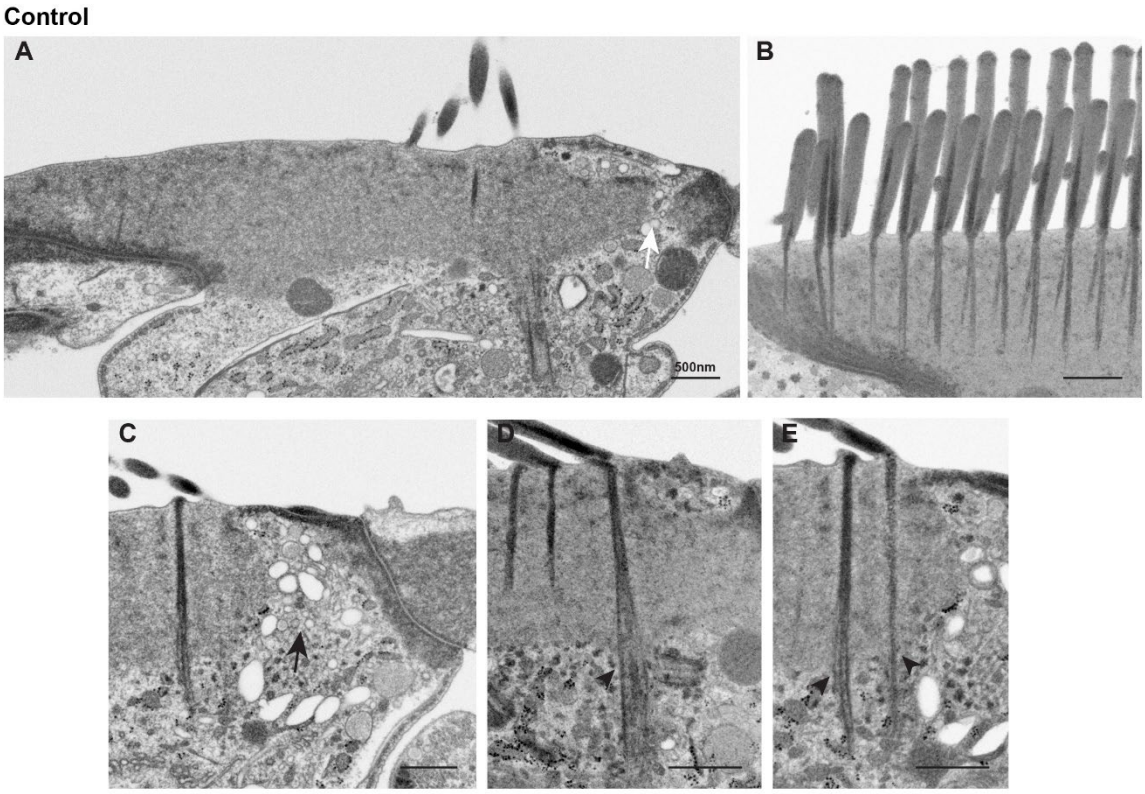

Figure 4.8 Typical F-actin compartments in control OHCs.
(A) Single FIB-SEM section of the cuticular plate. Actin meshwork of the cuticular plate is the bowl-shaped electron dense material that lacks mitochondria and vesicles. White arrow indicates vesicular traffic through the normally narrow path around the site of the retracted kinocilium. **(B)** A maximum intensity projection of straight rod-like stereocilia (tallest 1st and shorter 2nd row are shown; 2nd row rootlets are proportionally shorter). **(C)** A different neighboring cell from the same FIB-SEM block has a larger area that is empty of F-actin (black arrow). **(D-E)** Maximum intensity projections showing examples of over-elongated rootlet passing the cuticular plate F-actin meshwork (black arrowheads), compared to adjacent normal rootlets (without arrowheads) shown in (D). All intensity projections here are inverted for "TEM-like" image illustration. Scale bar in all images: 500 nm.

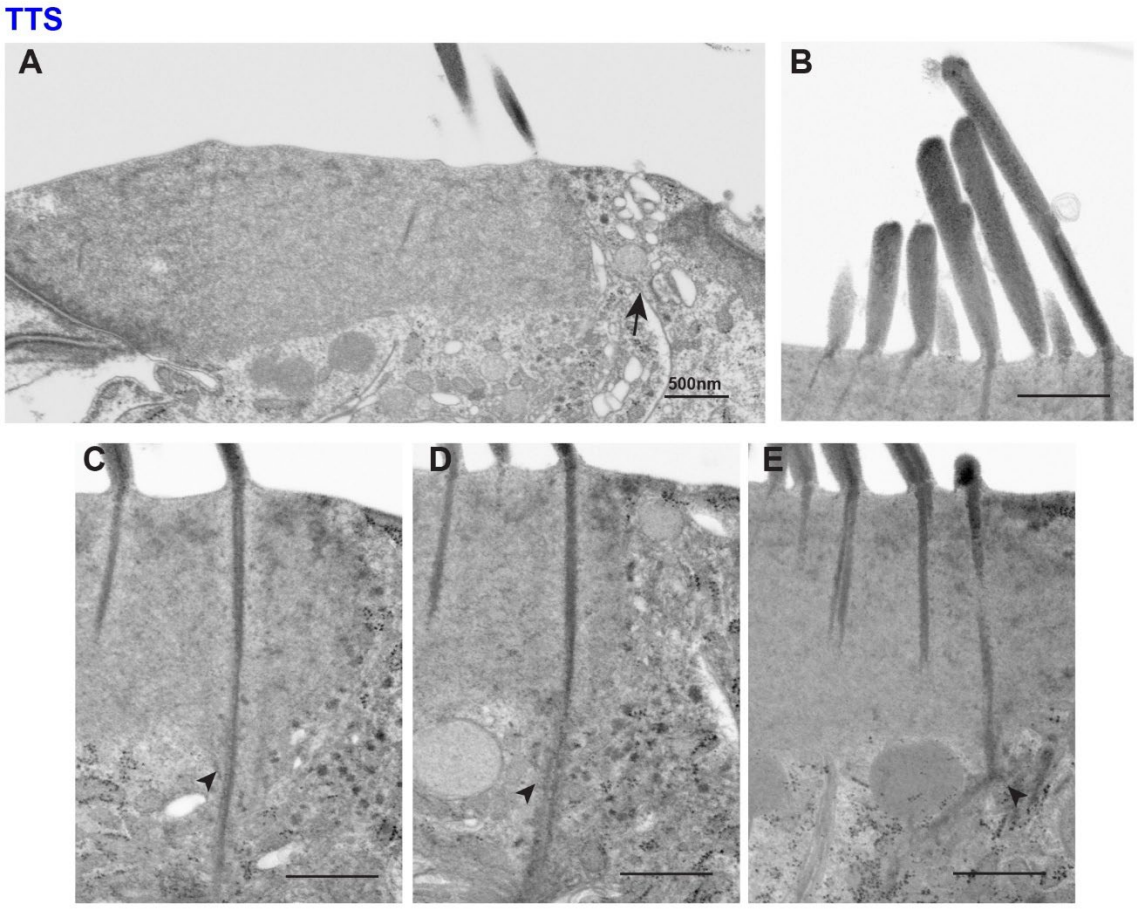

Figure 4.9 F-actin compartments in the OHCs exposed to noise producing TTS.
(A) Single FIB-SEM section of the cuticular plate. The electron dense material of the cuticular plate's actin meshwork lacking mitochondria and vesicles is shown. The area devoid of F-actin (black arrow) which is filled with vesicles becomes larger in TTS group compared to control. **(B)** A maximum intensity projection of straight rod-like stereocilia. **(C-D)** Maximum intensity projections showing examples of over-elongated rootlet passing the cuticular plate meshwork (black arrowheads), compared to adjacent normal rootlets (without arrowheads) shown in **(E)**. All intensity projections in this figure are inverted for "TEM-like" image illustration. Scale bar in all images: 500 nm.

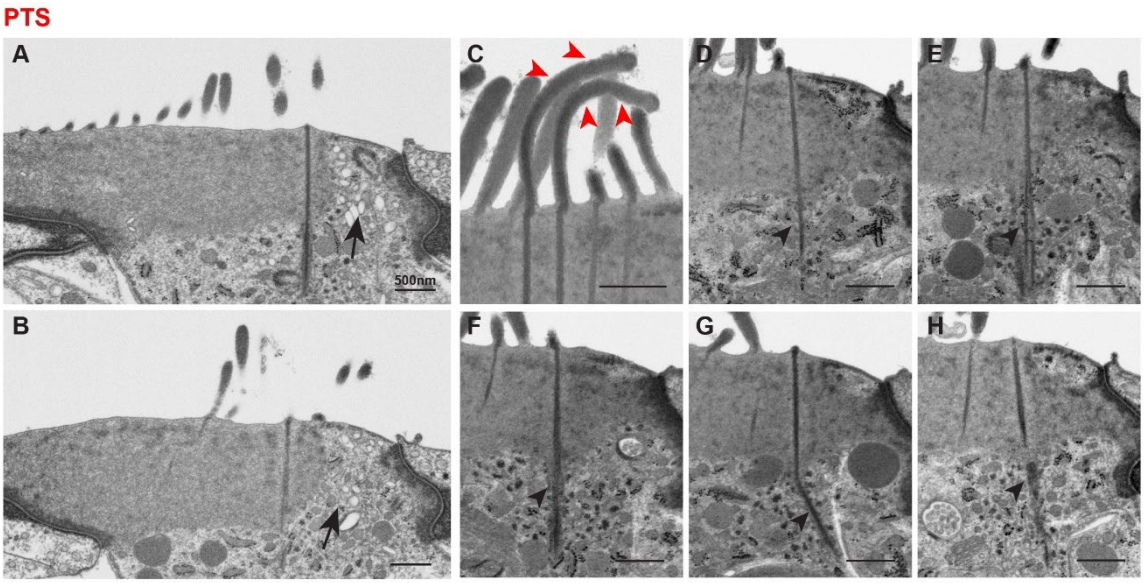

Figure 4.10 Disruption of F-actin within the shafts of stereocilia is a key pathology in OHCs induced by noise producing PTS.
(A-B) Single FIB-SEM sections of the cuticular plate from two different neighboring cells in the same FIB-SEM block. The area empty of F-actin becomes even larger after PTS exposure suggesting significant loss of actin (black arrows). **(C)** A maximum intensity projection of stereocilia shows striking bending of their shafts (red arrowheads). **(D-H)** Maximum intensity projections of over-elongated rootlets (black arrow heads) demonstrating that they are also present in PTS. In some cases, the over-elongated part of a rootlet looks disconnected (H). All intensity projections in this figure are inverted for "TEM-like" image illustration. Scale bar in all images: 500 nm.

CHAPTER 5. DISCUSSION

This project identifies the noise-induced damage to the actin structures in the mammalian hair cell bundles, immediately after exposure. We have found: i) disorganization of F-actin within the shafts of stereocilia in PTS but not control or TTS, ii) mechanical damage to the rootlets that is initiated in TTS and became more pronounced in PTS, and iii) noise-induced loss of actin from the cuticular plate in both TTS and PTS. We speculate that presumable depolymerization of actin within the stereocilia shafts and the cuticular plate is induced by global increase in $[Ca^{2+}]_i$ and subsequent activation of Ca^{2+}-dependent proteins such as calpains or actin severing molecules. The key take-home finding is that disorganization of F-actin within the shafts of stereocilia, immediately after exposure, distinguishes between TTS and PTS.

5.1 Noise exposure causes disorganization of actin within the shafts of stereocilia

In this study, we show that noise results in disruption, presumably depolymerization, of the F-actin core within the shafts of stereocilia in both IHCs and OHCs in PTS but not in TTS. FIB-SEM images of the IHCs stereocilia shafts reveal prominent disorganization in the packing of actin filaments (figure 4.2). Since these phenomena seem to occur in all stereocilia within a cell, it must be regulated globally i.e., at the level of a cell but not an individual stereocilium. We speculate that noise-induced depolymerization of F-actin core might be triggered by global change in intracellular $[Ca^{2+}]$ within a cell, which is known to increase during hair cell bundle overstimulation (Fridberger et al. 1998). The exact molecular mechanism requires further investigation.

It is known that unlike other actin compartments in hair cells, stereocilia have specialized actin cytoskeleton within their shafts. Their F-actin core is a paracrystalline

structure (Tilney et al. 1980) that is composed of parallel filaments that are rigid due to crosslinking by espin (Zheng et al. 2000), plastin-1(Taylor et al. 2015), and fascin-2 (Shin et al. 2010). Actin crosslinker/bundler espin binds F-actin at high affinity and is known to be relatively insensitive to Ca^{2+}, and therefore believed to protect F-actin from Ca^{2+} induced changes (Zheng et al. 2000). Furthermore, given their primary role in mechanotransduction, stereocilia are distinct cellular compartments because they exhibit special mechanisms for Ca^{2+} extrusion. They lack mitochondria and have unusually high density of Ca^{2+} ATPase pumps, known as PMCA2, specifically expressed along plasma membrane of stereocilia shafts to ensure removing Ca^{2+} upon entry through MET channels during mechanical stimulation (Yamoah et al. 1998; Dumont et al. 2001; Fettiplace and Nam 2019), (refer to figure 1.10 in Chapter 1). Therefore, we speculate that in TTS, transient or slight increases in $[Ca^{2+}]_i$ within stereocilia could be tolerated by the PMCA2 Ca^{2+} extrusion machinery and may not be sufficient to induce changes in the actin cytoskeleton within the stereocilia shafts (figure 4.2 E , left). In contrast, in PTS, persistent or extensive increase in $[Ca^{2+}]_i$ may exceed the extrusion capacity of PMCA2. This initiates increase of $[Ca^{2+}]_i$ inside the cell, and thereby activates Ca^{2+}-dependent mechanisms of cytoskeleton remodeling within a cell that include changes of F-actin in the stereocilia shafts (figure 4.2 E, right). Correspondingly, irreversible changes (such as disruption) of F-actin within the shafts of stereocilia are deleterious to the function of stereocilia and result in PTS. This is not surprising because the F-actin core of mammalian hair cells is known to be only dynamic at the tips of the stereocilia and is highly stable with minimal or no turnover within the shafts (Zhang et al. 2012; Drummond et al. 2015; Narayanan et al. 2015).

It is important to mention that due to the limited resolution, unlike IHCs, we could not resolve the packing of F-actin in OHCs. However, bending of the OHC stereocilia at their mid-shaft in PTS (figure 4.10 C) is a sign of disorganization (depolymerization), which we expect to be similar to that in IHCs. As previously mentioned, actin filaments within stereocilia shafts are highly rigid, and therefore can only be bent if disassembled. We also want to note that EM images by Liberman have previously illustrated that the shafts of stereocilia exhibited patches that were empty of actin in PTS hair cells several months after noise exposure (Liberman 1987), (refer to figure 2.1 B, left in Chapter 2). Here, in our FIB-SEM experiments, we capture the short-term effects of noise and reveal that the loss of actin, seen by Liberman, is likely preceded by disorganization of the actin filaments, presumably their severing and disassembly during noise exposure (figure 4.2 C). Indeed Ca^{2+}-dependent actin severing and capping proteins like gelsolin are known to be present in stereocilia (Mburu et al. 2010), and are possibly activated upon overwhelming increase in Ca^{2+} in PTS (figure 4.2 E, right).

5.2 Noise causes loss (disorganization) of actin within the cuticular plate

We have observed disorganization/shrinkage of the actin meshwork within the cuticular plate during noise exposure in IHCs and OHCs in both TTS and PTS. We hypothesize that disruption of actin within the cuticular plate might represent an early manifestation of the same Ca^{2+}-dependent mechanisms that, upon larger Ca^{2+} load, result in disorganization of F-actin within stereocilia. In this case, shrinkage of the cuticular actin meshwork may be caused by activation of Ca^{2+}-dependent proteases such as calpains, of which multiple isoforms (1-3) and (5-13) have been detected in adult hair cells (SHIELD 2012).

Interestingly, unlike in stereocilia where only PTS produces disruption of actin (figure 4.2 A-C), both TTS and PTS cause shrinkage of the actin within the cuticular plate (figure 4.6 B and C). Moreover, this shrinkage seems to be worse in PTS than TTS as the actin meshwork is severely interrupted by the formation of islands at the edges of the cell in IHCs (figure 4.6 E). This is also not surprising because the stereocilia and the cuticular plate compartments are fundamentally different on the structural and cellular basis. Stereocilia project from the apical surface of the hair cell while the cuticular plate is a part of the hair cell body. Unlike $[Ca^{2+}]_i$ control by PMCA2 inside stereocilia (Yamoah et al. 1998; Dumont et al. 2001), the resting level of Ca^{2+} within the cuticular plate is primarily maintained by Ca^{2+} buffers (Hackney et al. 2005) and PMCA1 (Dumont et al. 2001). Therefore, differences in the levels of Ca^{2+} or any Ca^{2+}-dependent events in the cuticular plate versus that of stereocilia are expected. Additionally, unlike the F-actin core within stereocilia, the gel-like actin meshwork of the cuticular plate forms randomly organized filaments which lacks espin but exhibits spectrin (Slepecky and Ulfendahl 1992; Furness et al. 2008; Liu et al. 2019) and alpha-actinin (Slepecky and Chamberlain 1985; Slepecky and Ulfendahl 1992), refer to (Chapter 1). Both molecules are known to be classical substrates for calpains that are highly sensitive to changes in Ca^{2+} (reviewed in (Lebart and Benyamin 2006)). Therefore, disorganization of actin within the cuticular plate may require smaller increase in $[Ca^{2+}]_i$ compared to that in stereocilia. This is consistent with the fact that although Ca^{2+} may increase to a lesser degree in TTS than in PTS, it may be sufficient to induce changes in the actin cytoskeleton. Indeed, the observed decrease in the structural non-uniformity within the meshwork of the cuticular plate is happening in both TTS and PTS (figure 4.6 F). Ca^{2+} induced degradation of actin and other cytoskeletal proteins, (for

example by calpains), decreases the heterogenic composition of the cuticular plate, thereby making it more homogenous in TTS and PTS.

Based on the data of our study, we have concluded that damage to the actin within the cuticular plate could be repairable and is not the primary cause of PTS. This is anticipated also because, unlike the shafts of stereocilia (Zhang et al. 2012; Drummond et al. 2015; Narayanan et al. 2015), F-actin within the cuticular plate is as dynamic as that in the tips of stereocilia (Zhang et al. 2012).

5.3 Appearance of dense actin structures within the shafts of stereocilia in IHCs

We observed "rootlet-like", aberrant dense actin structures within the shafts of stereocilia, which are not caused by noise exposure because they are equally present in the control and noise exposed stereocilia (figure 4.4 A-D). This suggests that stereocilia bundles can persist with these dense structures, and they do not seem to interfere with the hair cell's mechanosensitivity, as seen in the ABR assessments (figure 4.1 A, controls). One possibility on how these dense structures form is that they might be inherent to the stereocilia shafts. This means that they are locally generated during normal formation of the actin paracrystalline throughout mammalian postnatal development. An alternative possibility is that they are acquired by abnormal bundling of F-actin within the shafts of stereocilia, likely due to local mechanical damage induced by normal acoustic stimulation throughout life. If this is true, such mechanical damage does not alter hearing thresholds implicating a negligible effect on the mechanical properties of the stereocilia.

The latter phenomenon seems plausible considering the previously proposed models on the sliding of actin filaments during mechanical deflection of the stereocilia. According to the classical model suggested by Tilney and colleagues, when stereocilia

bend during sound-induced stimulation, parallel actin filaments within their shafts slide against each other (Tilney et al. 1983). Based on Tilney's idea, a second model recently proposed by (Kitajiri et al. 2010) suggests that filaments within the shafts of stereocilia are rigid and do not slide during deflection because they are crosslinked with espin (Zheng et al. 2000), plastin 1 (Taylor et al. 2015), and fascin 2 (Shin et al. 2010). Instead, only at the pivot point, actin filaments within the rootlet could freely shear against one another because they lack crosslinkers but are wrapped around by TRIOBP (Kitajiri et al. 2010; Pacentine et al. 2020). (See illustration of sliding filaments within the rootlets during normal stimulation, figure 4.4 E, left). It is not surprising that during long term and excessive mechanical deflection of the stereocilia throughout the lifespan, harsh sliding of the F-actin within the rootlets could propagate up into filaments within the shaft forcing them to slide (figure 4.4 E, middle). Consequently, sliding of the filaments could mechanically break crosslinkers within the stereocilia shafts, and filaments free of crosslinkers could become transiently spaced at variable distances (figure 4.4 E, right). As an attempt for repair, adjacent filaments may be bundled TRIOBP-4 isoform that is present in stereocilia shafts (Kitajiri et al. 2010), resulting into formation of dense structures that look like rootlets. Indeed, it was previously demonstrated that free actin filaments are robustly bundled by TRIOBP *in-vitro* (Kitajiri et al. 2010).

We note that formation of the abnormally dense actin structures within the shafts of stereocilia appears to be different from the F-actin disorganization produced in PTS. At least in both control and TTS stereocilia, in which we solely observe "rootlet-like" dense structures (figure 4.4 A and B), signs of striations and/or compact actin are indicative of intact filaments (figure 4.2 A and B). This evidence implies that the PTS associated

disorganization of F-actin (figure 4.2 C), is caused by a different mechanism than potential breakage of the crosslinkers due to noise overstimulation. Indeed, we do not observe traces of filaments in the stereocilia with disorganized actin in PTS, strongly suggesting their disassembly. Additionally, unlike the F-actin core within the shafts of stereocilia (Zhang et al. 2012; Drummond et al. 2015; Narayanan et al. 2015), crosslinker proteins like facsin-2 has been shown to have fast turnover (Roy and Perrin 2018), and therefore their mechanical damage is likely reversable.

5.4 Expansion of the rootlets during noise exposure

In this study we show that noise exposure expands stereocilia rootlets - they become thicker, hollow, or splayed, and their diameters become progressively larger going deeper into the cuticular plate. Interestingly, these noise-induced rootlet changes are reminiscent to hollow rootlets seen in the mutant (*Ankrd24*$^{KO/KO}$) mice lacking ankyrin-repeat protein (ANKRD24), an essential molecule for rootlet insertion and restraining their F-actin within the cuticular plate (Krey et al. 2022). According to our data, lower rootlets of the 1st row stereocilia seem to be thicker compared to other rows even in control hair cells, independent of noise exposure. Their thickness becomes variable deeper within the cuticular plate, again independent of noise exposure (figure 4.5 C). In contrast, lower rootlets in the 2nd row stereocilia of control unexposed stereocilia get thinner deeper into the cuticular plate. However, after noise, they start to widen in TTS, and their widening becomes significantly pronounced in PTS (figure 4.5 B). Hence, this strongly suggests that the noise exposure affects the molecular machinery that is mechanically connecting the rootlet to the actin meshwork and restraining it within the cuticular plate.

As previously discussed in Chapter 1, the lower part of the rootlet is embedded within the cuticular plate to maintain a well-anchored upright stereocilia throughout life. Within the cuticular plate's actin meshwork, the rootlet is somewhat fully isolated by an "empty" space that lacks actin (Tilney et al. 1980; DeRosier and Tilney 1989; Furness et al. 2008), but contains a number of molecules forming a complex that is crucial for anchoring the rootlet (Pacentine et al. 2020). Among them, rootlet bundler TRIOBP-5 (Katsuno et al. 2019) and spectrin, which makes up rings around the lower rootlets (Liu et al. 2019), are the key proteins maintaining the rootlets (figure 4.5 D, left). Moreover, the recently identified ANKRD24 physically interacts with TRIOBP-5, and the two of them are hypothesized to encircle the lower rootlet and keep their shape within the cuticular plate (Krey et al. 2022), (figure 4.5 D, left). Indeed, in the *Triobp*$^{\Delta ex9\text{-}10/\Delta ex9\text{-}10}$ mutant mice, stereocilia bundles have abnormal rootlets (Katsuno et al. 2019). Similarly, Krey et al. have recently found that in the *Triobp*$^{\Delta ex9\text{-}10/\Delta ex9\text{-}10}$ mutant hair cells, ANKRD24 seems to be disappear, and in *ankrd24*$^{KO/KO}$ mutants, TRIOBP-5 is abnormally localized (Krey et al. 2022). This strongly indicates that all these proteins are critical for the presence of each other as they work in concert for proper rootlet function and preventing their damage during normal mechanical stimulation. However, during intense overstimulation, they can also be susceptible to damage. Interestingly, mice lacking ANKRD24 not only have hollow rootlets but are also more susceptible to noise exposure (Krey et al. 2022). Additionally, definition of spectrin rings has been shown to be affected after intense noise exposure causing PTS (Liu et al. 2019).

As previously mentioned, the current belief is that only actin filaments within the rootlets slide relative to each other during sound stimulation (Kitajiri et al. 2010; Pacentine

et al. 2020). However, in the case of acoustic overstimulation, harsh sliding of these filaments could cause local mechanical breakage between the rootlet and the anchoring complex which connects it to the cuticular plate meshwork. For example, physical connection between ANKRD24 and the rootlet-TRIOBP-5 structures may no longer be intact after exposure, and hence restriction of F-actin of the lower rootlet within the cuticular plate could be lost (figure 4.5 D, middle). Non-restricted filaments become further apart forming hollow rootlets (figure 4.5 D, right), similar to that previously reported in *Ankrd24*$^{KO/KO}$ mice (Krey et al. 2022). Likewise, intense sliding of F-actin within rootlets may break their connection with the thin filaments which connect them to the actin meshwork of the cuticular plate (figure 4.5 D, middle and right). Although it is not currently known, we also speculate that if any of these molecules is somehow physically connected to spectrin, it is likely that spectrin will also be damaged around the rootlets (figure 4.5 D, middle and right).

Since damage to the rootlet seems to be mechanical, it is expected that some rootlets are more severely affected after acoustic trauma. The evidence for this speculation can be inferred from our observation of separate classes of damaged row 2 rootlets in PTS. Class II rootlets are thicker compared to class I, due to their large splaying towards their ends (Figure 4.5 B, bottom EM images). This strongly suggests that the severity of damage could depend on the location and the degree of broken molecules after overstimulation.

CHAPTER 6. CONCLUSION

The goal of this doctoral project is to identify the immediate (within minutes) effects of acoustic exposure on the stereocilia bundles in the auditory hair cells. Key summary findings of the work presented in this dissertation are:

- Disruption of F-actin core in the shafts stereocilia in PTS but not in TTS. This is an "all or none" effect of noise within a cell. It is likely a consequence of global change within the hair cell, such as Ca^{2+}-dependent depolymerization of F-actin.
- Formation of the distinct "rootlet-like" actin structures within the shafts of stereocilia not caused by noise exposure.
- Expansion (widening) of the lower rootlet within the cuticular plate, starting in TTS and becoming more striking in PTS. This damage seems to be row-specific and variable among effected rootlets. It is likely local, due to excessive sliding of the rootlet and mechanical breakage of the molecules connecting it to the cuticular plate.
- Re-arrangement (depolymerization) of actin within the cuticular plate's meshwork in both TTS and PTS, altering positioning of stereocilia. Similar to the stereocilia, possibly initiated by global increase in Ca^{2+} but perhaps at a lower Ca^{2+} concentration.

The only noise-induced ultrastructural damage that consistently differs between TTS and PTS, in both IHCs and OHCs, is the disorganization of F-actin in the shaft of stereocilia. It does make sense that this damage is not repairable because the shaft of stereocilia is the compartment where F-actin is known to be highly stable, with minimal or no turnover.

REFERENCES

Akil, O., Oursler, A. E., Fan, K. and Lustig, L. R. (2016). "Mouse Auditory Brainstem Response Testing." Bio Protoc **6**(6).

Baughman, J. M., Perocchi, F., Girgis, H. S., Plovanich, M., Belcher-Timme, C. A., Sancak, Y., Bao, X. R., Strittmatter, L., Goldberger, O., Bogorad, R. L., Koteliansky, V. and Mootha, V. K. (2011). "Integrative genomics identifies MCU as an essential component of the mitochondrial calcium uniporter." Nature **476**(7360): 341-345.

Baumeister, W., Grimm, R. and Walz, J. (1999). "Electron tomography of molecules and cells." Trends Cell Biol **9**(2): 81-85.

Békésy, G. V. (1960). Experiments in Hearing. New York, Toronto, London, McGraw-Hill Book Company, INC.

Belyantseva, I. A., Perrin, B. J., Sonnemann, K. J., Zhu, M., Stepanyan, R., McGee, J., Frolenkov, G. I., Walsh, E. J., Friderici, K. H., Friedman, T. B. and Ervasti, J. M. (2009). "Gamma-actin is required for cytoskeletal maintenance but not development." Proc Natl Acad Sci U S A **106**(24): 9703-9708.

Bergeron, S. E., Zhu, M., Thiem, S. M., Friderici, K. H. and Rubenstein, P. A. (2010). "Ion-dependent polymerization differences between mammalian beta- and gamma-nonmuscle actin isoforms." J Biol Chem **285**(21): 16087-16095.

Beurg, M., Fettiplace, R., Nam, J. H. and Ricci, A. J. (2009). "Localization of inner hair cell mechanotransducer channels using high-speed calcium imaging." Nat Neurosci **12**(5): 553-558.

Bielefeld, E. C., Kopke, R. D., Jackson, R. L., Coleman, J. K., Liu, J. and Henderson, D. (2007). "Noise protection with N-acetyl-l-cysteine (NAC) using a variety of noise exposures, NAC doses, and routes of administration." Acta Otolaryngol **127**(9): 914-919.

CDC. (2018, 2018). "Loud Noise Can Cause Hearing Loss." Retrieved 11/28/2023, 2023, from https://www.cdc.gov/nceh/hearing_loss/public_health_scientific_info.html.

CDC. (2020, 2020). "Too Loud! For Too Long!" Retrieved 11/29/2023, 2023, from https://www.cdc.gov/vitalsigns/hearingloss/index.html.

Chen, Y. S., Tseng, F. Y., Liu, T. C., Lin-Shiau, S. Y. and Hsu, C. J. (2005). "Involvement of nitric oxide generation in noise-induced temporary threshold shift in guinea pigs." Hear Res **203**(1-2): 94-100.

Cheng, P. W., Liu, S. H., Young, Y. H., Hsu, C. J. and Lin-Shiau, S. Y. (2008). "Protection from noise-induced temporary threshold shift by D-methionine is associated with preservation of ATPase activities." Ear Hear **29**(1): 65-75.

DeRosier, D. J. and Tilney, L. G. (1989). "The structure of the cuticular plate, an in vivo actin gel." J Cell Biol **109**(6 Pt 1): 2853-2867.

Drummond, M. C., Barzik, M., Bird, J. E., Zhang, D. S., Lechene, C. P., Corey, D. P., Cunningham, L. L. and Friedman, T. B. (2015). "Live-cell imaging of actin dynamics reveals mechanisms of stereocilia length regulation in the inner ear." Nat Commun **6**: 6873.

Dumont, R. A., Lins, U., Filoteo, A. G., Penniston, J. T., Kachar, B. and Gillespie, P. G. (2001). "Plasma membrane Ca2+-ATPase isoform 2a is the PMCA of hair bundles." J Neurosci **21**(14): 5066-5078.

Elkon, R., Milon, B., Morrison, L., Shah, M., Vijayakumar, S., Racherla, M., Leitch, C. C., Silipino, L., Hadi, S., Weiss-Gayet, M., Barras, E., Schmid, C. D., Ait-Lounis, A., Barnes, A., Song, Y., Eisenman, D. J., Eliyahu, E., Frolenkov, G. I., Strome, S. E., Durand, B., Zaghloul, N. A., Jones, S. M., Reith, W. and Hertzano, R. (2015). "RFX transcription factors are essential for hearing in mice." Nat Commun **6**: 8549.

Fettiplace, R. (2017). "Hair Cell Transduction, Tuning, and Synaptic Transmission in the Mammalian Cochlea." Compr Physiol **7**(4): 1197-1227.

Fettiplace, R. and Nam, J. H. (2019). "Tonotopy in calcium homeostasis and vulnerability of cochlear hair cells." Hear Res **376**: 11-21.

Fridberger, A., Flock, A., Ulfendahl, M. and Flock, B. (1998). "Acoustic overstimulation increases outer hair cell Ca^{2+} concentrations and causes dynamic contractions of the hearing organ." Proc Natl Acad Sci U S A **95**(12): 7127-7132.

Frolenkov, G. I., Belyantseva, I. A., Friedman, T. B. and Griffith, A. J. (2004). "Genetic insights into the morphogenesis of inner ear hair cells." Nat Rev Genet **5**(7): 489-498.

Fuchs, P. A. and Glowatzki, E. (2015). "Synaptic studies inform the functional diversity of cochlear afferents." Hear Res **330**(Pt A): 18-25.

Furness, D. N. (2015). "Molecular basis of hair cell loss." Cell Tissue Res **361**(1): 387-399.

Furness, D. N., Katori, Y., Mahendrasingam, S. and Hackney, C. M. (2005). "Differential distribution of beta- and gamma-actin in guinea-pig cochlear sensory and supporting cells." Hear Res **207**(1-2): 22-34.

Furness, D. N., Mahendrasingam, S., Ohashi, M., Fettiplace, R. and Hackney, C. M. (2008). "The dimensions and composition of stereociliary rootlets in mammalian cochlear hair cells: comparison between high- and low-frequency cells and evidence for a connection to the lateral membrane." J Neurosci **28**(25): 6342-6353.

Hackney, C. M., Mahendrasingam, S., Penn, A. and Fettiplace, R. (2005). "The concentrations of calcium buffering proteins in mammalian cochlear hair cells." J Neurosci **25**(34): 7867-7875.

Hadi, S., Alexander, A. J., Vélez-Ortega, A. C. and Frolenkov, G. I. (2020). "Myosin-XVa Controls Both Staircase Architecture and Diameter Gradation of Stereocilia Rows in the Auditory Hair Cell Bundles." J Assoc Res Otolaryngol **21**(2): 121-135.

Harrison, R. V. (1988). The Biology of Hearing and Deafness Springfield, Illinois, Charles C Thomas.

Haruta, T. (2018). "Comparison of 3D Imaging Methods in Electron Microscopy for Biomaterials." JEOL NEWS **53**(8).

Kachar, B., Battaglia, A. and Fex, J. (1997). "Compartmentalized vesicular traffic around the hair cell cuticular plate." Hear Res **107**(1-2): 102-112.

Kaltenbach, J. A., Falzarano, P. R. and Simpson, T. H. (1994). "Postnatal development of the hamster cochlea. II. Growth and differentiation of stereocilia bundles." J Comp Neurol **350**(2): 187-198.

Karavitaki, K. D. and Corey, D. P. (2010). "Sliding adhesion confers coherent motion to hair cell stereocilia and parallel gating to transduction channels." J Neurosci **30**(27): 9051-9063.

Katsuno, T., Belyantseva, I. A., Cartagena-Rivera, A. X., Ohta, K., Crump, S. M., Petralia, R. S., Ono, K., Tona, R., Imtiaz, A., Rehman, A., Kiyonari, H., Kaneko, M., Wang, Y. X., Abe, T., Ikeya, M., Fenollar-Ferrer, C., Riordan, G. P., Wilson, E. A., Fitzgerald, T. S., Segawa, K., Omori, K., Ito, J., Frolenkov, G. I., Friedman, T. B. and Kitajiri, S. I. (2019). "TRIOBP-5 sculpts stereocilia rootlets and stiffens supporting cells enabling hearing." JCI Insight **4**(12).

Kawashima, Y., Géléoc, G. S., Kurima, K., Labay, V., Lelli, A., Asai, Y., Makishima, T., Wu, D. K., Della Santina, C. C., Holt, J. R. and Griffith, A. J. (2011). "Mechanotransduction in mouse inner ear hair cells requires transmembrane channel-like genes." J Clin Invest **121**(12): 4796-4809.

Kazmierczak, M., Harris, S. L., Kazmierczak, P., Shah, P., Starovoytov, V., Ohlemiller, K. K. and Schwander, M. (2015). "Progressive Hearing Loss in Mice Carrying a Mutation in Usp53." J Neurosci **35**(47): 15582-15598.

Kazmierczak, P., Sakaguchi, H., Tokita, J., Wilson-Kubalek, E. M., Milligan, R. A., Müller, U. and Kachar, B. (2007). "Cadherin 23 and protocadherin 15 interact to form tip-link filaments in sensory hair cells." Nature **449**(7158): 87-91.

Kiernan, A. E., Steel, K. P. and Fekete, D. M. (2002). 22 - Development of the Mouse Inner Ear. Mouse Development. J. Rossant and P. P. L. Tam, Elsevier Inc**:** 539-566.

Kitajiri, S., Sakamoto, T., Belyantseva, I. A., Goodyear, R. J., Stepanyan, R., Fujiwara, I., Bird, J. E., Riazuddin, S., Riazuddin, S., Ahmed, Z. M., Hinshaw, J. E., Sellers, J., Bartles, J. R., Hammer, J. A., 3rd, Richardson, G. P., Griffith, A. J., Frolenkov, G. I. and Friedman, T. B. (2010). "Actin-bundling protein TRIOBP forms resilient rootlets of hair cell stereocilia essential for hearing." Cell **141**(5): 786-798.

Konings, A., Van Laer, L. and Van Camp, G. (2009). "Genetic studies on noise-induced hearing loss: a review." Ear Hear **30**(2): 151-159.

Kopke, R., Bielefeld, E., Liu, J., Zheng, J., Jackson, R., Henderson, D. and Coleman, J. K. (2005). "Prevention of impulse noise-induced hearing loss with antioxidants." Acta Otolaryngol **125**(3): 235-243.

Kozel, P. J., Davis, R. R., Krieg, E. F., Shull, G. E. and Erway, L. C. (2002). "Deficiency in plasma membrane calcium ATPase isoform 2 increases susceptibility to noise-induced hearing loss in mice." Hear Res **164**(1-2): 231-239.

Krey, J. F., Liu, C., Belyantseva, I. A., Bateschell, M., Dumont, R. A., Goldsmith, J., Chatterjee, P., Morrill, R. S., Fedorov, L. M., Foster, S., Kim, J., Nuttall, A. L., Jones, S. M., Choi, D., Friedman, T. B., Ricci, A. J., Zhao, B. and Barr-Gillespie, P. G. (2022). "ANKRD24 organizes TRIOBP to reinforce stereocilia insertion points." J Cell Biol **221**(4).

Kujawa, S. G. and Liberman, M. C. (2009). "Adding insult to injury: cochlear nerve degeneration after "temporary" noise-induced hearing loss." J Neurosci **29**(45): 14077-14085.

Kurabi, A., Keithley, E. M., Housley, G. D., Ryan, A. F. and Wong, A. C. (2017). "Cellular mechanisms of noise-induced hearing loss." Hear Res **349**: 129-137.

Kurima, K., Ebrahim, S., Pan, B., Sedlacek, M., Sengupta, P., Millis, B. A., Cui, R., Nakanishi, H., Fujikawa, T., Kawashima, Y., Choi, B. Y., Monahan, K., Holt, J. R., Griffith, A. J. and Kachar, B. (2015). "TMC1 and TMC2 Localize at the Site of Mechanotransduction in Mammalian Inner Ear Hair Cell Stereocilia." Cell Rep **12**(10): 1606-1617.

Le Prell, C. G., Yamashita, D., Minami, S. B., Yamasoba, T. and Miller, J. M. (2007). "Mechanisms of noise-induced hearing loss indicate multiple methods of prevention." Hear Res **226**(1-2): 22-43.

Lebart, M. C. and Benyamin, Y. (2006). "Calpain involvement in the remodeling of cytoskeletal anchorage complexes." Febs j **273**(15): 3415-3426.

Lehnhardt, E. and Lehnhardt, M. (2003). Functional Anatomy, Physiology and Pathology of the Auditory System. COMENIUS 2.1 ACTION. Qualification of educational staff working with hearing-impaired children (QESWHIC), Socrates Education and Culture.

Liberman, M. C. (1987). "Chronic ultrastructural changes in acoustic trauma: serial-section reconstruction of stereocilia and cuticular plates." Hear Res **26**(1): 65-88.

Liberman, M. C. (2016). "Noise-Induced Hearing Loss: Permanent Versus Temporary Threshold Shifts and the Effects of Hair Cell Versus Neuronal Degeneration." Adv Exp Med Biol **875**: 1-7.

Liberman, M. C. and Beil, D. G. (1979). "Hair cell condition and auditory nerve response in normal and noise-damaged cochleas." Acta Otolaryngol **88**(3-4): 161-176.

Liberman, M. C. and Dodds, L. W. (1987). "Acute ultrastructural changes in acoustic trauma: serial-section reconstruction of stereocilia and cuticular plates." Hear Res **26**(1): 45-64.

Liu, Y., Qi, J., Chen, X., Tang, M., Chu, C., Zhu, W., Li, H., Tian, C., Yang, G., Zhong, C., Zhang, Y., Ni, G., He, S., Chai, R. and Zhong, G. (2019). "Critical role of spectrin in hearing development and deafness." Sci Adv **5**(4): eaav7803.

Manley, G. A. and Gummer, A. W. (2017). The Cochlea: What It Is, Where It Came From, and What Is Special About It. Understanding the Cochlea. A. N. Popper and R. R. Fay. Swistzerland, Springer International Publishing AG. **62:** 351.

Marcus, D. C. (1998). Acoustic Transduction. Cell Physiology Source Book, second edition. N. Sperelakis. San Diego, CA, Academic Press.

Mburu, P., Romero, M. R., Hilton, H., Parker, A., Townsend, S., Kikkawa, Y. and Brown, S. D. (2010). "Gelsolin plays a role in the actin polymerization complex of hair cell stereocilia." PLoS One **5**(7): e11627.

McGrath, J., Roy, P. and Perrin, B. J. (2017). "Stereocilia morphogenesis and maintenance through regulation of actin stability." Semin Cell Dev Biol **65**: 88-95.

Minami, S. B., Yamashita, D., Schacht, J. and Miller, J. M. (2004). "Calcineurin activation contributes to noise-induced hearing loss." J Neurosci Res **78**(3): 383-392.

Müller, M., von Hünerbein, K., Hoidis, S. and Smolders, J. W. (2005). "A physiological place-frequency map of the cochlea in the CBA/J mouse." Hear Res **202**(1-2): 63-73.

Narayan, K. and Subramaniam, S. (2015). "Focused ion beams in biology." Nat Methods **12**(11): 1021-1031.

Narayanan, P., Chatterton, P., Ikeda, A., Ikeda, S., Corey, D. P., Ervasti, J. M. and Perrin, B. J. (2015). "Length regulation of mechanosensitive stereocilia depends on very slow actin dynamics and filament-severing proteins." Nat Commun **6**: 6855.

Natarajan, N., Batts, S. and Stankovic, K. M. (2023). "Noise-Induced Hearing Loss." J Clin Med **12**(6).

Ohlemiller, K. K. and Gagnon, P. M. (2007). "Genetic dependence of cochlear cells and structures injured by noise." Hear Res **224**(1-2): 34-50.

Ohlemiller, K. K., McFadden, S. L., Ding, D. L., Flood, D. G., Reaume, A. G., Hoffman, E. K., Scott, R. W., Wright, J. S., Putcha, G. V. and Salvi, R. J. (1999). "Targeted deletion of the cytosolic Cu/Zn-superoxide dismutase gene (Sod1) increases susceptibility to noise-induced hearing loss." Audiol Neurootol **4**(5): 237-246.

Ohlemiller, K. K., McFadden, S. L., Ding, D. L., Lear, P. M. and Ho, Y. S. (2000). "Targeted mutation of the gene for cellular glutathione peroxidase (Gpx1) increases noise-induced hearing loss in mice." J Assoc Res Otolaryngol **1**(3): 243-254.

Ohlemiller, K. K., Wright, J. S. and Dugan, L. L. (1999). "Early elevation of cochlear reactive oxygen species following noise exposure." Audiol Neurootol **4**(5): 229-236.

Pacentine, I., Chatterjee, P. and Barr-Gillespie, P. G. (2020). "Stereocilia Rootlets: Actin-Based Structures That Are Essential for Structural Stability of the Hair Bundle." Int J Mol Sci **21**(1).

Pan, B., Akyuz, N., Liu, X. P., Asai, Y., Nist-Lund, C., Kurima, K., Derfler, B. H., György, B., Limapichat, W., Walujkar, S., Wimalasena, L. N., Sotomayor, M., Corey, D. P. and Holt, J. R. (2018). "TMC1 Forms the Pore of Mechanosensory Transduction Channels in Vertebrate Inner Ear Hair Cells." Neuron **99**(4): 736-753.e736.

Peddie, C. J., Genoud, C., Kreshuk, A., Meechan, K., Micheva, K. D., Narayan, K., Pape, C., Parton, R. G., Schieber, N. L., Schwab, Y., Titze, B., Verkade, P., Aubrey, A. and Collinson, L. M. (2022). "Volume electron microscopy." Nat Rev Methods Primers **2**: 51.

Perrin, B. J. and Ervasti, J. M. (2010). "The actin gene family: function follows isoform." Cytoskeleton (Hoboken) **67**(10): 630-634.

Perrin, B. J., Sonnemann, K. J. and Ervasti, J. M. (2010). "β-actin and γ-actin are each dispensable for auditory hair cell development but required for Stereocilia maintenance." PLoS Genet **6**(10): e1001158.

Pickles, J. O., Comis, S. D. and Osborne, M. P. (1984). "Cross-links between stereocilia in the guinea pig organ of Corti, and their possible relation to sensory transduction." Hear Res **15**(2): 103-112.

Pollock, L. M. and McDermott, B. M., Jr. (2015). "The cuticular plate: a riddle, wrapped in a mystery, inside a hair cell." Birth Defects Res C Embryo Today **105**(2): 126-139.

Puel, J. L., Ruel, J., Gervais d'Aldin, C. and Pujol, R. (1998). "Excitotoxicity and repair of cochlear synapses after noise-trauma induced hearing loss." Neuroreport **9**(9): 2109-2114.

Quirk, W. S. and Seidman, M. D. (1995). "Cochlear vascular changes in response to loud noise." Am J Otol **16**(3): 322-325.

Reynolds, R. P., Kinard, W. L., Degraff, J. J., Leverage, N. and Norton, J. N. (2010). "Noise in a laboratory animal facility from the human and mouse perspectives." J Am Assoc Lab Anim Sci **49**(5): 592-597.

Roy, P. and Perrin, B. J. (2018). "The stable actin core of mechanosensory stereocilia features continuous turnover of actin cross-linkers." Mol Biol Cell **29**(15): 1856-1865.

Rzadzinska, A. K., Schneider, M. E., Davies, C., Riordan, G. P. and Kachar, B. (2004). "An actin molecular treadmill and myosins maintain stereocilia functional architecture and self-renewal." J Cell Biol **164**(6): 887-897.

Saunders, J. C. and Flock, A. (1986). "Recovery of threshold shift in hair-cell stereocilia following exposure to intense stimulation." Hear Res **23**(3): 233-243.

Scheffer, D. I., Zhang, D. S., Shen, J., Indzhykulian, A., Karavitaki, K. D., Xu, Y. J., Wang, Q., Lin, J. J., Chen, Z. Y. and Corey, D. P. (2015). "XIRP2, an actin-binding protein essential for inner ear hair-cell stereocilia." Cell Rep **10**(11): 1811-1818.

Schneider, M. E., Belyantseva, I. A., Azevedo, R. B. and Kachar, B. (2002). "Rapid renewal of auditory hair bundles." Nature **418**(6900): 837-838.

SHIELD. (2012). Retrieved 01/2/2024, 2024, from https://shield.hms.harvard.edu/gene_search.html.

Shih, C. P., Chen, H. C., Lin, Y. C., Chen, H. K., Wang, H., Kuo, C. Y., Lin, Y. Y. and Wang, C. H. (2019). "Middle-ear dexamethasone delivery via ultrasound microbubbles attenuates noise-induced hearing loss." Laryngoscope **129**(8): 1907-1914.

Shin, J. B., Longo-Guess, C. M., Gagnon, L. H., Saylor, K. W., Dumont, R. A., Spinelli, K. J., Pagana, J. M., Wilmarth, P. A., David, L. L., Gillespie, P. G. and Johnson, K. R. (2010). "The R109H variant of fascin-2, a developmentally regulated actin crosslinker in hair-cell stereocilia, underlies early-onset hearing loss of DBA/2J mice." J Neurosci **30**(29): 9683-9694.

Slepecky, N. and Chamberlain, S. C. (1985). "Immunoelectron microscopic and immunofluorescent localization of cytoskeletal and muscle-like contractile proteins in inner ear sensory hair cells." Hear Res **20**(3): 245-260.

Slepecky, N. B. and Ulfendahl, M. (1992). "Actin-binding and microtubule-associated proteins in the organ of Corti." Hear Res **57**(2): 201-215.

Taylor, R., Bullen, A., Johnson, S. L., Grimm-Günter, E. M., Rivero, F., Marcotti, W., Forge, A. and Daudet, N. (2015). "Absence of plastin 1 causes abnormal maintenance of hair cell stereocilia and a moderate form of hearing loss in mice." Hum Mol Genet **24**(1): 37-49.

Tilney, L. G., Derosier, D. J. and Mulroy, M. J. (1980). "The organization of actin filaments in the stereocilia of cochlear hair cells." J Cell Biol **86**(1): 244-259.

Tilney, L. G., Egelman, E. H., DeRosier, D. J. and Saunder, J. C. (1983). "Actin filaments, stereocilia, and hair cells of the bird cochlea. II. Packing of actin filaments in the stereocilia and in the cuticular plate and what happens to the organization when the stereocilia are bent." J Cell Biol **96**(3): 822-834.

Tilney, L. G., Saunders, J. C., Egelman, E. and DeRosier, D. J. (1982). "Changes in the organization of actin filaments in the stereocilia of noise-damaged lizard cochleae." Hear Res **7**(2): 181-197.

Tilney, L. G., Tilney, M. S. and DeRosier, D. J. (1992). "Actin filaments, stereocilia, and hair cells: how cells count and measure." Annu Rev Cell Biol **8**: 257-274.

Vélez-Ortega, A. C., Freeman, M. J., Indzhykulian, A. A., Grossheim, J. M. and Frolenkov, G. I. (2017). "Mechanotransduction current is essential for stability of the transducing stereocilia in mammalian auditory hair cells." Elife **6**.

Vélez-Ortega, A. C. and Frolenkov, G. I. (2019). "Building and repairing the stereocilia cytoskeleton in mammalian auditory hair cells." Hear Res **376**: 47-57.

Wagner, E. L., Im, J. S., Sala, S., Nakahata, M. I., Imbery, T. E., Li, S., Chen, D., Nimchuk, K., Noy, Y., Archer, D. W., Xu, W., Hashisaki, G., Avraham, K. B., Oakes, P. W. and Shin, J. B. (2023). "Repair of noise-induced damage to stereocilia F-actin cores is facilitated by XIRP2 and its novel mechanosensor domain." Elife **12**.

WHO. (2023, 2023). "Deafness and hearing loss." Retrieved 11/28/2023, 2023, from https://www.who.int/news-room/fact-sheets/detail/deafness-and-hearing-loss.

Xu, K., Xu, B., Gu, J., Wang, X., Yu, D. and Chen, Y. (2023). "Intrinsic mechanism and pharmacologic treatments of noise-induced hearing loss." Theranostics **13**(11): 3524-3549.

Yamane, H., Nakai, Y., Takayama, M., Iguchi, H., Nakagawa, T. and Kojima, A. (1995). "Appearance of free radicals in the guinea pig inner ear after noise-induced acoustic trauma." Eur Arch Otorhinolaryngol **252**(8): 504-508.

Yamoah, E. N., Lumpkin, E. A., Dumont, R. A., Smith, P. J., Hudspeth, A. J. and Gillespie, P. G. (1998). "Plasma membrane Ca2+-ATPase extrudes Ca2+ from hair cell stereocilia." J Neurosci **18**(2): 610-624.

Zhang, D. S., Piazza, V., Perrin, B. J., Rzadzinska, A. K., Poczatek, J. C., Wang, M., Prosser, H. M., Ervasti, J. M., Corey, D. P. and Lechene, C. P. (2012). "Multi-isotope imaging mass spectrometry reveals slow protein turnover in hair-cell stereocilia." Nature **481**(7382): 520-524.

Zheng, L., Sekerková, G., Vranich, K., Tilney, L. G., Mugnaini, E. and Bartles, J. R. (2000). "The deaf jerker mouse has a mutation in the gene encoding the espin actin-bundling proteins of hair cell stereocilia and lacks espins." Cell **102**(3): 377-385.

VITA

Education

University of Kentucky, College of Medicine, Lexington, KY August 2018 – Present
Doctor of Philosophy in Physiology
Program: Integrated Biomedical Sciences
Department: Physiology
Lab Mentor: Dr. Gregory I. Frolenkov
Dissertation: Disorganization of Actin Within the Shafts of Stereocilia is a Key Difference Between Temporary and Permanent Noise-Induced Hearing Loss (NIHL)
Doctoral Defense Date: April 15th, 2024

University of Kentucky, College of Medicine, Lexington, KY August 2018
Master of Science in Medical Sciences
Lab Mentor: Dr. Gregory I. Frolenkov
Thesis: Myosin-XVa is Key Molecule in Establishing the Architecture of Mechanosensory Stereocilia Bundles of the Inner Ear Hair Cells

University of Kentucky, College of Arts and Sciences, Lexington, KY May 2013
Bachelor of Science in Biology with Honors. (Pre-Medicine Program Curriculum)
Minor: Arabic and Islamic Studies

Professional Positions

Graduate Research Assistant 2018 – Present
Dr. Gregory Frolenkov's Laboratory
Department of Physiology, University of Kentucky College of Medicine

Senior Teaching Assistant Fall 2023
Elementary Physiology Laboratory (PGY 208-201)
Department of Physiology, University of Kentucky College of Medicine

Graduate Research-Master's Student 2015 – 2018
Dr. Gregory Frolenkov's Laboratory

Postbaccalaureate Research- Volunteer 2013 – 2015
Dr. Gregory Frolenkov's Laboratory

Awards and Honors

Best Poster Presentation Award October 2021
University of Kentucky Dept. of Physiology Research Retreat

Research Fund Support 5T32GM118292-04 (PI: Bret N. Smith) July 2019 – June 2020
The "Graduate Training in Integrative Physiology" grant by the American National Institute of Health (NIH) is awarded to selected to graduate students in the University of Kentucky Dept. of Physiology.

First Prize Best Poster Presentation May 2018
University of Kentucky Dept. of Physiology Research Retreat

Meritorious Graduate Student Poster Presentation Award March 2017
The Kentucky Chapter of the American Physiological Society

Cum Laude Honors in Biology degree May 2013

Poster/Podium Presentations

Regional Meetings:

Hadi S, Alexander AJ, Velez-Ortega AC, Frolenkov GI (2017) "Myosin-15a is Essential for Gradation of Stereocilia Heights and Diameters in the Mechanosensory Bundle of the Auditory Hair Cells." *5th Annual Meeting of the Kentucky Chapter of the American Physiological Society*, Bowling Green, KY, Abst. 7. **(Best poster award)**

National Meetings:

Shadan Hadi, Gregory Frolenkov (2024) "Disruption of F-Actin Within the Shafts of Stereocilia is a Key Difference Between Temporary and Permanent Noise-Induced Hearing Loss." *Association for Research in Otolaryngology*, Anaheim, CA. Abst.SU-80

Ghazaleh Behnammanesh, **Shadan Hadi**, Abigail Dragich, Xiayi Liao, Mi-Jung Kim, Lijin Dong, Benjamin Perrin, Shinichi Someya, Gregory I Frolenkov, Jonathan Bird (2024) "Myosin 15 Isoform 3 Traffics the Elongation Complex to the Tips of Row 1 Stereocilia and is Required for Their Maintenance in the Adult Hair Cells." *Association for Research in Otolaryngology*, Anaheim, CA. Abst.Podium#19

Abigail Dragich, Savita Sharma, **Shadan Hadi**, Craig Vander Kooi, Gregory Frolenkov (2024) "G-a Interacting Protein, C-terminus 3 (GIPC3) Regulates Vesicular Trafficking in Mammalian Auditory Hair Cells." *Association for Research in Otolaryngology*, Anaheim, CA. Abst.S-34

Savita Sharma, Abigail Dragich, **Shadan Hadi**, Gregory Frolenkov, Craig Vander Kooi (2024) "Structural Basis of G-A Interacting Protein, C-Terminus 3 (GIPC3) Function as an Adaptor for Myosin-6-Dependent Transport." *Association for Research in Otolaryngology*, Anaheim, CA. Abst.M-43

Shadan Hadi, Gregory Frolenkov (2023) "Immediate Effects of Noise Damage on the Actin Structures Supporting Stereocilia in Mammalian Auditory Hair Cells." *Association for Research in Otolaryngology*, Orlando, FL. Abst.MO-141.

Hesam Babahosseini, Inna A, Belyantseva, Rizwan Yousef, Risa Tona, **Shadan Hadi**, Sayaka Inagaki, Elizabeth Wilson, Shin-Ichiro Kitajiri, Gregory I. Frolenkov, Thomas B. Friedman, Alexander X. Cartagena-Rivera. "Triobp Promotes Unbalanced Bidirectional

Radial Stiffness Gradients Within the Mammalian Organ of Corti." *Association for Research in Otolaryngology*, Orlando, FL. Abst.Podium#31.

Ghazaleh Behnammanesh, **Shadan Hadi**, Mi-Jung Kim, Lijin Dong, Shinichi Someya, Gregory I Frolenkov, Jonathan Bird (2023) "Myosin 15 Isoform 3 Traffics the Elongation Complex in Postnatal Hair Cells and is Required for Hearing." *Association for Research in Otolaryngology*, Orlando, FL. Abst.SA-108.

Isabel Aristizabal, Arnaud Giese, Abigail Dragich, Sofia Zuluaga-Osorio, **Shadan Hadi**, Saima Riazuddin, Zubair Ahmed, Gregory I Frolenkov (2023) "The Calcium and Integrin-Binding Protein 2 (CIB2) Transmits the Force to the Mechanotransducer of Mammalian Auditory Hair Cells." *Association for Research in Otolaryngology*, Orlando, FL. Abst.Podium#28.

Shadan Hadi, Mike Grossheim, Gregory I. Frolenkov (2022) "Immediate Effects of Noise Exposure to the Actin Structures Supporting Stereocilia Bundles in Mammalian Auditory Hair Cells." *Molecular Biology of Hearing and Deafness*, Iowa City, IA. Abst.PS-51.

Isabel Aristizabal-Ramirez, Arnaud P.J. Giese, Abigail K. Dragich, K. Sofia Zuluaga-Osorio, Julie Watkins, **Shadan Hadi**, Saima Riazuddin, Zubair M. Ahmed, Gregory I. Frolenkov (2022) "Deafness-associated Variant of the Calcium and Integrin-Binding Protein 2 (CIB2) Slows Down Force Transmission to the Mechanotransducer Channels in Mammalian Auditory Hair Cells." *Molecular Biology of Hearing and Deafness*, Iowa City, IA. Abst. Podium.

K. Sofia Zuluaga-Osorio, Isabel Aristizabal-Ramirez, Rizwan Yousaf, Elizabeth Wilson, Sayaka Inagaki, **Shadan Hadi**, Thomas B. Friedman, Inna A. Belyantseva, Gregory I. Frolenkov (2022) "Taperin deficiency increases nonlinearity of stereocilia bundle motion and transduction current-displacement relationship in mammalian auditory hair cells." *Midwest Auditory Research Conference,* Ann Arbor, MI. Abst. Podium.

K. Sofia Zuluaga-Osorio, Isabel Aristizabal-Ramirez, Rizwan Yousef, Elizabeth Wilson, Sayaka Inagaki, **Shadan Hadi**, Thomas Friedman, Inna Belyantseva, Gregory Frolenkov (2022) "Taperin is Not Essential for Mechanotransduction but Contributes to the Linearity of Hair Bundle Motion." *Association for Research in Otolaryngology*, Virtual meeting, Abst. PS.

Mark T McClendon, **Shadan Hadi**, Gregory Frolenkov, A. Catalina Velez-Ortega (2022) "Dynamic Changes in Stereocilia Cytoskeleton Alignment Driven by Mechanotransduction in Auditory Mammalian Hair Cells." *Association for Research in Otolaryngology*, Virtual meeting, Abst. PS.

Isabel Aristizabal, Arnaud Giese, Abigail Dragich, Sofia Zuluaga-Osorio, Julie Watkins, **Shadan Hadi**, Saima Riazuddin, Zubair Ahmed, Gregory Frolenkov (2022) "Calcium and Integrin-Binding Protein 2 (CIB2) is Essential for Force Transmission to the

Mechanotransducer Channels of the Mammalian Auditory Hair Cells." *Association for Research in Otolaryngology*, Virtual meeting, Abst. PS.
Hadi S, Alexander AJ, Velez-Ortega AC, Frolenkov GI (2019) "Myosin-XVa is Controls both Staircase Architecture and Diameter Gradation in the Stereocilia Bundles of the Auditory Hair Cells." *Midwest Auditory Research Conference,* Springfield, IL. Abst. PS-28.

Hadi S, Alexander AJ, Velez-Ortega AC, Frolenkov GI (2019) "The Short Isoform of Myosin-XVa is Required not only for Staircase Architecture but also for Gradation of Stereocilia Diameters in the Auditory Hair Cells." *Association for Research in Otolaryngology*, Baltimore, MD, Abst. PS-448.

Hadi S, Alexander AJ, Velez-Ortega AC, Frolenkov GI (2018) "Myosin-XVa is Essential to Form the Gradation of Stereocilia Diameters Within the Hair Bundles of Inner but not Outer Hair Cells." *Association of Research in Otolaryngology,* San Diego, CA, Abst. PS-125.

Hadi S, Alexander AJ, Velez-Ortega AC, Frolenkov GI (2017) "Different Role of Myosin-15a in the Development of Inner and Outer Hair Cells: Stereocilia Number and Diameter." *Association for Research in Otolaryngology*, Baltimore, MD, Abst. PS-773.

Hertzano R, Milon B, Margulies Z, McMurray M, **Hadi S**, Mitra S, Frolenkov GI (2017) "RFX Transcription Factors are Necessary for Hair Cell Terminal Differentiation but not for Survival of Mature Hair Cells." *Association for Research in Otolaryngology*, Baltimore, MD, Abst. PS-96.

Elkon R, Milon B, Morrison L, Shah M, Vijayakumar S, Rarcherla M, Leitch C, Silipino L, **Hadi S**, Schmid C, Barnes A, Song Y, Eisenman D, Eliyahu E, Frolenkov G, Strome S, Durand B, Zaghloul N, Jones S, Reith W, Hertzano R (2016) "RFX Transcription Factors are Essential for Survival of the Terminally Differentiating Outer Hair Cells in Mice." *Association for Research in Otolaryngology*, San Diego, CA, Abst. PS-292.

Publications

Isabel Aristizábal-Ramírez, Abigail K. Dragich, Arnaud P.J. Giese, K. Sofia Zuluaga-Osorio, Julie Watkins, Garett K. Davies, **Shadan E. Hadi**, Saima Riazuddin, Craig W. Vander Kooi, Zubair M. Ahmed, Gregory I. Frolenkov. "Calcium and Integrin-binding protein 2 (CIB2) controls force sensitivity of the Mechanotransducer channels in cochlear outer hair cells". *bioRxiv*. 2023 Jul. doi**:**10.1101/2023.07.09.545606.

Babahosseini H, Belyantseva IA, Yousaf R, Tona R, **Hadi S**, Inagaki S, Wilson E, Kitajiri SI, Frolenkov GI, Friedman TB, Cartagena-Rivera AX. "Unbalanced bidirectional radial stiffness gradients within the organ of Corti promoted by TRIOBP." *Proc Natl Acad Sci U S A*. 2022 Jun 28;119(26):e2115190119. doi: 10.1073/pnas.2115190119.

Hadi S, Alexander AJ, Vélez-Ortega AC, Frolenkov GI. "Myosin-XVa Controls Both Staircase Architecture and Diameter Gradation of Stereocilia Rows in the Auditory Hair

Cell Bundles." *J Assoc Res Otolaryngol*. 2020 Apr;21(2):121-135. doi:10.1007/s10162-020-00745-4

Elkon R, Milon B, Morrison L, Shah M, Vijayakumar S, Racherla M, Leitch CC, Silipino L, **Hadi S**, Weiss-Gayet M, Barras E, Schmid CD, Ait-Lounis A, Barnes A, Song Y, Eisenman DJ, Eliyahu E, Frolenkov GI, Strome SE, Durand B, Zaghloul NA, Jones SM, Reith W, Hertzano R "RFX Transcription Factors are Essential for Hearing in Mice." *Nat Commun*. 2015 Oct 15;6:8549. doi: 10.1038/ncomms9549.

Shadan Hadi